Alma Mater Studiorum · Università di Bologna

Scuola di Scienze
Dipartimento di Fisica e Astronomia
Corso di Laurea Magistrale in Fisica

Computational modelling to characterize dendrimer nanocarriers for siRNA delivery in Chronic Obstructive Pulmonary Disease

Relatore:
Prof. Gastone Castellani

Correlatore:
Prof. Andrea Danani

Presentata da:
Cecilia Magatti

Anno Accademico 2016/2017

Abstract

La Broncopneumopatia Cronica Ostruttiva (BPCO) è un'infiammazione polmonare progressiva caratterizzata da limitazione di flusso espiratorio. Ad oggi a livello mondiale si stima che 328 milioni di persone siano affette da BPCO e si prevede che diventi la quarta causa di morte entro il 2030 con più di 65 milioni di casi l'anno.
Il successo dei trattamenti medici mediante acidi nucleici, come DNA e silencing interference RNA è fortemente legato al design di efficienti tecnologie di rilascio. I dendrimeri cationici rappresentano un'interessante possibilità come vettori grazie a noti vantaggi di efficienza, di basso costo, di produzione e di versatilità d'applicazione nel trattamento di molteplici malattie e disturbi.
Il presente lavoro di tesi, svolto presso l'Istituto Dalle Molle di Studi sull'Intelligenza Artificiale di Lugano (CH), ha avuto lo scopo di investigare a livello computazionale su scala atomica il meccanismo di legame di diversi dendrimeri con un modello di siRNA, per l'ottenimento di efficienti sistemi di rilascio per il trattamento di BPCO.
In primo luogo sono stati realizzati i modelli di tre dendrimeri con differente funzionalizzazione ed è stato eseguito uno studio preliminare di caratterizzazione in acqua. In seguito, mediante la dinamica molecolare è stato analizzato il complesso, esplorandone le caratteristiche di legame in termini energetici e strutturali.
Si è evidenziato come i cambiamenti conformazionali e la presenza di cariche sulla superficie dei dendrimeri condizionassero il legame con il siRNA.
La diversa funzionalizzazione dei dendrimeri infatti influisce fortemente sulla topologia e sulle proprietà fisico-chimiche che guidano l'interazione con gli agenti terapeutici e l'ambiente. I risultati di questo lavoro apportano un contributo significativo al futuro design di vettori di acidi nucleici selettivi, caratterizzati dal miglior compromesso tra stabilità del complesso e abilità di rilascio del sistema.

Contents

Chapter 1

Introduction

This chapter introduces the present master thesis research, together with its aims and objectives; It describes some details on the biological background of gene therapy. At the end there is a summary about the organization of all the chapters treated in this work.

Chronic obstructive pulmonary disease (COPD) is a progressive inflammatory lung disease usually progressive and associated with an enhanced chronic inflammatory response in the airways and the lung to noxious particles or gases. Targeting and silencing the TNF-α gene by siRNA, through engineered dendrimers able to prevent lung inflammation, is a promising research line for the treatment of COPD pioneered by the group of Prof. Fattal and Prof. Majoral, France. In multidrug therapeutic regimen (as in COPD), an easier administration as well as a reduced number of therapeutics and adverse effects, represent a promising strategy to enhance the therapy success. In this connection, it is well recognized that bioavailability of therapeutic agents depends on both patients inhalation technique and size of drug-NPs delivered. In this context, dendrimers size controllability and customizability offer a powerful property to ensure ad hoc size for different inhalator condition and different patient features. Finally, it is now accepted that TNF-α system shows several polymorphisms that can affect the therapy efficacy. Therefore, the ability to specifically silence TNF-α production in peculiar cells (AMs) could overcome limitations due to population heterogeneity and reduce adverse effect due to off-targeting (local effect through mannosylateddendrimer administered by inhalation).
In this work we focus the attention on design and optimize novel dendrimers for siRNA delivery targeting COPD. In order to model an ad hoc dendrimer-based system suitable for inhalator purpose and able to guarantee an high TNF-α silencing, an accurate evaluation of the physicochemical and molecular properties of the different dendrimers is necessary. In particular our modelling activity will allow to characterize how different functionalizations may modify dendrimer properties in term of interaction with cell membrane of the lung tissue.

Aim of the Thesis

The aim of this thesis is to build advance particle designs for improved deposition and interaction with lung tissue. The main goal is to use computational methods to investigate the behaviour of different dendrimers in water and in complex with siRNA and to improve the characterization of the complex during the molecular dynamics simulations. Due to the particular structures assumed by dendrimers after complexation with siRNA it would be interesting to study which characteristics it shows,in order to evaluate siRNA-dendrimer interaction to ensure an appropriate loading and delivery of the therapeutic agent.

The present manuscript is divided in several sections briefly described as following:

- Chapter 1 is the present introductory part.

- Chapter 2 introduces the scientific background concerning the use of gene therapy for pulmonary disease. In detail, firstly it gives a description of COPD inflammation and TNF-α receptor. Furthermore, it provides a detailed description of strategies for gene therapy and the usage of non viral vectors. The third section is focused on the main role of siRNA in the gene silencing process, including advantages of siRNA therapy for treatment of lung inflammation. The use of nanoparticles in siRNA therapy is explained with a special focus on cationic polymers as dendrimers. Finally, a specific section for the description of dendrimers structures and properties is dedicated with the attention on their conformational characteristics in order to improve their efficacy within the siRNA complex.

- Chapter 3 provides a theoretical overview of the methods used in this work with particular emphasis on the physical and biophysical aspects. In particular, the aim of this Chapter is to explore a connection between simulation and statistical mechanics and describe the theory underlying the present master thesis work, in order to provide an explanation of the physical background behind computational methods. After a presentation of computational molecular modelling, a description of Molecular Mechanics and Molecular s approaches is provided. In the last section an overview is given which covers enhanced sampling methods.

- Chapter 4 gives a panoramic of three types of functionalized dendrimers characterization. Particularly it describes a Molecular Dynamics study to evaluate the behaviour of different generations of three dendrimers, with same core and branches structure but different terminal groups. In particular, the role of pyrrolidinium, piperazinium and morpholidinium as terminal group

will be investigate in order to understand the variations in physicochemical properties of dendrimer surface.

- Chapter 5 includes a description of the model of siRNA and its complex with different dendrimers. The chapter presents a molecular modelling strategy to design optimized dendrimer-based carries for siRNA to be delivered by inhalation route in COPD treatment. In details, in silico simulations has been performed to evaluate the siRNA-dendrimer interaction. Classical MD has been employed to ensure an appropriate siRNA loading and delivery in presence of different dendrimers functionalized by pyrolidinium, piperazinium and morpholidinium surface groups.
- Chapter 6 is devoted to general conclusions of this work.

Chapter 2

Use Of Nanoparticles In Gene Therapy For COPD

This chapter presents an overview of the scientific background underlying thesis work. In detail, firstly it gives a description of COPD inflammation and TNF-α receptor. Furthermore, it provides a detailed description of strategies for gene therapy and the usage of non viral vectors. The third section is focused on the main role of siRNA in the gene silencing process, including advantages of siRNA therapy for treatment of lung inflammation. The use of nanoparticles in siRNA therapy is explained with a special focus on cationic polymers as dendrimers. Finally, a specific section for the description of dendrimers structures and properties is dedicated with the attention on their conformational characteristics in order to improve their efficacy within the siRNA complex.

2.1 Chronic Obstructive Pulmonary Disease (COPD)

Chronic obstructive pulmonary disease (COPD), is a collective nomenclature which includes chronic pulmonary emphysema (CPE) and chronic bronchitis, is a progressive inflammatory lung disease which is characterized by a persistent airflow limitation, is usually progressive and associated with an enhanced chronic inflammatory response in the airways and the lung to noxious particles or gases. It is generally accepted that cigarette smoking is the most important risk factor for COPD; other factors that can be contributed to the disease progression are: prolonged and intense exposure to air pollution, noxious dusts and chemicals [1] (Fig. 2.1).
Inflammatory mediators induce mucus hypersecretion, oedema and inhibition of tissue repair. These detrimental mechanisms are prompted by smoke, which all contribute to the respiratory dysfunctions.
This chronic inflammatory response may induce parenchymal tissue destruction (resulting in emphysema) and disrupt normal repair and defense mechanisms (resulting in small airway fibrosis), leading to the loss of alveolar attachments to the small

airways and decreases lung elastic recoil. These pathological changes lead to air trapping and progressive airflow limitation, and in turn to breathlessness and other characteristic symptoms of COPD. The risk of future exacerbations is estimated by the severity of airflow limitation and the history of previous exacerbations. COPD is a leading cause of morbidity and mortality worldwide and results in an economic and social burden that is both substantial and increasing, an estimated number of 328 million people have COPD worldwide (168 million men and 160 million women) [2] with the possibility of becoming the fourth leading cause of death in the world by 2030 with more than 65 million people dying from COPD every year [3]. A new approach is necessary to improve therapy efficacy and safety; in fact the

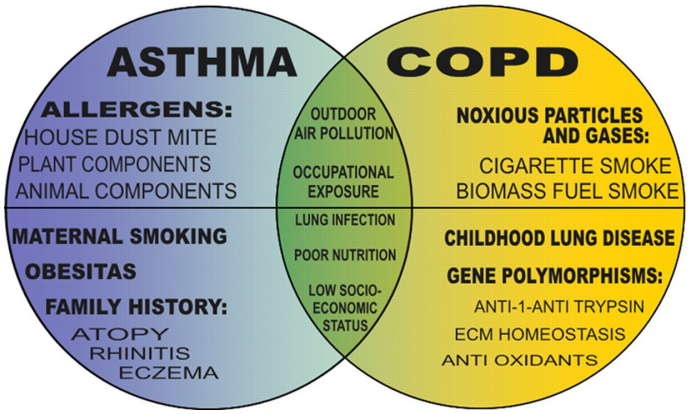

Figure 2.1: *Representation of airway disease risk factors. Both asthma and COPD hold pathologic features belonging to environmental risk factors, sharing outdoor air pollutants and occupational exposures, and personal risk factors, sharing lung infections, poor nutrition and low socioeconomic status [4].*

treatment of COPD, according to GOLD classification based on symptom and risk evaluation, includes theophylline, long-acting muscarinic antagonists, long acting beta-2 agonists (LABAs), LABA/inhaled glucocorticoids (GCs) combinations and the phosphodiesterase-4 inhibitor roflumilast.
Furthermore, an exhortation to treat COPD with systematic GCs for 7 to 14 days is included in current guidelines for patients with acute exacerbations, instead of intermittent systemic corticosteroid use, as a result of the association of the latter with concomitant adverse effects such as osteoporosis, hyperglycaemia, upper gastrointestinal haemorrhage, muscle weakness and acute psychosis [5], [6].

2.1.1 Inflammation

The association of airways inflammation and lung pathology in smokers has long been suspected, moreover many animal model studies and *in vitro* experiments have investigated the role of specific inflammatory cells and molecules in COPD

[7]. Whereas Alveolar Macrophages (AMs) are the predominant cell type found in airways, they, and to a lesser extent epithelial cells, play a critical role in the physiopathology of COPD and are a major target for therapy (Fig. 2.2).
AMs extracted from COPD patients have a stimulated secretion of inflammatory proteins, including certain cytokines, chemokines, reactive oxygen species and elastolytic enzymes[8].
Among those factors, the genetic contribution to the disease has been implicated. Although the nature of the genetic influences remains undefined, factors that regulate the inflammatory responses to direct exposure of inhaled insults are important in the pathogenesis of COPD [9]. In particular, COPD patients show an increased expression

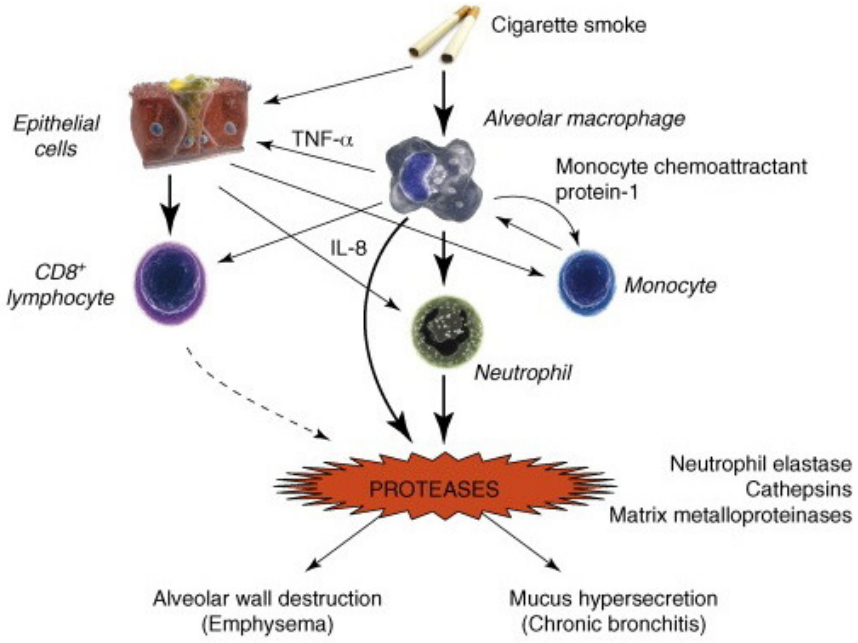

Figure 2.2: *Chronic inflammation in COPD is driven initially by cigarette smoking and other inhaled irritants, which induce a specific pattern of inflammation that predominantly involves the peripheral airways and lung parenchyma [10].*

of Tumor Necrosis Factor (TNF), which has been implicated in several inflammatory conditions. TNF-α also operates at an early stage in the inflammatory cascade and plays an important role in many inflammatory diseases of lungs [11].

2.1.2 TNF-alpha

TNF-α is a multifunctional and potent pleiotropic cytokine and is a modulator of the immune and inflammatory responses; it has been implicated in a variety of autoimmune diseases, including asthma [9]. Among various proinflammatory cytokines involved in the pathogenesis of COPD, tumor necrosis factor (TNF)-α plays a pivotal role in the release of other cytokines and induction of chronic inflammation

[12]. It has been widely accepted that TNF-α correlates with associated symptoms of COPD such as weight loss (25% of patients with COPD will develop cachexia) due to accelerated metabolism and protein turnover [13].
TNF-alpha (TNF-α) exerts a variety of effects, such as growth promotion, growth inhibition, angiogenesis, cytotoxicity, inflammation, and immunomodulation. It was hypothesised that TNF-α could be used as a potential effective target for the treatment of COPD; however, because the multiple effects of this cytokine, it is fundamental to attack specific processes with a selective approach.
Anti-TNF-α and TNF receptor inhibitors (e.g. infliximab, golimumab and etanercept) are considered as potential new medications in asthma and COPD management [14], [15]. However, whereas TNF-α inhibitors are effective in a relatively small subgroup of patients with severe asthma, they have shown to be ineffective in COPD [11], [16]. The failure of the above mentioned inhibitors has been related to the TNF-α polymorphisms associated with clinical features of COPD [17].

2.2 Gene Therapy

In the last two decades the use of nucleic acids as drugs has been claimed to be an important future direction of molecular medicine. Particularly, nanomedicine owns many important applications, one of which is gene delivery, which consists in a powerful approach for the treatment genetic diseases [18] as well as an alternative method to traditional chemotherapy used in treating cancer.

2.2.1 Strategies

Depending on the type of nucleotide molecule that is used, gene therapy can be divided into two possible categories: function enhancement (i.e., by using plasmid DNA (pDNA)) and function inhibition (i.e., by using oligomeric genetic material such as antisense oligonucleotides (ON), siRNA or DNAzyme), respectively, via different mechanisms [19].
In general, a delivery system should help to target the therapeutic nucleic acid to the desired site of action and facilitate efficient intracellular trafficking, typically to the nucleus [20] (once the complexes have reached the target cells they need to be taken up efficiently and then processed in the appropriate fashion to allow efficient transfer from the endosome to the cytoplasm and, finally, the nucleus).
This requires effective traversing of intracellular compartments and the lack of efficiency for these steps probably represents one of the key limitations of synthetic gene delivery systems [21].
The use of a *vector* enables the cellular uptake of the genetic material and protects against intracellular enzymatic degradation, in fact free oligonucleotides and DNA

are rapidly degraded by serum nucleases in the blood when injected intravenously [22]. The attentions of my research are focused on designing effective carrier vectors that compact and protect oligonucleotides for gene therapy.

2.2.2 Nonviral Gene Delivery

Viral carriers have been used as available vehicles for efficient gene transfer into most tissues, because they exhibit high efficiency at delivering both DNA and RNA to numerous cell lines. Nevertheless, there are great problems associated with viral vector systems, starting from toxicity, immunogenicity, and limitations with respect to scale-up procedures [23].
Hence, considering the biosafety, drawbacks of viral approach and also costs, the nonviral vectors for siRNA delivery are increasingly regarded as the best alternatives to viral ones [24].
Nonviral gene therapy or other nucleic acid therapies have been proposed to treat more serious diseases which require systemic administration for the gene to enter the target cells affected by genetic diseases, viral infections or cancer.
Nonviral vectors rely on their ability to bind and to condense genetic material into such a form that it can navigate through various extra- and intracellular barriers to the cell nucleus, where genes can be expressed.

2.3 The Role of siRNA

As an alternative to DNA-involved gene transfer, RNAi mediated by small interfering RNA (siRNA), provides another approach by employing RNA as a powerful tool that can be used to specifically silence gene expression, and for this reason has been recognized as a therapeutic agent for the treatment of a variety of diseases, including viral infections, cancer, and autoimmune disorders [25],[26],[27].
SiRNAs were discovered by showing that the introduction of a long double-stranded RNA (dsRNA) into a variety of hosts could induce post-transcriptional silencing of all homologous host genes and/or transgenes [28], [29].
RNA interference (RNAi) is the mechanism adopted by most eukaryotic cells, where by small double-stranded RNA (dsRNA) molecules control gene expression by potent degradation of its complementary messenger RNA (mRNA) sequence [22].

2.3.1 Gene Silencing Process

In the general RNAi process, long transcripts of double-stranded RNA (dsRNA) are cleaved into short 21-25 nucleotide dsRNA, referred to as siRNA by the help of an endoribonuclease Dicer [24].

The resulting siRNA molecule is then assembled to a multiprotein complex, the RNA-induced silencing complex (RISC) to form RISC-siRNA complex in the cytoplasm. Functional RISC contains four different subunits, including helicase, exonuclease, endonuclease, and homology-searching domains. After activation, when siRNA binds to RISC, the duplex siRNA is unwound by helicase, resulting in two single strands allowing the antisense strand to bind to the targeted RNA molecule (mRNA) [30]. The endonuclease hydrolyzes the target messenger RNA (mRNA) homologous at the site where the antisense strand is bound.
Binding of siRNA strand-incorporated RISC to the target mRNA complementary to a single siRNA strand by base-pairing recognition initiates the cleavage of the mRNA strand within the target site. This leads to translational repression followed by mRNA degradation, consequently knocking down the expression of the corresponding protein and allowing the RISC complex to interact with other molecules from the mRNA pool for a repetitive action of mRNA degradation [22]. The process is known

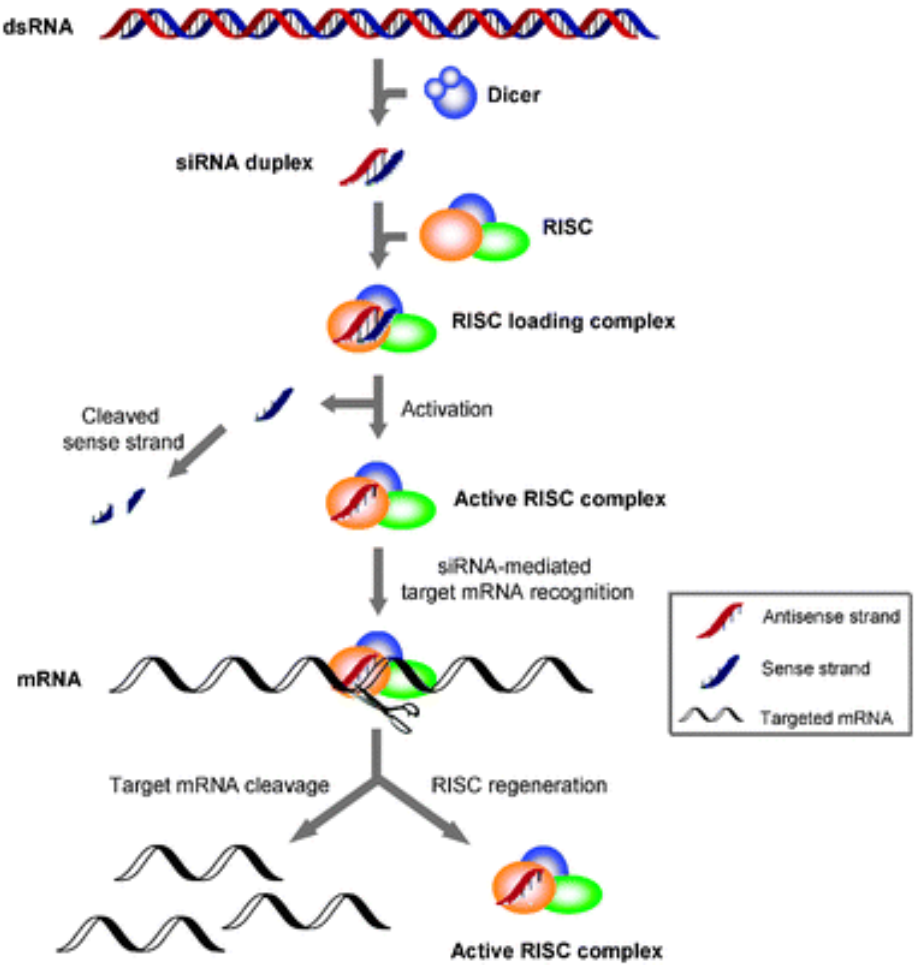

Figure 2.3: *Representation of the mechanism of RNA interference and gene silencing process [31].*

as gene silencing and is highly effective and specific, thanks to the fact that one

nucleotide mismatch between the target mRNA and the siRNA can prevent the recognition and thus the silencing process (Fig. 2.3).

2.3.2 Advantages of siRNA Therapy

The ability to repress translation of any disease-causing protein through gene silencing process makes RNAi a potent strategy to tackle disease progression over conventional therapeutics. Since the discovery of gene silencing by introduction of doublestranded RNA, RNA interference is widely used in functional genomics and drug development [28], [32].
Nevertheless, the successful use of this molecule faces challenges for in vivo delivery [33]. The protection of siRNA from degradation and the promotion of targeted intracellular delivery for effective knockdown of protein synthesis with minimal side-effects are the primary requirement for a good and efficient delivery system.
Compared to other RNA molecules causing gene-specific silencing via the RNAi pathway, as siRNA, shRNA and miRNA, the antisense strand of siRNA is complementary to the mRNA target and has higher target recognition and binding compared to other RNA molecules, in which the complementarity with the target mRNA is partial [34].
Design and synthesis of RNAi molecules complementary to any gene are relatively easy and can be applied using well demonstrated strategies over synthesis of other small molecule [22].

2.3.3 Drawbacks

Since siRNA can target even mRNAs which their translated proteins are located inside cells, it has to be delivered into the cytosol of target cells because of its poor stability in physiological fluids. Thus, the naked siRNA is highly unstable and rapidly degraded by serum nucleases when administered systemically, furthermore it induces an immune response and activates circulating mononuclear phagocytosis as a defense mechanism against viral infection [35].
Moreover, by interfering with other endogenous miRNA pathways siRNA exhibits off-target gene silencing effects, contrasting siRNA sequences against the same gene can generate similar gene silencing signatures. Off-target gene silencing occurs when other mRNA transcripts partially hybridize with the administered siRNA [36].

2.3.4 Targeting and Silencing the TNF-alpha Gene by siRNA

The siRNA therapy is used for treatment of lung inflammation using cationic phosphorous dendrimers as transfection agents. Knocking down gene expression using small interfering RNA (siRNAs) has raised a lot of interest in designing new pathways for therapeutics. A more selective and effective strategy could be represented by silencing of the TNF-α gene by siRNA. Differently from systemic antibodies/inhibitors,

siRNA-targeted delivery through inhalation can potentially contain the effect to specific cells or histological areas such as lung AMs in the case of COPD.

2.4 Nanoparticles for siRNA Delivery

As already mentioned, oligonucleotides cannot cross membranes by passive diffusion and they are characterized by a very inefficient intracellular delivery [37], therefore, despite siRNA's potential strong efficacy, they need to be delivered by nano-systems which need several key requirements [38], [39], [40]:

- protection from degradation in biological fluids
- increase cellular uptake
- favour subcellular distribution

Thus, the success of gene silencing applications based on the use of synthetic siRNA critically depends on efficient intracellular delivery. Compared with viral counterparts and liposomes, nanoparticles-mediated siRNA delivery is a potentially attractive alternative due to low toxicity and immunogenicity by design, and allow for industrial production involving good manufacturing practice [41] and amenability to synthetic modification to incorporate functional elements for targeting and improved delivery, Fig. 2.4. As a result, a significant amount of research in the past decade has focused on designing cationic compounds that can form complexes with DNA or RNA and can avoid both in vitro and in vivo barriers for gene delivery [23].

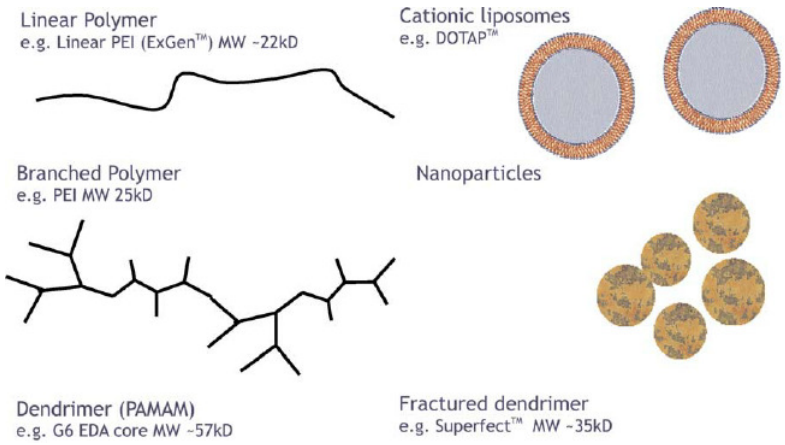

Figure 2.4: *Examples of synthetic vectors. Synthetic gene delivery vectors are based on a number of different, normally cationic materials which support the packaging of the nucleic acid into nanoparticles. The most important classes of materials are cationic polymers and cationic lipids. The lipids are based on self-aggregating small cationic amphiphiles whereas the cationic polymers form complexes through multivalent electrostatic interactions. [20].*

2.4.1 Cationic Polymers as siRNA Delivery Systems

A key for the successful delivery of siRNA or pDNA in cationic assemblies is the formation of highly compacted nanostructures generally termed "complexes" that decrease the hydrophilicity, charge, and size of nucleic acids. The formation of complexes is mediated by electrostatic interactions between the protonated (positively charged) amine groups in the carrier backbone and the negatively charged phosphate groups of the nucleotides [19].
Polycationic branched macromolecules such as dendrimers show a strong binding affinity for RNA molecules and, hence, can provide an effective, reproducible, and relatively non-toxic method for transferring siRNAs into animal cells [42]. These vectors possess cationic nature (e.g., cationic cell penetrating peptides, cationic polymers, dendrimers, and cationic lipids) and complex siRNA by electrostatic interaction [43].
Commonly used classes of synthetic vectors are based on various cationic lipids or polymers and, depending on the synthetic vector material used, the resulting particles have also been termed lipoplex, polyplex, or dendriplex, when dendrimers are being used [20].
In general, cationic polymers are advantageous in gene delivery due to their (i) high stability, (ii) well-defined size and low polydispersity index, and (iii) great variety of molecular weights, architectures (linear, branched, dendrimeric), and functional groups. [19]. The design of binding agents devoted creating high-affinity complexes with nucleic acids is a key point in the development of nanocarriers for gene therapy and, in particular, the study of their multivalent recognition ability of strengthening binding is extremely important to generate systems with potential biomedical applications [44].

2.4.2 Multivalent Ligands

Understanding the factors that influence the interactions between nucleic acids and vectors is an important prerequisite for their controlled manipulation. A key role in this phenomenon is played by the multivalency principle, which implies that the strength of a multivalent binding interaction can be much stronger than the sum of a corresponding number of monovalent interactions [18].
Multivalency is defined as a type of binding in which multiple ligands are attached to a single molecular scaffold and used to interact with another entity that displays multiple binding sites which are complementary to the ligands [45]. For example, the ionic interaction between a protonated amine and the phosphate backbone of DNA forms the basis for most synthetic DNA binding molecules used for gene delivery. However an individual binding unit with one protonated amine cannot efficiently bind to the phosphate backbone of DNA under physiological conditions, and to

achieve high-affinity binding, multivalent ligands must be utilized [45], [46].
While the number of binding sites and sizes of the molecules increase, the binding event also becomes more complex to understand and tune. Polyvalent interactions therefore give rise to special phenomena such as cooperativity and multivalency, and the design of such binding systems requires a detailed understanding of the delicate [47], [48] balance between binding entropy and enthalpy.
The binding of two molecules, both having multiple recognition sites, may occur with an affinity greater than the sum of the corresponding monovalent interactions, a phenomenon that has been defined as the "cluster effect". Multivalent binding between nanoscale objects has recently emerged as one of the most powerful methods for the assembly of functional supramolecular materials with applications in nanotechnology.
Multivalent ligands can function as inhibitors or effectors of biological processes. Potent inhibitory activity can arise from the high functional affinities of multivalent ligand-receptor interactions. Effector functions, however, are influenced not only by apparent affinities but also by alternate factors, including the ability of a ligand to cluster receptors. By altering multivalent ligand architecture, ligands with preferences for different binding mechanisms would be generated. The structural parameters that were varied include scaffold shape, size, valency, and density of binding elements, the architecture of a multivalent ligand is a key parameter in determining its activity as an inhibitor or effector [47].

2.5 Dendrimers

Dendrimers are globular, synthetic and highly branched macromolecules that have repetitive structures [49], [50] with a spherical shape that grows in generation. The

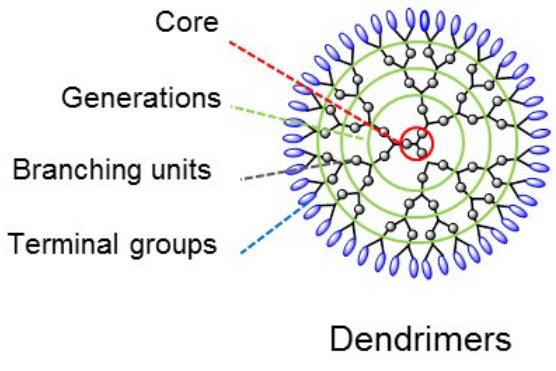

Figure 2.5: *Schematic structure of dendrimers [51].*

name originated from the Greek word *Dendron* meaning tree and *Meros* meaning part, which depicts a structure that consists of a central core molecule that acts as a root,

from which a number of tree-like arms originates in a symmetrical manner (Fig. 2.5).

2.5.1 Structure and Main Properties

The peculiarity of dendrimers compared to other classical macromolecules is due to their defined architecture, in particular three distinct characteristics [24]:

1. a central core to define the interior size, the branch number and direction
2. layers of repetitive units (termed generations G) radically attached to the central core, that also regulate the molecular size and the flexibility;
3. the presence of active terminal groups (and then surface charge) to present the chemical property and the interaction possibility.

The core of a dendrimer is denoted as generation zero, in the Fig. 2.6 is shown how the valency of the core determines the starting number of branching points.
Indeed, their structure grows regularly with the generation dendrimers with high generation numbers having a high density of primary amine groups on the surface which make them efficient for binding nucleic acid molecules. An increase in the generation number affects the shape of a dendrimer. Dendrimers of lower generations have a planar or elliptical shape, whereas dendrimers of higher generations typically have a spherical structure with a hydrophobic interior core, useful for the encapsulation of bioactive molecules [52]. Thus, higher generations present not only a higher electrostatic potential to attract oppositely charged target molecules but also a higher level of backfolding and surface crowding [53].
The possibility to carefully increase the number of "branched layer" (generation) and therefore to finely tune surface properties and the structure flexibility, represents a remarkable feature of this family of nano tools [54]. Reactive end-groups of dendrimers

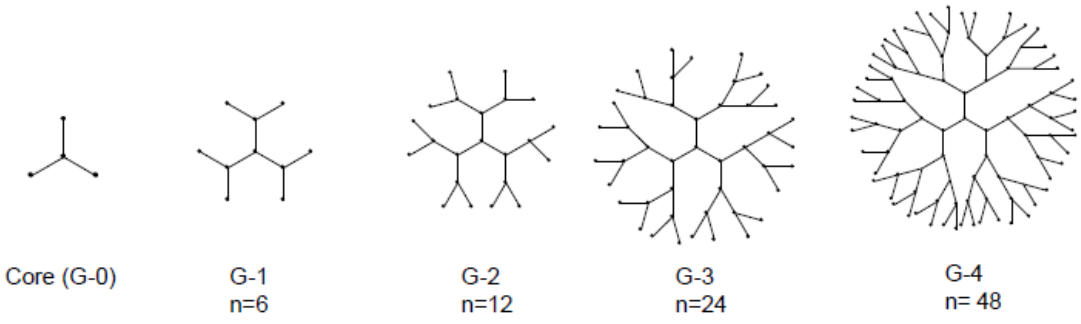

Figure 2.6: *Representation of dendrimers of generations 1 to 4. The n denotes number of terminal functional groups [22].*

allow the addition of repetitive units or branching in a controllable manner and versatility by modification of the end groups for multiple copies of various ligands

including therapeutics and imaging agents for biomedical applications [55].
Moreover the ordered structure is characterized by strong symmetry and periodicity and the surface can be functionalized in many ways to modulate the physicochemical properties of the final construct [56], [57].
Thanks to the high degree of versatility and a very large number of potential applications, dendrimers are emerging as a new class of structure with outstanding features for nanomedicine [58].
Branched macromolecules, dendrimers and dendrons, are not afflicted by problems of polydispersity. Indeed, such molecules can be considered to constitute a unique nanoscale construction kit, with each generation of growth modifying the size of the building block. In addition, dendrons can display a high density of functional surface groups that can offer multiple simultaneous interactions. This leads to enhanced binding - the multivalent effect, which is correlated with the dendritic generation and constitutes an additional advantage of dendritic polymers over their linear analogues [46]. With regards to this, in the last study particular attention has been given to these characteristics of the terminal groups, in connection with the multivalency effect that is the most important property recognized [59], [60].

2.5.2 Dendrimers as Delivery Vectors

Thanks to their multivalent structure and due to the fact that the success of medical treatment with DNA and siRNA is strongly related with the design of efficient delivery technologies, dendrimers offer considerable advantages in binding nucleic acid [61], for this reason in the last decade their structures has been proposed as ideal candidates to deliver and release genetic material inside cells [23], [62], [20], [63].
The low-cost and adjustable controlled release DNA delivery systems have important advantages over other DNA delivery methods, including DNA protection before release, site-specific delivery using implantable polymers, and long-term release without repeat administration [64].
The properties such a high ratio of multivalent surface moieties to molecular volume make dendrimers highly interesting for the development of synthetic (non-viral) vectors for therapeutic nucleic acids [20].

2.5.3 Dendrimers as siRNA Delivery Vectors

Among versatile non-viral vectors, dendrimer-based siRNA carriers have been gradually explored since their performance in DNA delivery was approved (Fig. 2.7). There are basically three means to optimize the dendrimer structure for lowering the cytotoxicity as well as improving the delivering efficiency [24]:

1. synthesis of new dendritic structure or the use of new core unit for dendrimer preparation;

2. functionalization of the interior or exterior part of dendrimer molecules;

3. employing other biocompatible/bioactive molecules to form effective complexes with dendrimers.

In particular, polycationic dendrimers represent a promising strategy for delivering siRNA in lung [18].
The positively charged primary amine groups on the surface of these dendrimers allows electrostatic interaction with negatively charged siRNA molecules [22].
However, in order to design an ad hoc dendrimer-based system suitable for inhalational purposes and be able to guarantee high TNF-alfa silencing, an accurate evaluation of the physicochemical and molecular properties of the different dendrimers is necessary.
After lung administration, nanoparticles (NPs) should be internalized by alveolar macrophages (AMs). To further increase the cellular pool of NPs their surface may be functionalized by dendrimers to specifically bind the C-type lectin receptor on AMs membrane and reduce side effects [65], [66], [67].

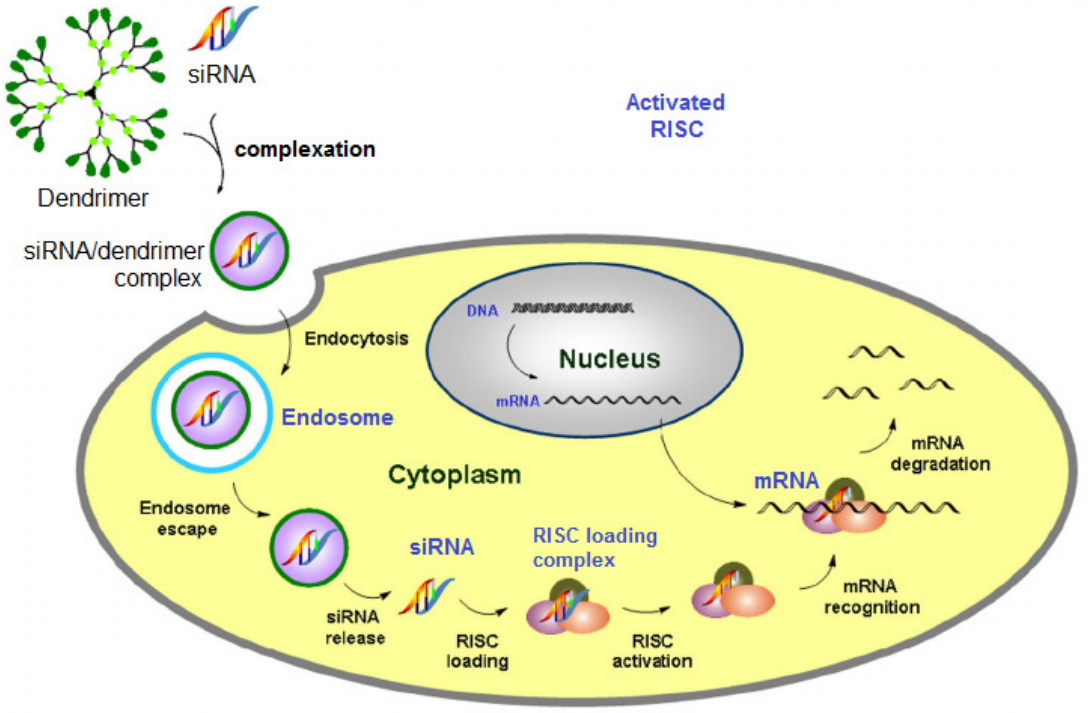

Figure 2.7: *The proposed mechanism of dendrimer mediated siRNA delivery and gene silencing. [New J. Chem. 2012; 36:256-63] - adapted by [31].*

2.5.4 Surface Modification for Improved Efficacy with siRNA

Surface functionalization of nanocarriers with a wide variety of polymers and targeting ligands is a promising approach to achieve specific functions [68].

As said previously, the multivalent recognition of DNA and siRNA by dendrimers is strictly related to their structural flexibility, in terms of the ability to orient and use their surface charges in a cooperative way [69], accordingly the descriptor of "flexible" behaviour is refered to local structure and do not necessarily communicate global structure of dendrimers.
Thus the multivalent polycationic surface is able to generate multiple strong ionic interactions with the charged phosphate groups of nucleic acids [69] and this is the reason of such high affinity toward DNA and siRNA. Furthermore, the structural modifications of dendritic generations due to binding with nucleic acids indicate the ability to adapt to a charged target.
Comparing different generations of dendrimer their number of charged surface groups grows exponentially with higher generation, so that the global attraction with nucleic acids grows too. Moreover, the study of the multivalent behaviour of these molecules takes into account that not all of these charged groups are actively participating in the binding, this because the multivalent binding action of multiple surface groups cannot be explained as a simple attraction (it is a balance between the amount of charge and ability to use these charges efficiently) but it is related to the molecular flexibility. There is a limit in the advantage that is possible to obtain simply by adding charged groups to the structure. This depends on the surface density and makes the difference in treating dendrimers as flexible molecules rather than as rigid spheres [42].
To utilize dendrimers for energetically favorable binding interactions, they should be designed in such a way that the number of binding interactions is maximized while internal strain in the bound molecules is minimized [70].

Chapter 3

Materials And Methods

The aim of this Chapter is to explore a connection between simulation and statistical mechanics and describe the theory underlying the present master thesis work, in order to provide an explanation of the physical background behind computational methods. After a presentation of computational molecular modelling, a description of Molecular Mechanics and Molecular Dynamics approaches is provided. In the last section an overview is given which covers enhanced sampling methods.

3.1 Computational Molecular Modeling

Modeling the behaviour of physical systems with mathematical equations has been one of the main aims of scientists, since the beginning of modern science. A model is a powerful tool, which allows to predict with a certain degree of confidence the results of an experiment or the consequences of an event without having to materially reproduce such experiment/event.
Computational molecular modeling is an excellent tool which scientists use to visualize molecules. The tool represents molecular structures numerically, and simulates the atomic and molecular interactions that govern microscopic and macroscopic behaviours of physical systems with the equations of quantum and classical physics; it includes all theoretical methods and computational techniques used to describe complex biophysical systems in terms of a realistic atomistic description, aimed at understanding and predicting their macroscopic properties.
These properties are not found analytically because of the large number of molecules that generally constitute molecular systems, the problem being solved through numerical methods, which thanks to their low-scale level of description are able to discover the features of the case study and to create a point connection between laboratory experiments and theory.
The most accurate techniques can be considered the quantum mechanics/molecular mechanics methods (QM/MM), whose aim is to solve the wavefunction of a system

using the Born-Oppenheimer approximation. This approximation breaks the wave-function into two separated terms, namely an electronic one and a nucleic one [71]. QM/MM methods can describe the evolution of a molecular system in a very accurate way, however, because of their similar accuracy, such methods are inadequate to simulate systems which are larger than about hundred atoms, hence not very useful for characterizing biological complexes.
At an upper level (spatial scale of nanometer and time scale of nanosecond), Molecular Dynamics and Montecarlo simulations are powerful tools of investigation: indeed, these two methods are the ones that are most used in biomolecular modeling, because they are the ones that best cover the temporal and spatial scales that are involved in processes of particular interest, for example, protein folding [72].
In particular, Molecular Dynamics (MD), solving Newton's second law represents a powerful multidisciplinary method at the nanoscale level based on physics, chemistry, statistical and molecular mechanics and it is applied in fields such as material science, computational chemistry, drug design and computational biology to understand the structure and the dynamics of proteins, protein folding and unfolding, multi-scale modelling, molecular docking and receptor-ligand interaction, transport and diffusion properties of molecules.

3.2 Molecular Mechanics

Differently from quantum mechanical methods, which is based on Schrödinger equation and deals with the electronic motions in the system and examines structures as a function of electron distribution, the Molecular Mechanics (MM) method uses Newtonian mechanics to model molecular systems, analysing the system as a set of atoms interacting through a potential energy function.
The most important theoretical bases of MM are founded on the important results produced by analytical mechanics. The core of the MM approach is the set of the equations and parameters used to describe the potential energy function V of a molecular system, also known as force field.
Several force-fields are available for molecular simulations. The choice of the force-field strongly depends on the system which has to be simulated and also on the simulated conditions (e.g., explicit/implicit water, ions, etc.). Among the most commonly used potential energy functions are the AMBER, CHARMM, GROMOS and OPLS/AMBER force fields.

3.2.1 Potential Energy Function

Atom interactions are taken into account in terms of potential energies, from which information about the forces is extracted. Potential energy is a multidimensional

function which depends on the spatial coordinates r_i of all the N atoms that constitute the system. It is the sum of two different contributions, which are a function of the coordinates r_i of all the N atoms in the system:

$$E(r^N) = E_B(r^N) + E_{NB}(r^N) \tag{3.1}$$

where E_B is the sum of all the functional expressions describing the bond interactions among the atoms in the system and E_{NB} is the sum of the functional expressions describing the nonbond interactions in terms of Van der Waals and electrostatic contributions. The two terms in equation (1) can be expressed as:

$$E_B(r^N) = E_{bonds}(r^N) + E_{angles}(r^N) + E_{dihedrals}(r^N) \tag{3.2}$$

$$E_{NB}(r^N) = E_{Coulomb}(r^N) + E_{VdW}(r^N) \tag{3.3}$$

The potential energy function can be described as:

$$\begin{aligned} V(r^N) = {} & \frac{1}{2}k_{ij}[r_{ij} - r_{0,ij}]^2 + \frac{1}{2}\xi_{ijk}(\cos(\theta_{ijk}) - \cos(\theta_{0ijk}))^2 \\ & + \phi_{ijkl}\left(1 + \cos\left(n\phi_{ijkl} - \phi_{0ijkl}\right)\right) + 4\epsilon_{ij}\left[\left(\frac{\sigma_{ij}}{r_{ij}}\right)^{12} - \left(\frac{\sigma_{ij}}{r_{ij}}\right)^{6}\right] + \frac{q_i q_j}{4\pi\epsilon_0\epsilon_r r_0} \end{aligned} \tag{3.4}$$

where the first three terms in the sum represent the bond interactions, while the last two represent the non-bond interactions.

3.2.2 Treatment of bond and non-bond interactions

In equation 4 there are several terms that can be distinguished in bond and non-bond interactions. In particular, the mathematical term that describes the interaction due to the covalent bond is:

$$E_{bond} = \frac{1}{2}k_{ij}[r_{ij} - r_{0,ij}]^2 \tag{3.5}$$

The variable is r_{ij} and the other two parameters (k_{ij}, $r_{0,ij}$) that appear in the equation have a well-defined physical meaning. k_{ij} represents the bond stiffness, while $r_{0,ij}$ is the equilibrium distance, and depends on the atom types that are bonded. This association of atomic bond interactions with an equation that resembles a simple elastic spring was discovered to be a very good (as well as computationally cheap) approximation.

The angle bond contribution includes all interactions among the three atoms (represented by indices i, j and k), that are covalently bound together. The potential energy is expressed as a function of the angle θ_{ijk}, formed by the three atoms, the equilibrium angle, $\theta_{0,ijk}$, and the stiffness, ξ_{ijk}, of the bond angle:

$$E_{angle} = \frac{1}{2}\xi_{ijk}(\cos(\theta_{ijk} - \cos(\theta_{0ijk}))^2 \tag{3.6}$$

The dihedral bond interactions, that are usually called proper dihedral interactions, involve four atoms (i, j, k, and l), that are covalently bound one after the other one.

$$E_{dihedral} = \phi_{ijkl}[1 + \cos(n\phi_{ijkl} - \phi_{0ijkl})] \tag{3.7}$$

The potential energy is described as a function whose variables are the stiffness of the dihedral angle, ξ_{ijlk}, the dihedral angle ϕ_{ijkl} between vectors that are normal to the planes that are identified by the atoms i, j, and l, and atoms j, k and l respectively, and the equilibrium dihedral angle, named $\phi_{0,ijkl}$.
The last two terms of Eq. 4 belong to the group of non-bonded interactions. There are a number of non-bonded interactions that act in nature. However but just the two main ones are usually included into the force fields, and they are the Van der Waals and Coulomb energies.
The Coulomb energy, E_{Coul}, takes into account the electrostatic interactions between charged particles, while the Lennard-Jones energy, E_{LJ}, accounts for a combination of excluded volume effects and Van der Waals interactions. Coulomb interactions are active between any two charged particles (also just partially charged), i and j in the equation. The strength of the interaction depends on the quantity of the charges, q_i and q_j, as well as the relative distance r_{ij} among them.

$$E_{Coul} = \frac{q_i q_j}{4\pi\epsilon_0\epsilon_r r_0} \tag{3.8}$$

The energy depends on the distance between the particles r_{ij}, which implies that the Coulomb interaction is a long-range one.
Alternatively, the Lennard-Jones energy describes two kinds of forces that work combined on two different distance-ranges:

$$E_{LJ} = 4\epsilon_{ij}[(\frac{\sigma_{ij}}{r_{ij}})^{12} - (\frac{\sigma_{ij}}{r_{ij}})^{6}] \tag{3.9}$$

The first term represents the very short-range repulsion due to overlapping by electron orbitals. The second one describes the long-distance Van der Waals attraction energy. The two fixed parameters, σ_{ij} and ϵ_{ij}, depend on the atom types and specifically indicate, respectively, the shortest distance for which the Lennard-Jones energy is zero and the depth of the potential well. The calculation of non bond-forces is extremely complicated in terms of computational effort, because the number of the non-bond interactions increases as the square of the number of atoms in the system. To properly reduce the computational effort, the non-bond interactions are computed by applying the distance cutoff. With the application of the cutoff distance, every interaction between two atoms is computed only if their distance is smaller than the cutoff chosen. In Fig. 3.1 the summary of interaction terms in a typical biomolecular Force Field is reported, as described in the paragraph.

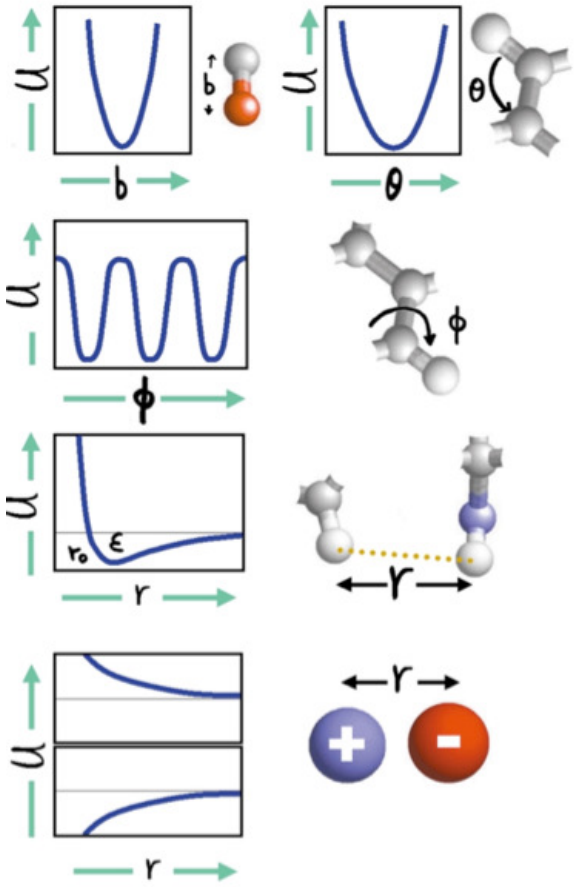

Figure 3.1: *Summary of interaction terms in a typical biomolecular Force Field [73].*

3.2.3 Periodic Boundary Conditions

In the computational models often used are the Periodic Boundary Conditions (PBC), in order to circumvent the natural finite size of the simulation box, the edge effects. All the atoms are put in a space-filling box, usually filled with water (implicitly or explicitly modelled), surrounded by translated copies of itself as shown in Fig. 3.2, with the aim of removing boundaries of the system. Thus, when a dynamic step pushes a particle out through one side of the simulation box, with PBC the particle is re-positioned on the opposite side. Moreover, in order to avoid self-interactions with periodic copies, the simulation box and the interaction cutoff distance has to be comparable. The inaccuracies resulting from the presence of PBC are expected to be less severe than the errors resulting from an artificial boundary with vacuum. In the minimum image convention, which states that with periodic boundary conditions cut-off distance should be small enough to avoid a particle seeing itself in the adjacent box, each individual particle in the simulation interacts with the closest image of the remaining particles in the system, which is repeated infinitely if PBC are settled

on. Applying a cutoff distance is not a problem for short range interactions as the Lennard-Jones potential which decreases very rapidly, but the long-range interaction model requires the use of more accurate methods (e.g., shift function, and switch functions) with the aim of avoiding discontinuities in the potential energy calculation.

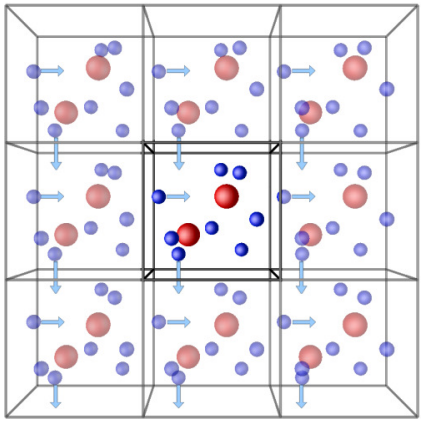

Figure 3.2: *This figure represents the periodic boundary conditions. The central box, with the molecules of interest in red and the water in blue, is replicated in copies of itself.*

3.2.4 Potential Energy Minimization

The Potential Energy function is a complex multidimensional function of molecular system coordinates. Minimum points of the Potential Energy Surface (PES) correspond to local stable states of the system. Any movement away from this configuration, is characterized by higher energy. The minimum with the lowest energy is known as global minimum. The process of energy minimization is able to reduce the potential energy of the system. To identify the minimum point of the PES there are two different approaches to the minimization problem: derivative methods and non-derivative methods.
Energy minimization is widely present in a molecular dynamics simulation, especially for simulation of complex system, such as macromolecules.

3.3 Molecular Dynamics

Molecular Dynamics (MD) is a technique that solves the Newton's equations of motion for a system constituted by interacting atoms. The main principle consists of establishing the temporal evolution of the atomic positions. For this, the system is modeled as a mass set of atoms or molecules. This is a deterministic method, which means that the future state of the system is completely determined by its present state.

Employing Newton's equation implies the use of classical mechanics to describe the motion of the atoms:

$$m_i \frac{d^2 r_i}{dt^2} = F_i \tag{3.10}$$

with i = 1, 2,..., N. The force F_i is the vectorial sum of all the forces that act on the ith particle of the system: these forces are all derived from a function $V(r^N)$ that includes and describes how all the particles interact each other. This function is the called potential energy function, and it is related to the force F_i of the previous equation through

$$V(r^N) = -\nabla F_i \tag{3.11}$$

The equations of motion are solved by integrating the above equations using small time steps, whose order of magnitude is usually between 1 and 10 fs.
This means that during the simulation, at every time step, the position and the velocity of every single atom in the system are calculated. At each step, the initial positions and velocities of all the atoms in the molecular system need to be known and these are the input data. The forces alternatively are calculated through the potential energy. While the positions are usually accessible from the crystallographic structures that are present in some apposite databases (like for example PDB Data Bank), the velocities are almost never known, so they need to be assigned, at least for the first iteration. This can be done using a Maxwell-Boltzmann distribution at a specific temperature, for example 300 K, that is the temperature that is normally used for biological systems.
As indicated, the initial configuration of the molecular system usually comes from experimental data, especially crystallographic structures. These experimental techniques usually bring to data that represent systems is very far from the equilibrium. Thus an energy minimization is required to be performed before running MD simulations. From a practical point of view, what is done is to reduce interaction forces among atoms that are excessively large, i.e. to relax the system.
The MD approach uses conservative force-fields as "constitutive laws" for the simulated systems which are function of the atomic positions only. This implies that the electronic motions are not considered. However electrons are supposed to adjust their dynamics instantly following the atomic position, as the Born-Oppenheimer approximation demands. A force-field is a set of parameters which specifies the functional expressions describing interactions among atoms. The force-field parameters take into account all the static properties of the system, e.g. covalent bond constants, whereas the atom positions or velocities describe the dynamics of the system. In particular, the force-field parameters represent the constants of the functional expressions describing all bond and non-bond interactions among atoms.
Several force-fields are available for molecular simulations: the choice of the force-field strongly depends on the system which has to be simulated and also on the

simulated conditions (e.g., explicit/implicit water, ions, etc.).

3.4 Statistical Ensembles

There is a strong connection between computer simulations of biochemical systems and Statistical Mechanics. Simulations give microscopical properties (e.g. atomic positions and velocities), and the equivalent of experimental measurements are represented by statistical averages over microscopical configurations.
To compute the macroscopic properties it is necessary to generate a representative statistical ensemble, which defines all the accessible physical states of a molecular system.
The identification of the appropriate *statistical ensemble* and the issue of *ergodicity* are the main points in the computer simulations. In particular, the physical characteristics of a system are translated in weighting prescriptions for the points (q, p) of the *phase space* $D \times \mathbb{R}^{3N}$ of N-particles system

$$\left.\begin{array}{l} r \equiv (r_1, ..., r_N) \in D \subset \mathbb{R}^{3N} \\ p \equiv (p_1, ..., p_N) \in \mathbb{R}^{3N} \end{array}\right\} \Rightarrow (r, p) \in D \times \mathbb{R}^{3N} \tag{3.12}$$

Within a statistical ensemble, given an observable $A(r, p)$, the calculation of the mean value $\langle A \rangle$ is expressed as the statistical average

$$\langle A(r, p) \rangle = \int D \times \mathbb{R}^{3N} A(r, p) \mu(drdp) \tag{3.13}$$

where $\mu(drdp) = \rho(r, p)drdp$ is a probability measure and $\rho(r, p)$ indicates the probability density.
The points (r, p) represent the accessible *microstates* for the system, thus $\mu(drdp)$ represents relevant thermodynamic *macrostates* that the system could exhibit.
The practical computation of ensemble averages requires one to sample a set of configurations $(r^n, p^n)_{n=1,...,M}$ from the probability measure $\mu(drdp)$ ("trajectory" in the *phase space*). After sampling, the approximation

$$\langle A(r, p) \rangle_\mu \simeq \frac{1}{M} \sum_{n=1}^{M} A(r^n, p^n) \tag{3.14}$$

estimates the mean value of a given observable A.
Following the identification of the correct thermodynamic ensemble, the simulation is able to perform the requested sampling. The actual interpretation for times Δt between sampled points and for the total duration of the sampling $\tau = M\Delta t$ depends upon the specific simulation choices, and the M number of sampled points. This is connected to the *ergodicity*. In fact the ergodicity condition is fulfilled when almost all

the phase space is sampled, within the interval τ. Consequently, with a *time* average approximation the Eq. 14 becomes

$$\langle A(t)\rangle_\tau = \frac{1}{\tau}\int_0^\tau A(r(t), p(t))dt \tag{3.15}$$

as if we are following the solution $(r(t), p(t))$ of some kind of equations of motion in phase space. The ergodic hypothesis assumes that the time averages of Eq. (2.5) on very long trajectories and the ensemble averages of Eq. (2.2) converges (at least in the thermodynamic limit). To make use of this hypothesis, the interval τ has then to be sufficiently long to ensure that almost all the phase space is explored.
The equilibrium is defined by an *ensemble* of states, and while the low-energy states are more probable that high-energy ones, the latter will also appear in the ensemble due to thermal fluctuations, with a probability given by the Maxwell-Boltzmann distribution. At equilibrium, the instantaneous temperature of the system evolved around the target temperature T. Most natural phenomena exhibit a wide range of characteristic time scales.
In a MD simulation the integration time-step has to be commensurate with the fastest internal dynamics (typically $\triangle$t $\sim$ 1 fs). This sets a limit to the available total simulated time and, consequently, to the ability of a simulation to reproduce some classes of events. There are, indeed, phenomena that happen at time scales several order of magnitude larger than the integration time scale.
Similarly, systems which are characterized by rare events or systems that exhibits metastabilities (in which thermodynamical wells are separated by very high, non-thermal free energy barriers) highly suffer for the time scale separation. Systems which exhibit the above features are non-ergodic in practice from the simulation point of view.

3.4.1 Implementation scheme

In Fig. 3.3 is presented the MD implementation scheme, where the initial positions and velocities are provided as input data. Starting from the atomic positions r_i, the potential energy V is calculated and models the interaction between atoms; the scheme continues with the calculation of the forces F_i acting on each atom, by deriving the potential energy function. Where upon the integration of the equation of motion leads to the calculation of new position r_i and velocities v_i.
The cycle goes on for a number of steps until the equilibrium and the convergence of the computed equilibrium property are reached. Finally, using the output trajectory of the MD, the macroscopic thermodynamic properties (e.g., temperature, energy, pressure) can be calculated as time averages.

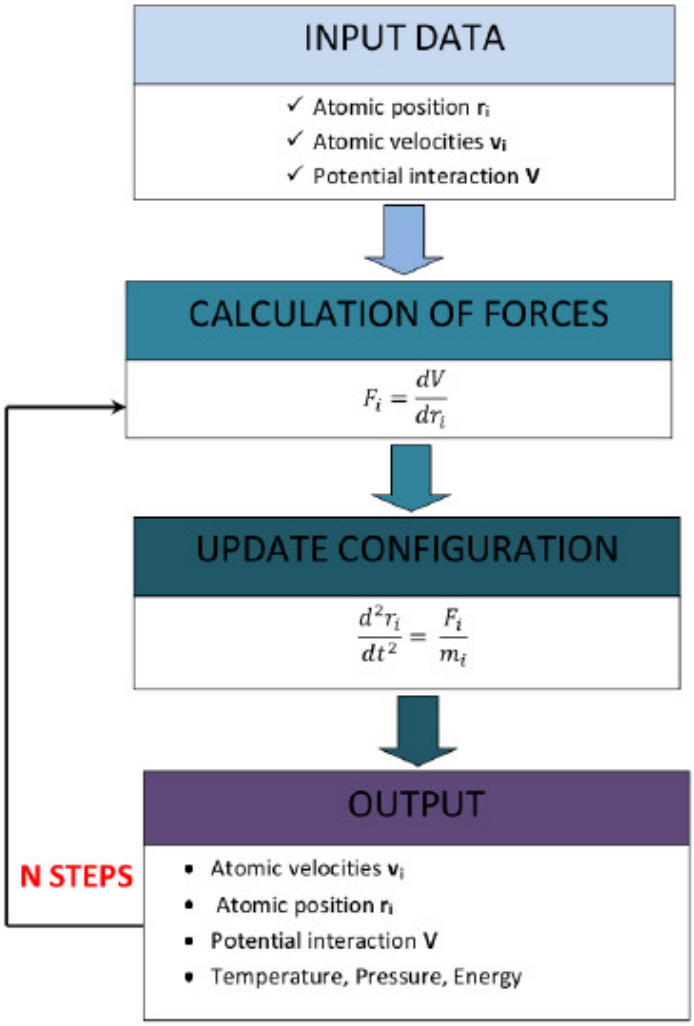

Figure 3.3: *Implementation scheme of Molecular Dynamics, in which the initial positions and velocities are provided as input data.*

3.5 Enhanced Sampling Methods

When the thermodynamic equilibrium properties are based on free energies (e.g. binding constant, solubility, relative stability of molecular conformation, etc.), classical MD is not sufficient and is limited by two important causes:

- high computational costs, due to the large number of interacting atoms, which can reach the number of hundreds of thousands or even millions, leading to an incorrect estimation of the macroscopic thermodynamic property under investigation;
- rough energy landscapes, with many local minima frequently separated by high-energy barriers, causing the system being trapped in a relative free en-

ergy minimum, impeding thermal fluctuations which might never be able to overcome the energy barriers.

To solve the problem, a vast variety of methods has been developed. Some aim to reduce the number of degrees of freedom of the problem, some others to enhance the sampling resorting to non-Boltzmann probability weight factor simulations. A solution is constituted by the coupling of classical MD with more complicated sampling techniques, e.g. replica exchange MD, metadynamics, umbrella sampling which allow the system conformation to escape from energy wells.

3.6 Metadynamics

Metadynamics is a non-equilibrium molecular dynamics method which accelerates the sampling of the multidimensional free energy surfaces by adding an external bias potential as a function of the collective variables [74]. The bias potential discourages the system from revisiting previous sampled region and allows one to surmount energy barriers. Consider a N-particles system, interacting with the potential V(r), and

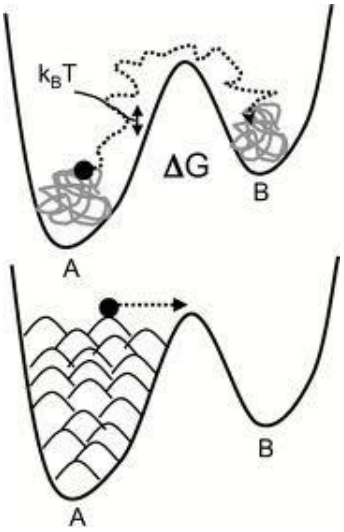

Figure 3.4: *View of metastable systems. The barrier crossing is a stochastic event because the order of magnitude of the free energy barrier is much higher than the thermal energy k_BT. The wells indicated as A and B are then metastable states.*

evolving under the action of a dynamics having a canonical equilibrium distribution at a temperature T. For system wherein the dynamics is stuck in some local minimum of $V(r)$, the escape probability is very low (Fig. 3.4). The idea of metadynamics is to add a history-dependent potential to bias the system not to return to previously visited points in the configurational space [75]. In basic implementations of metadynamics

at time t the bias potential is:

$$V_G(S,t) = \int_0^t dt' w exp(-\sum_{i=1}^{d} \frac{(S_i(R) - S_i(R(t')))^2}{2\sigma_i^2}) \tag{3.16}$$

where S is a set of d functions of the microscopic coordinates R of the system; ω is an energy rate and σ_i is the width of the Gaussian. The energy rate (w) is constant and usually expressed in terms of a Gaussian height W and a deposition length τ_G ($\omega = W/\tau_G$). Metadynamics shows the advantage of accelerating the sampling of rare events by pushing the system away from local free-energy minima and exploring new reaction pathways as the system tends to escape the minima passing through the lowest free-energy saddle point. Furthermore the bias potential VG provides an unbiased estimate of the underlying free:

$$V_G(S, t \longrightarrow \infty) = -F(S) + C \tag{3.17}$$

in which C is an additive constant and the free energy $F(S)$ is defined as

$$F(S) = -\frac{1}{\beta} ln(\int dR \delta(S - S(R)) exp^{-\beta U(R)}) \tag{3.18}$$

with $\beta = \frac{1}{k_B T}$ and $U(R)$ is the potential energy function.

3.6.1 The choice of Collective Variables (CV)

The relevant dynamics of the system will be encoded in a suitable formed reaction coordinate, called $\xi(r)$. Equivalently, the CV retains all the information about the relevant changes in the system (the slow or rare event) without taking into account all the microscopic details of the dynamics of the system. To this extent, an appropriate definition for a CV set should satisfy two properties: a) to clearly distinguish between different states of the system and b) to describe all the slow degrees of freedom related to the process of interest. In particular, if the wrong reaction coordinate is chosen, or if an important collective variable is neglected, then a strong bias in the reconstruction is introduced. Thus, the biased dynamics could be affected by hysteresis effects leading to a wrong evaluation of the free energy landscape. A possible check to evaluate the quality of a chosen CV is to investigate whether the metadynamics along that coordinate is able to sample ergodically the reduced space. Given these indications, every possible function $\xi(r)$ of the spatial coordinates is eligible to be a reaction coordinate. For example, geometry related variables (distances, angles, dihedrals, gyration radius, ...) or interaction variables (potential energy, coordination number, hydrogen bonds, ...) could be addressed for metadynamics. An operative scheme for a simulation may be the following:

1. run a standard MD simulation to monitor the evolution of the selected reaction coordinate $\xi(r)$. This is useful to establish the characteristic size of the variation

of the variables in unbiased condition, that is the size of the smallest feature of interest in the free energy landscape;

2. guess the parameter (σ, τ_G, ω) for the algorithm to work;

3. start metadynamics and during the run, collect the deposited Gaussians for further free energy estimate;

4. monitor the explored positions in order to evaluate the diffusivity in the CV space and stop the reconstruction at time t'.

During the run, the bias potential will in time fill all the minima of the free energy landscape. The bias itself (the sum of all deposited Gaussians) will be the estimate of the free energy for a sufficient long simulation time. After this simulation time, the dynamics of the reaction coordinates will be nearly diffusive or, equivalently, the probability density of the biased system becomes nearly uniform. The slow deposition argument does not give a real proof of convergence of the bias potential to the free energy density function. However, it is clear that the filling process is able at least to give an estimation that oscillates around the real free energy function F(z). An estimate of the error of metadynamics is possible by means of averaging processes that benefit from this oscillation around the real value.
Two principal drawbacks are present in metadynamics technique: firstly, the free energy estimation does not converge to a definite value but fluctuates around the correct result and this creates a large difficult to understand when the simulation has to stop, secondly the problem is that the selection of CVs has an high impact on the correct estimation of the free energy.

3.6.2 Umbrella Sampling

A fundamental thermodynamic equation that describes the free energy for the formation of a biological complex (i.e. protein-ligand) relates free energy to changes in enthalpy and entropy:

$$\Delta G = \Delta H - T\Delta S \tag{3.19}$$

where ΔG is the difference in Gibbs free energy of the binding reaction, and represent changes in enthalpy and entropy, respectively, and T is the temperature of the system. It is useful to know how the free energy changes as a function of reaction coordinates. Here it is useful to introduce the concept of the potential of mean force (PMF) [76], that for a system with N atoms describes an average force over all the configurations of all the $n+1...N$ atoms acting on a atoms j at any fixed configuration.

Weighted Histogram Analysis Method (WHAM)

A common technique used to calculate the Potential of Mean Force (PMF) along a given reaction coordinate is Umbrella Sampling (US) (Fig. 3.5). PMF is a type of experiment done in molecular dynamic simulations which computes how a system's energy changes as a function of some specific reaction coordinate parameters. The umbrella sampling is designed to overcome limited sampling at energetically unfavorable configurations by restraining the simulation system with an additional, usually harmonic, potential:

$$w_i(\xi) = \frac{1}{2}K_i(\xi - xi_i)^2 \tag{3.20}$$

Then, a series of separate umbrella simulations are conducted with this potential; these simulations restrain the system at position $\xi_i (i = 1, ..., N_w)$ with a force constant K_i. Umbrella histograms $h_i(\xi)$ are recorded from each N_w umbrella simulation, and are called *umbrella windows*; they represent the probability distributions $P_i(\xi)$ along the reaction coordinate biased by the umbrella potential. The most commonly used method to unbiased the distribution $P_i(\xi)$ and compute the PMF from histograms is the weighted histogram analysis method (WHAM) [77]. Since the free energy is the change in PMF of a system along the reaction coordinate, WHAM estimates the statistical uncertainty of the unbiased probability distribution given the umbrella histogram followed by calculating the PMF with the smallest uncertainty.

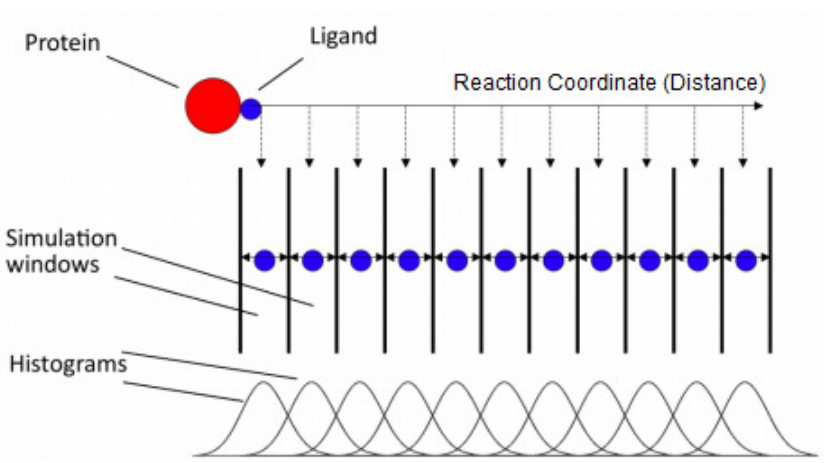

Figure 3.5: *Schematic representation of Umbrella Sampling method, for an example of protein-ligand interaction: protein (red circle) and ligand (blue circle). Along the reaction coordinate (protein-ligand distance) independent simulations are run with additional harmonic potential where ligand is restrained by its centre of mass. Each window provides with the probability of finding (histogram) according to the harmonic potential. Overlapping windows provide the input to weighted distribution analysis method which provides the Potential of Mean Force (PMF) (the free energy along the distance) of protein-ligand interactions [78].*

Chapter 4

Investigation Of Dendrimers By Molecular Dynamics

This chapter describes a Molecular Dynamics study to evaluate the behaviour of different generations of three dendrimers, with same core and branches structure but different terminal groups. In particular, the role of pyrolidinium, piperazinium and morpholidinium as terminal group will be investigate in order to understand the variations in physicochemical properties of dendrimer surface.

4.1 Introduction

The development of different dendrimers has biological and biomedical applications and is a promising alternative to synthetic polymers frequently used in drug delivery, as demonstrated by several theoretical and mathematical modelling. In fact, with advantages as low cost, ease of production, well-defined size and a good complexation with siRNA, dendrimers represent an attractive strategy to serve as drug carriers. Dendrimers show high versatility for application in the treatment of different diseases. Generally, the properties of therapeutics-loaded dendrimers directly depend on physicochemical, molecular and supramolecular characteristics. Moreover, a central point of all multivalent ligands is the important for biomedical applications of their multiple copies of binding units organized on a single scaffold [79].
Several recent studies have explored the poly(amidoamine) PAMAM dendrimers performance and the influence of structure of dendrimers on their properties [80], [81], [82], [83] and also five critical nanoscale design parameters were proposed by Tomalia (size, shape, surface chemistry, flexibility and architecture) [84].
In detail, glycodendrimers (such as mannose-functionalized dendrimers) have been described as promising tools due to the high biocompatibility degree [85]. An interesting property compared to other NPs is the potentiality to be customized in order to obtain either proinflammatory properties [86], or anti-inflammatory

features (e.g. mannose dendrimers) [87], [88], and thus for example preventing lung inflammation [65]. The structure of dendrimers in solution has been shown to be independent of concentration, unlike the linear polymer analogues [89].
In connection with siRNA delivery, fourth generation cationic phosphorus-containing dendrimers have been demonstrated to be good candidates for drug and gene delivery carriers after experiments in vivo [66] and they have shown to be effective in silencing TNF-α. Particularly, here the analysis will be focused on the role of pyrolidinium, piperazinium and morpholidinium as terminal group of the dendrimers, will be evaluated in order to understand which are the physicochemical and mechanical properties which may drive the experimentally identified effectiveness of specific dendrimer functionalization strategies.
In fact, dendrimer functionalizations strongly affect the topology and the physico-chemical properties of them, driving the interaction with therapeutic agents and the environment. Accordingly, conformational organization and assembly among components of dendrimers are still under investigation.

4.2 Materials and Methods

Three models of functionalized dendrimers have been developed in relation to atomistic coordinates and force-field parameters, using classical General Amber Force Field (GAFF).
The structures and properties of different dendrimers has been investigate using a computational approach based on classical Molecular Dynamics (MD), in terms of study of different conformational characteristics (i.e. core, generation and terminal groups) and physico-chemical characterization.

4.2.1 Model Development of Functionalized Dendrimers

The 3D models of three different dendrimers were developed starting from the stoichiometry and the knowledge about the physical and chemical properties of related atoms and bonds. All dendrimers are composed by a series of residues, starting from the first generation to four: a central core, a repetitive branch unit and a terminal surface group; with the growth of generation, a repetitive branch unit is added, as shown in Fig. 4.1.
The characteristic that differentiates the three functionalized dendrimers is the presence of specific terminal groups, which determines dendrimer properties among with surface charge, hydrophilic and hydrophobic area, ability of binding.
In particular, dendrimer terminal are constituted of **pyrolidinium** (in 16/CEF/051 dendrimer, here labeled **DP**); **morpholinium** (in 16/CEF/294 dendrimer, here labeled **DM**) and **piperidinium** (in mk016 dendrimer, here labeled **DG**).

The schemes of Fig. 4.2 show distinct structures for all the terminal groups, however all present positively charged nitrogen, an important factor that causes a not neutral total charge for the dendrimers.

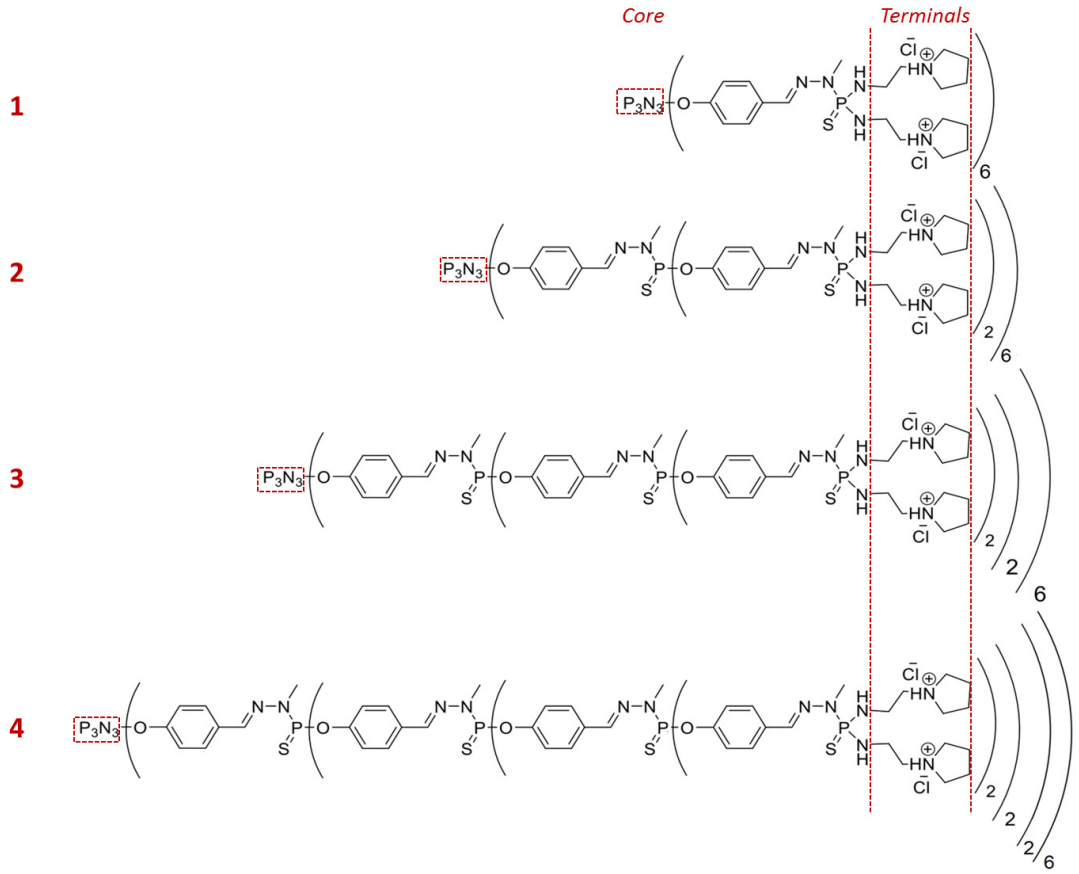

Figure 4.1: *Example of dendrimers considered for the proposed research, in figure are represented only dendrimers with pyrolidinium as the terminal group (16/CEF/051), also are shown different generations from one to four (corresponding to 1-4 of the scheme).*

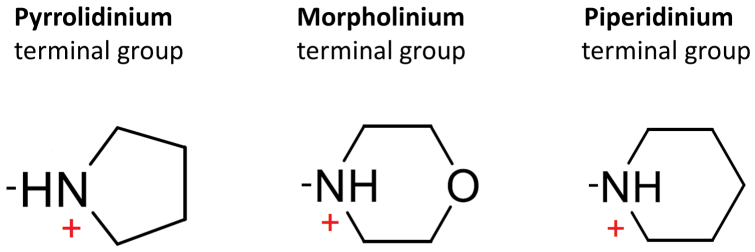

Figure 4.2: *Three different dendrimer terminal groups used in this work.*

After the building of the dendrimers structures partial charges were calculated considering separate residues by the RESP fitting method at the HF/6-31G level of theory using Gaussian09 on the RED server [90]; in this way a proper distribution of

the partial charges is obtained, which correctly takes into account the conformation of dendrimer and related bonds. Then, the topology and the parametrization were developed using leap module of AMBER 16. In the Table 4.1 below are schematized the characteristic of three dendrimers under investigation as a function of the four generations considered, in terms of total charge and number of atoms ascertained in different dendrimers.

generation	charge	16/CEF/051 number of atoms	16/CEF/294 number of atoms	mk016 number of atoms
G1	12	396	408	432
G2	24	912	936	984
G3	48	1944	1992	2088
G4	96	4088	4104	4296

Table 4.1: *Scheme of the characteristics of dendrimers simulated in this project. All the systems were solvated in a water box in presence of 150 mM NaCl concentration.*

4.2.2 Molecular Dynamics Simulations

Molecular Dynamics provides a molecular level picture of structure and dynamics, here MD simulations were performed using Gromacs-5 program [78]; the force field parameters for the atom types were obtained using the antechamber module [91]. The systems were solvated in a TIP3P water octahedron box and an appropriate number of ions (Cl- and Na+) was added to neutralize them using the leap module of AMBER 16 . Subsequently, after an energy minimization of 5000 steps of steepest descent energy, the system was equilibrated for 200 ps at 300 K and 1 atm (under NVT and NPT conditions, respectively) and finally 100 ns of classical molecular dynamics simulation was performed until stability is reached.
All these simulations were run under periodic boundary conditions (PBC) applied along the *xyz* coordinates and the equations of motion were integrated with a 2.0 fs time step, where the bonds constrained were treated with LINCS algorithm [92].
In order to characterize the energetic behaviour of the system and to study its stability, different properties were followed along the simulation, first at all those coming from characteristics of functional groups and different surface charge of dendrimers.

4.2.3 Analysis

During the course of simulations, with the aim of controlling the stability of dendrimers conformations obtained from modeling, some analysis have been performed, in particular the evolution in time of important parameters as Root-Mean-Square De-

viation (RMSD), Radius of Gyration R_g and Solvent Accessible Surface Area (SASA) is reported.
The Radius of Gyration (R_g) is a fundamental tool for the description of structural properties of dendrimers. This quantity represents the average distance between each atom in the structure considered and the center of mass of the dendrimer, as indicated by the eq. 1

$$R_g^2 = \frac{1}{N}\sum_{k=1}^{N}(r_k - r_{mean})^2 \tag{4.1}$$

and it takes into account the spatial distribution of the atom chain by mediating over all N molecular components [42].
Thus, R_g is a good indication of the shape of the molecule at each time: if a dendrimer is rigid, it will maintain a relatively steady value of radius of gyration over the simulation, differently, if is flexible, its R_g will change over time.
Another performed analysis was the evaluation of time evolution of Total Solvent Accessible Surface Area (SASA) for all the generations of three dendrimers under investigation. The extent to which a macromolecule interacts with its environment, the solvent, is naturally proportional to the degree to which it is exposed to these environment. The solvent-accessible surface area (SASA) is a geometric measure of this exposure, and therefore a dependency exists between SASA and environment free energy.

Cluster Analysis

With the aim of finding and studying the equilibrium conformations of three dendrimers, cluster analysis was performed. Using an unsupervised classification algorithm, clustering, structures that are similar to each other within a certain RMSD threshold are grouped together. The size of a cluster, the number of structures that belong to it, is also an indication of how favourable that particular region of the conformational landscape is in terms of free energy. In particular, GROMACS-5 implements an algorithm in the cluster program; here, we use the gromos clustering algorithm with a cutoff of 2.5 angstroms.
Briefly, the algorithm first calculates how many frames are within the threshold of each particular frame, based on the RMSD matrix, and then selects the frame with the largest number of neighbours to form the first cluster. These structures are removed from the pool of available frames, and the calculation proceeds iteratively, until the next largest group is smaller than a pre-defined number. Importantly, it also gave a PDB file with the centroid representative of the cluster. Furthermore, partition generated by clustering has been validated by visual inspection of the structures returned as cluster centers.
For the visual examination of the simulated systems it was employed the Visual

Molecular Dynamics (VMD) package [93]; using VMD tools the charge distribution difference are visible, showing how dendrimers stand in presents of a different number of residues and different terminal groups.

Equilibrium Quantitative Analysis of Dendrimers

Dendrimers flexibility was evaluated on a residue basis using the root mean square fluctuation (RMSF) of the positions of the center of mass for different repetitive units. The RMSF measures its deviation from the time-averaged position during the simulation:

$$RMSF(i) = \sqrt{< r_i^2 > - < r_i >^2} \tag{4.2}$$

where r_i is the coordinate vector for atom i and the $<>$ indicates a time-averaging. In general, calculation of the Root Mean Square Fluctuations (RMSF) is a measurement of the thermal motions of different residues. It captures, for each residue, the fluctuation about its average position, consequently, Root Mean Square Fluctuation (RMSF) curve is a good indicator for their fluctuation (and therefore for dendrimers fluctuation), consequently residues corresponding to higher values of generation express more flexibility during simulation.
Another evaluation was made on the Radial Distribution Function (RDF) to understand how the chlorine (negative ions) present in the solvent are positioned at equilibrium in reference to charged positively amines. Specifically, the charged amines arranged on terminal groups has been selected and taken as reference for the calculation of RDF. The Radial Distribution Function (RDF) or pair correlation function $g_{AB}(r)$ between particles of type A and B is defined as:

$$g_{AB}(r) = \frac{< \rho_B(r) >}{< \rho_B >_{local}} = \frac{1}{< \rho_B >_{local}} \frac{1}{N_A} \sum_{i \in A}^{N_A} \sum_{j \in B}^{N_B} \frac{\delta(r_{ij} - r)}{4\pi r^2} \tag{4.3}$$

with $< \rho_B(r) >$ the particle density of type B at a distance r around particles A, and $< \rho_B >_{local}$ the particle density of type B averaged over all spheres around particles A with radius r_{max}, usually half of the box length.

4.2.4 Adaptive Poisson-Boltzmann Solver Method

The average-linkage method implemented in the gmx cluster tool of the GROMACS-5 was used to perform cluster analysis, with aim to find the most populated cluster and use it as input for electrostatic calculation with APBS-method [94]. In the average-linkage method, the cluster similarity is assessed by computing the mean distance between members of each cluster, where the distance between structures is given by the Root Mean Square Deviation (RMSD) of the atomic positions after optimal superposition. Each system snapshot was considered as part of a cluster when its distance to any element of the cluster was less than a critical threshold.

Adaptive Poisson-Boltzmann Solver (APBS) is a software package designed to estimate the electrostatic interactions in the dendrimers, solving the equations of continuum electrostatics. The Poisson-Boltzmann (PB) equation is a non linear elliptic partial differential equation which is solved for the electrostatic potential, starting from Poisson's equation:

$$-\nabla\epsilon(x)\nabla\varphi(x) = \rho(x) \tag{4.4}$$

the basic equation for describing the electrostatic potential $\varphi(x)$ generated by a charge distribution $\rho(x)$ in a continuum model of a polarizable solvent with dielectric constant $\epsilon(x)$.

4.3 Results

4.3.1 Conformational Stability of Dendrimers

To evaluate the structural stability of MD simulations it was used the Root Mean Square Deviation (RMSD) as an indicator of convergence of the structure towards an equilibrium state; the gromacs program is used to examine the variation the RMSD from the original structure of the dendrimer as a function of time during the simulation. The RMSD plots (Fig. 4.3) show oscillating profiles with high deviations in the first 25 ns of simulation, then the profiles get stabilized and reach a constant behaviour as the simulation time progressed. In general, the value of RMSD increases with generation and reaches a stable value more rapidly in case of $16/CEF/051$ and $16/CEF/294$ dendrimers. In all cases a flat plot of RMSD value after the first 30 ns of simulation ensures that the system has reached stability. Also the time evolution of total Radius of Gyration (R_g) for all generations of three dendrimers is plotted, showing the stability of system reached after a little reorganization of the structures (Fig. 4.4).

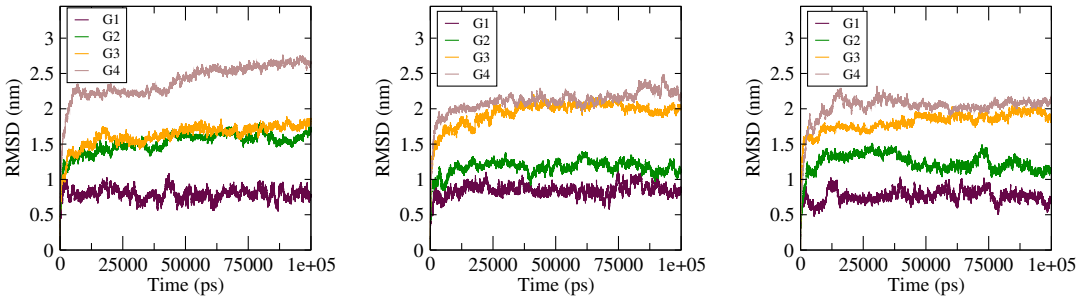

(a) (b) (c)

Figure 4.3: *Time evolution of total Root-Mean-Square Deviation (RMSD) for all generations of three dendrimers:* $16/CEF/051$ *(a);* $16/CEF/294$ *(b);* $mk016$ *(c).*

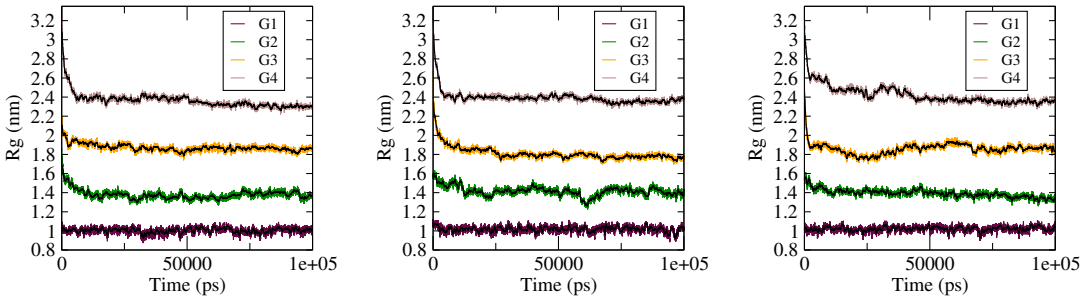

(a) (b) (c)

Figure 4.4: *Time evolution of total Radius of Gyration (R_g) for all generations of three dendrimers:* $16/CEF/051$ *(a);* $16/CEF/294$ *(b);* $mk016$ *(c).*

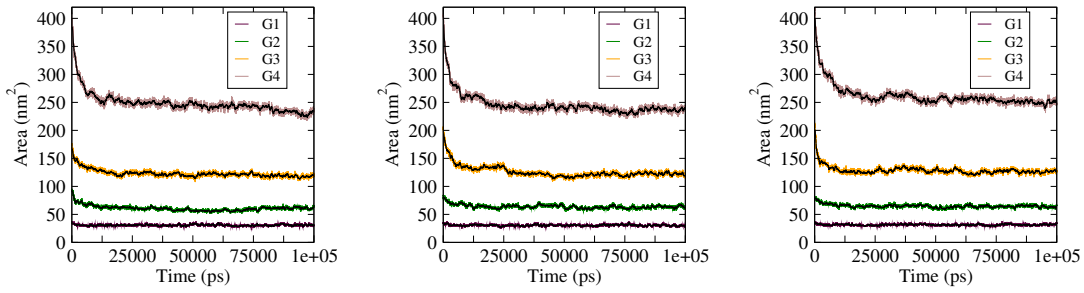

(a) (b) (c)

Figure 4.5: *Time evolution of total Solvent Accessible Surface Area (SASA) for all generations of three dendrimers:* $16/CEF/051$ *(a);* $16/CEF/294$ *(b);* $mk016$ *(c).*

Another important data is the time evolution of surface area; in detail, high SASA values represent a system that provide weaker environmental protection; here SASA values are plotted over the total simulation time of each dendrimer (Fig. 4.5).

4.3.2 Equilibrium Dendrimers Configurations

A comparison between equilibrium configurations in vacuum and in water is presented as a good indicator of how structures in solvent goes to a significant conformational reorganization, collapsing into a globular shape and drastically reducing the space taken.
The phenomenon is more accentuated for higher generations that undergo a strong reduction in water (Fig. 4.6-4.8). Otherwise, all dendrimers equilibrated in vacuum maintain a perfectly spherical and orderly shape, with terminal groups which form the outside of the sphere and with several space among different branches accessible to solvent.

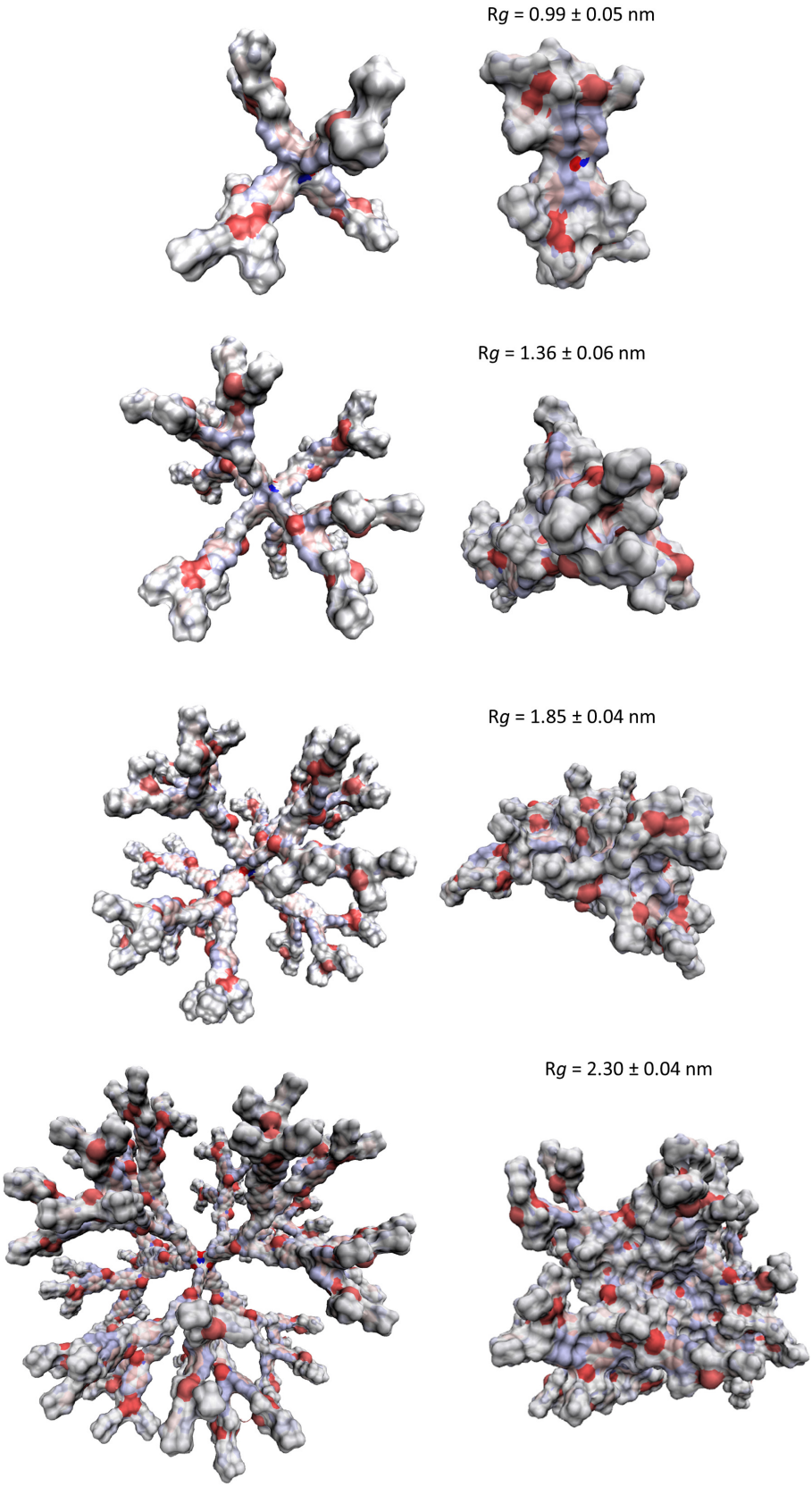

Figure 4.6: *Comparison of* 16/*CEF*/051 *dendrimers configuration after equilibration in vacuum (left) and in water (right): G1 (a); G2 (b); G3 (c); G4 (d).*

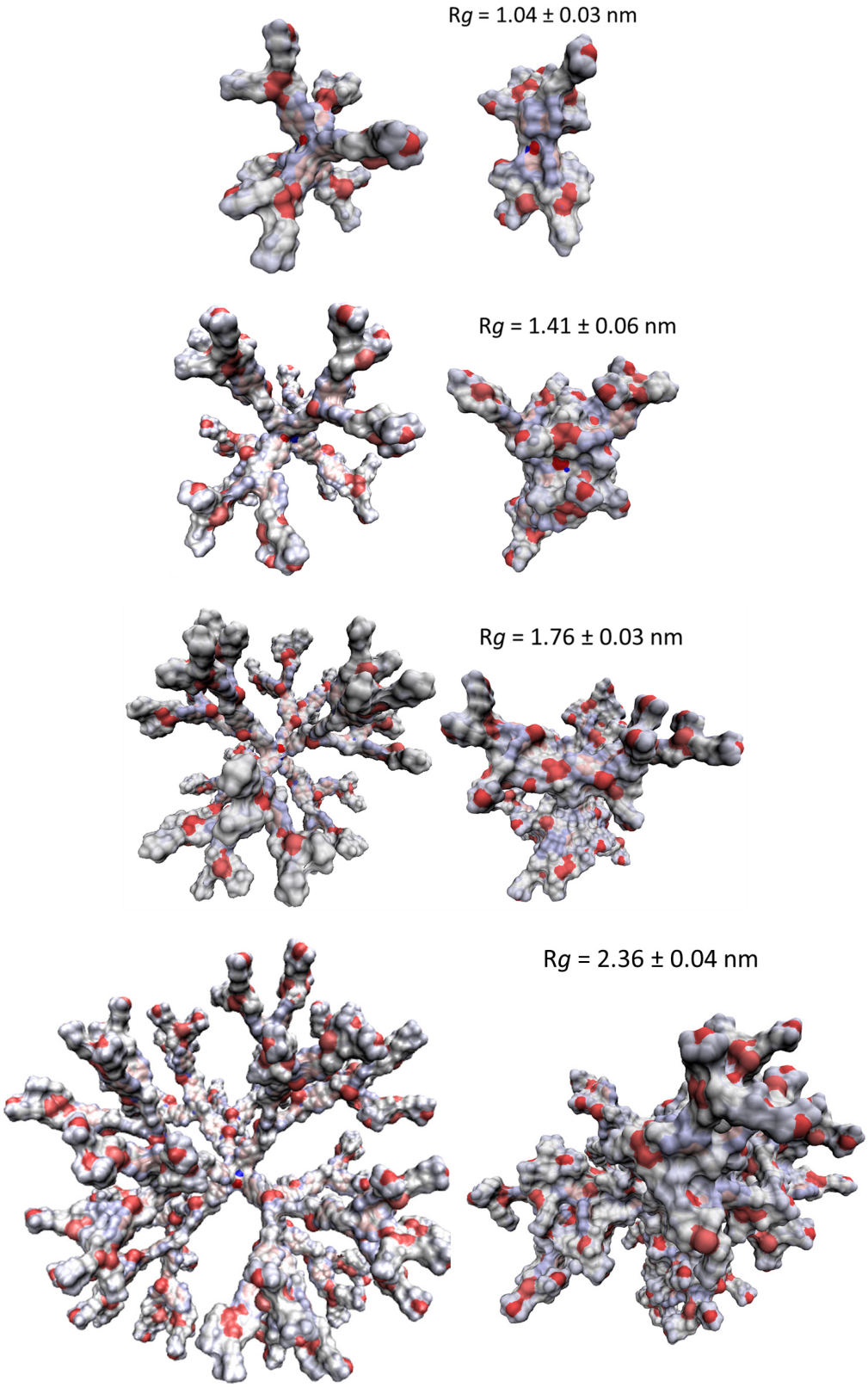

Figure 4.7: *Comparison of* 16/*CEF*/294 *dendrimers configuration after equilibration in vacuum (left) and in water (right): G1 (a); G2 (b); G3 (c); G4 (d).*

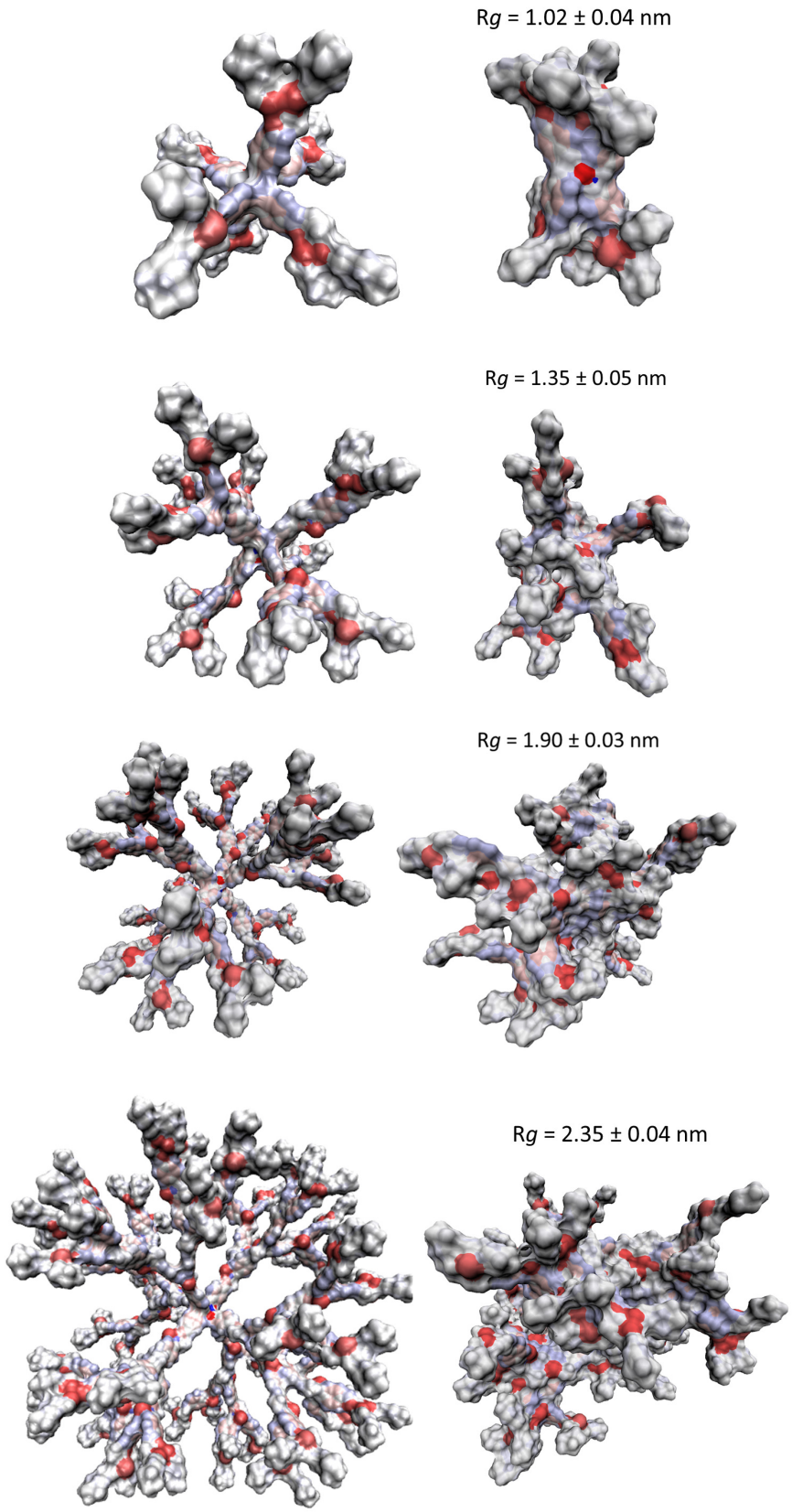

Figure 4.8: *Comparison of mk*016 *dendrimers configuration after equilibration in vacuum (left) and in water (right): G1 (a); G2 (b); G3 (c); G4 (d).*

The configurations obtained from cluster analysis have been used as reference for the equilibrium analysis of dendrimers. Then, equilibrium conformational energetic properties investigation of all three dendrimers was performed.
From the equilibrated phase of MD trajectories has been evaluated the distributions of Radius of Gyration, histogram below shows for all of the dendrimers the average values with relative standard deviations.
From profiles of time evolution of the radius of gyration is visible that R_g grows with generations and all dendrimers of G1 presents flat R_g plots for an average value around 1 nm that is almost identical to the value observed for the starting structure and consistent with a rigid framework. For all second generation structures is visible a little arrangement in the first 10 ns of simulation after which they get rapidly to a R_g around 2.45 nm.
In contrast, with the growing of generations dendrimers reorganize by collapsing from an initial, extended structure to a compact equilibrated globule corresponding to a significant reduction in radius of gyration (Fig. 4.9).
About that, dendrimers of third generation present a visible conformational reorganization, in particular for $16/CEF/051$, whose R_g goes from 2.4 nm at the beginning of simulation to 1.8 nm after 20 ns beyond which remains almost stable; R_g of *mk*016 shows variations up to 60 ns of simulation when reaches a flat trend around 1.9 nm; otherwise $16/CEF/051$ dendrimer quickly achieves a stable value of 1.9 nm without meaningful variations. Finally, for all G4 dendrimers it is highlighted a prominent reorganization over time starting from a value around 3.1 nm to 2.4 nm of R_g.

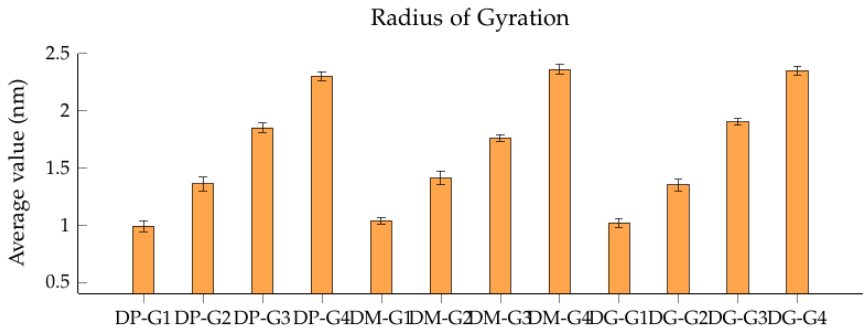

Figure 4.9: *Histograms of average values and standard deviation of equilibrium distribution of Radius of Gyration for* $16/CEF/051$, $16/CEF/294$ *and mk*016 *dendrimers (labelled: DP , DM and DG, respectively), comparing four different generations.*

Also for the Solvent Accessible Surface Area (SASA) it was calculated the distribution at equilibrium, in particular, are distinguished hydrophobic and hydrophilic components. The histograms below (Fig. 4.10) shows the results obtained as average values and relative standard deviation at equilibrium; the reference values of Total SASA are reported in Table 2.

As seen for R_g, this significant conformational reorganization for high generation is reflected also in the SASA plots where the effect is more pronounced for third and fourth generations. In details, for dendrimers of second generation the Solvent Accessible Surface Area starts from a value around 85 (95 nm for $16/CEF/051$) to 65 nm^2 after 25 ns of simulation. Otherwise, for $16/CEF/051$ and $mk016$ dendrimers of G4 generation the Solvent Accessible Surface Area starts from a value of 350 to 250 nm^2, with $16/CEF/051$ and $16/CEF/294$ that reach a flat plot after 20 ns of simulation and $mk016$ that manifests reorganization until 40 ns, it reflects a more flexible structure in higher generations compared to G1.

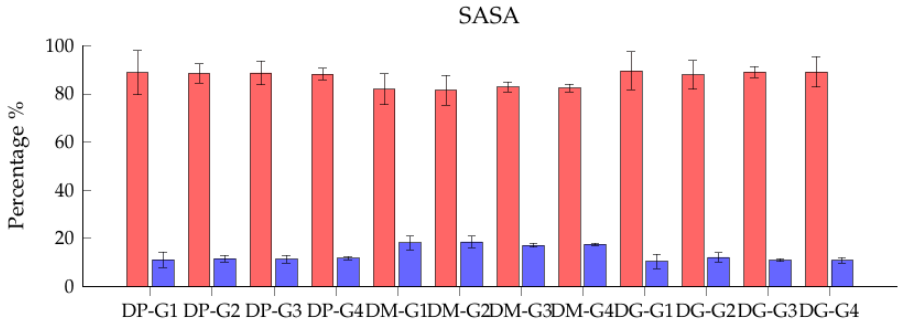

Figure 4.10: *Histograms of average values and standard deviation of equilibrium distribution of SASA components (hydrophobic in red and hydrophilic in blue) for all dendrimers, comparing four different generations.*

Another interesting analysis is about the different components of Solvent Accessible Surface Area, here plays a significant role the different composition of atoms in terminal groups of three dendrimers (4.2).
Firstly, it's immediately evident that there are no significant differences between the results of the four generations of dendrimers because for each dendrimer the value are similar, furthermore in accordance with the specific conformation and the number of atoms SASA exhibits an increase in value with generation.
Commensurate with the atoms disposition in dendrimers, in SASA histogram is visible that the most exposed sites are hydrophobic (around 88% of total value, with an higher value of 89 % for $mk016$ dendrimer), compared to 12 % of hydrophilic component.
Also, it is very interesting to note the difference made by the presence of oxygen in the terminal groups of $16/CEF/294$ dendrimers (in morpholinium); indeed it presents a notable value of hydrophilic component of around 18 %, considerably higher than others. Its notable to observe that the Solvent Accessible Surface Area calculated only for the core of dendrimers shows a flat trend around 2.2 nm^2 during the simulation, that indicates no significant variations of the core surface exposed over time.

	Hydrophobic (%)	Hydrophilic (%)	Total SASA (nm^2)
16/CEF/051-G1	88.9 ± 8.9	11.1 ± 2.2	31.1
16/CEF/051-G2	88.5 ± 4.0	11.5 ± 1.4	59.0
16/CEF/051-G3	88.7 ± 4.9	11.3 ± 1.6	120.3
16/CEF/051-G4	88.2 ± 2.4	11.7 ± 0.6	120.3
16/CEF/294-G1	81.9 ± 6.3	18.1 ± 2.9	29.8
16/CEF/294-G2	81.5 ± 6.1	18.5 ± 2.4	63.3
16/CEF/294-G3	82.8 ± 2.1	17.2 ± 0.7	122.6
16/CEF/294-G4	82.5 ± 1.6	17.5 ± 0.5	237.5
mk016-G1	89.6 ± 7.9	10.4 ± 2.9	31.8
mk016-G2	87.9 ± 5.9	12.1 ± 2.0	64.4
mk016-G3	89.1 ± 2.4	10.9 ± 0.6	126.9
mk016-G4	89.1 ± 6.3	10.9 ± 1.1	261.6

Table 4.2: *Solvent Accessible Surface Area components as a percentage of total (average value and standard deviation); in the last column are reported the Total SASA values.*

Therefore, it's useful to study the trend of the fluctuations of different residue of dendrimers to understand the movement and the flexibility of each one. In particular, it has been calculated thanks to the Root Mean Square Fluctuations (RMSF) measurement, that captures the variations about average positions.
From the plots in Fig. 4.11 (where is represented the average value of RMSF for every repetitive branching unit) is evident that the value of RMSF increases with the number of generation, but also is visible that all of the external branches presents an higher value of RMSF (as shows figures of G1-dendrimers).
For G1-dendrimers, $16/CEF/051$ exhibits the highest values of RMSF for terminal groups (0.61 nm); in all plots is visible that the core (AAA) doesn't present any fluctuation that reflects its rigid structure.
Finally, a very important aspect of analysis consists in the study of Radial Distribution Function of Cl ions around charged amines of terminal groups.
This analysis allows to establish the dendrimer's ability to attract negative ions (Cl), which depends mainly on generation and hence on the number of loaded amines present in the macromolecule terminal units.
RDF plots (reported in Fig. 4.12) the average density of Cl atoms at specific distance (coordinate **r**) relative to the amine of dendrimer at each simulation step.
It is worth noting that high peaks in a certain zone of these graphs correspond to areas of high atomic density and low atomic mobility.
The non-uniformity in peak height in the RDF profile suggests a difference in the ability of the two regions to readily vibrate.
An important result is the presence of a high peak in a specific distance from amines that correspond to the area of high atomic density and also low atomic mobility. That

is, the Cl center of mass shows an area of high atomic density at 0.5 nm from amines after which falls off rapidly for higher distances.
The curve for all generation is picked at this value and it takes into accounts the interaction distance between two charged atoms. It also indicates that a large part of the Cl takes part in the interaction.
Furthermore, RDF plots correctly exhibit an interesting dependence on dendrimer generation, and therefore dendrimer size. Infact, the number of ions considerably grows with generation and high ones exhibit low surface and very high energy.

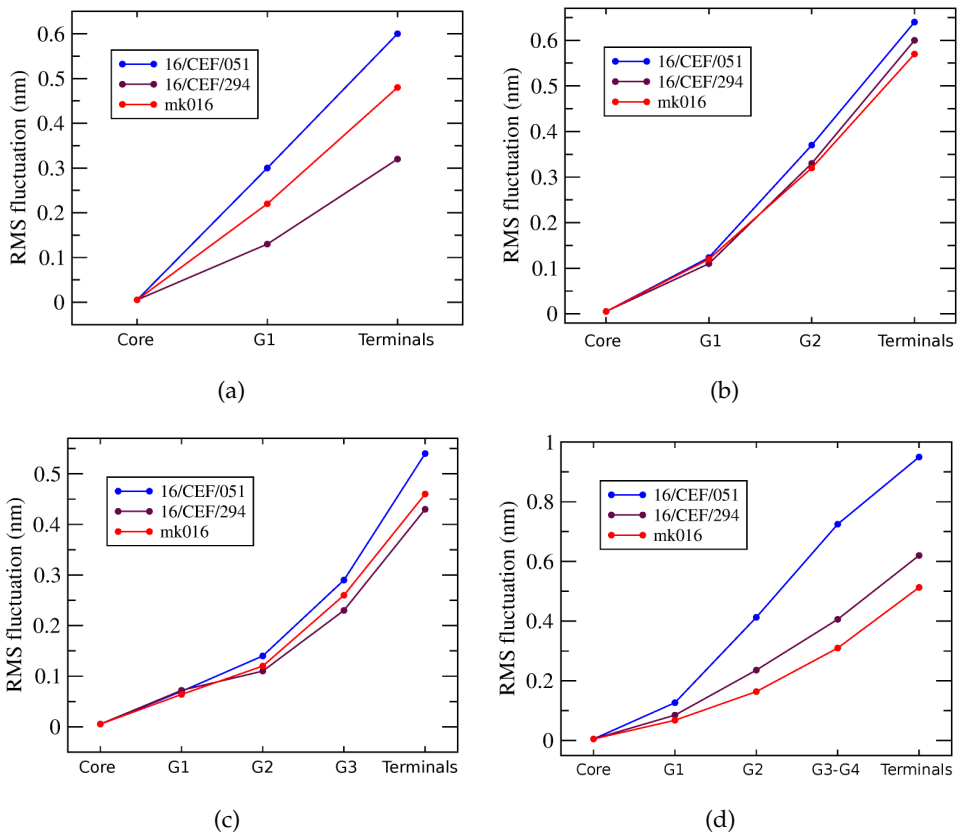

Figure 4.11: *Equilibrium Root-Mean-Square Fluctuation (RMSF) calculated in function of different residues for all dendrimers: G1 (a); G2 (b); G3 (c); G4 (d).*

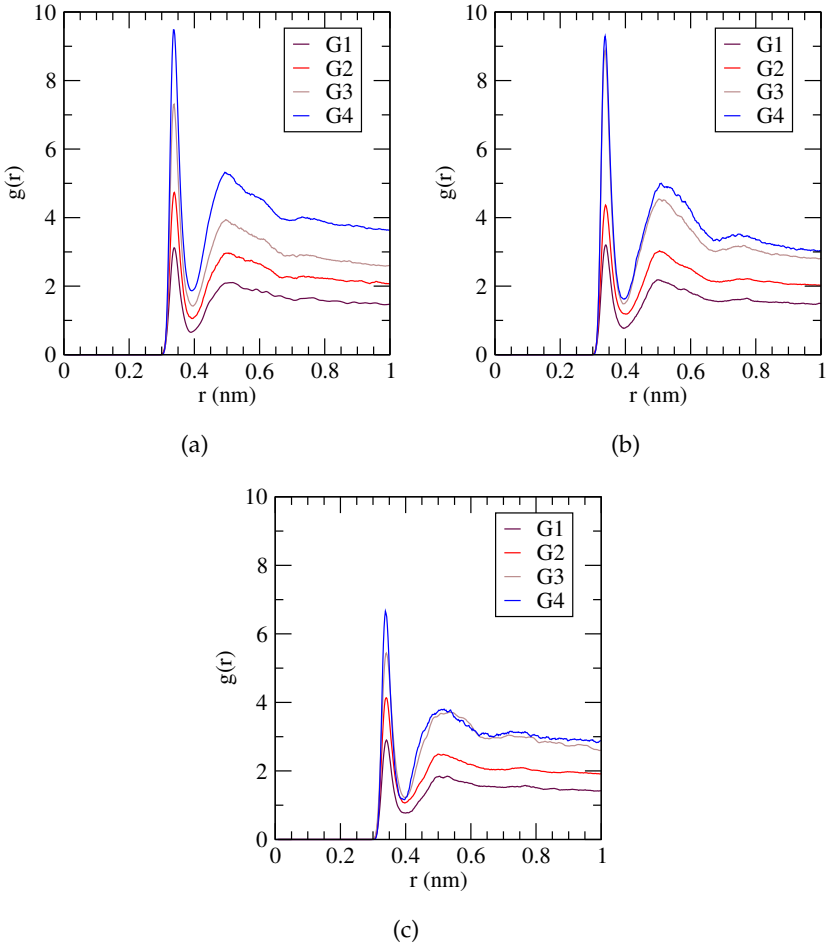

Figure 4.12: *Equilibrium Radial Distribution Function (RDF) of ions (Cl) in reference to amines of the terminal groups for three dendrimers:* 16/*CEF*/051 *(a),* 16/*CEF*/294 *(b) and mk*016 *(c), different four generations are comparised.*

Equilibrium Evaluation of Charges Effect

Below are reported the equilibrium configurations, corresponding to the cluster's arrangement, for every dendrimers, put side by side with the map of relative electrostatics interactions founded using Adaptive Poisson-Boltzmann Solver (APBS) method. The VMD molecular graphics software package provides support for both the execution of APBS and the visualization of the resulting electrostatic potentials (the "Color Scale Data Range" was fixed to -10 to 10), the results are reported in Fig 4.13-4.15. The principal feature of APBS images is the overall positive electrostatic potential of the dendrimers, which will plays a significant role in the interaction with siRNA. In the color scale the negative net charges are colored red, while the positive net charges blue.

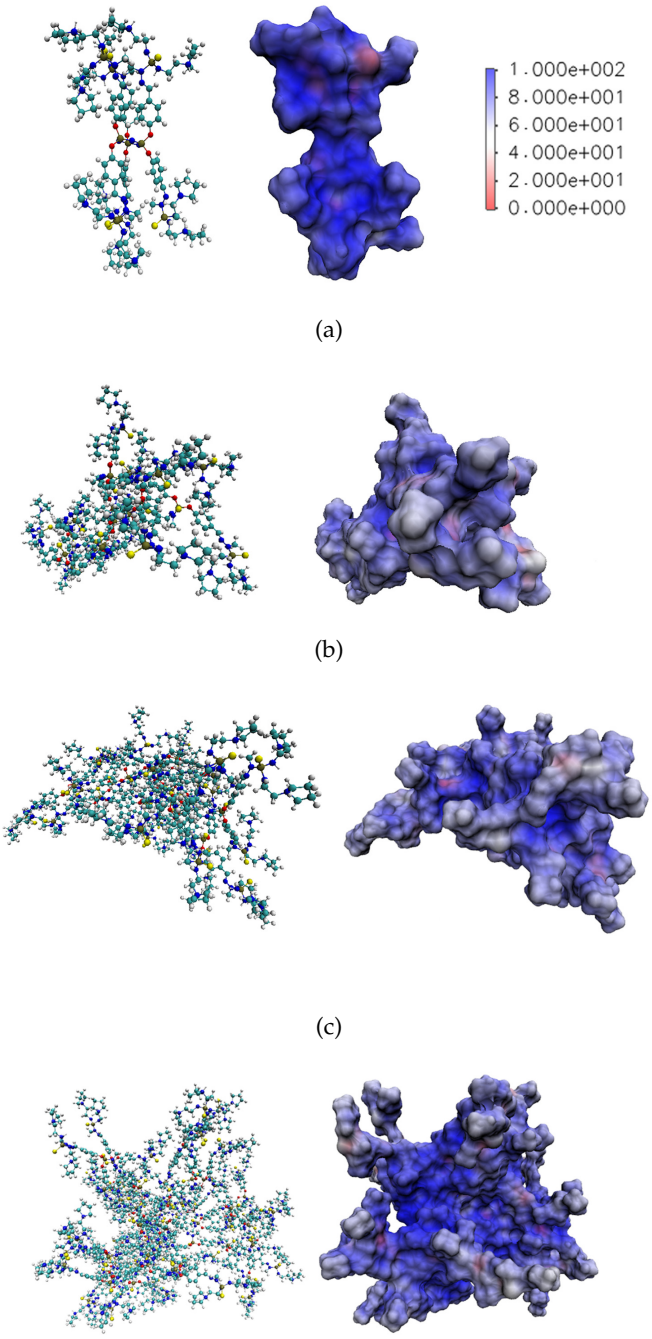

(a)

(b)

(c)

(d)

Figure 4.13: *Equilibrium configuration of* $16/CEF/051$ *dendrimers (left) and map of electrostatics interactions (right) founded using Adaptive Poisson-Boltzmann Solver (APBS) method: G1 (a); G2 (b); G3 (c); G4 (d).*

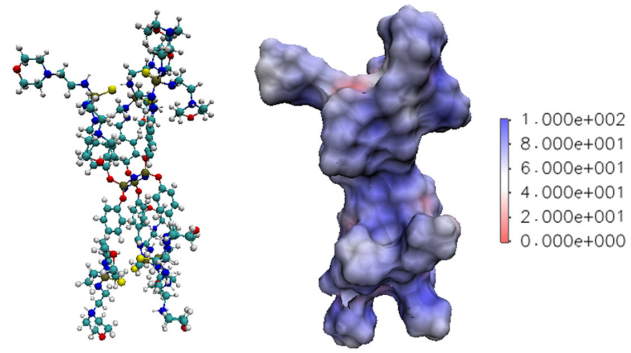

(a)

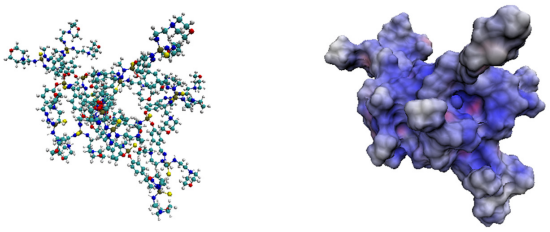

(b)

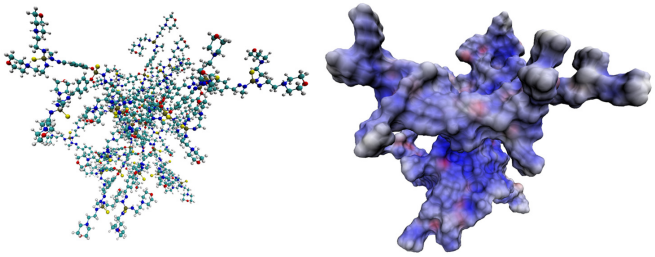

(c)

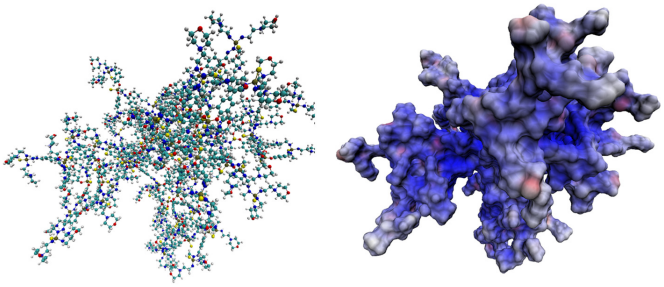

(d)

Figure 4.14: *Equilibrium configuration of* $16/CEF/294$ *dendrimers (left) and map of electrostatics interactions (right) founded using Adaptive Poisson-Boltzmann Solver (APBS) method: G1 (a); G2 (b); G3 (c); G4 (d).*

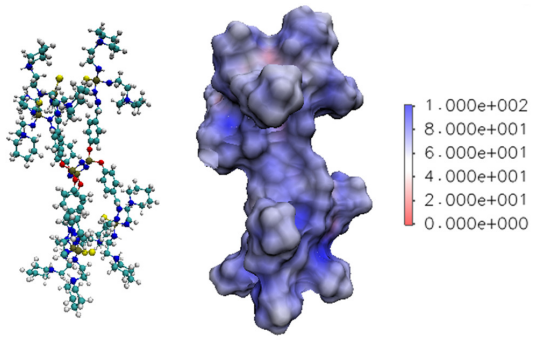

(a)

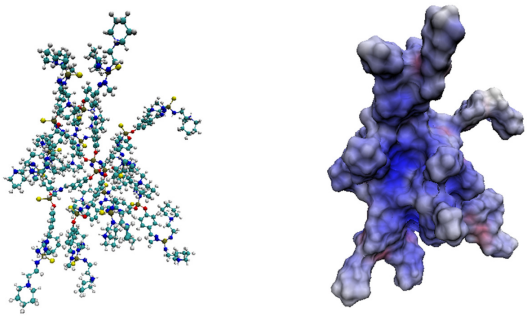

(b)

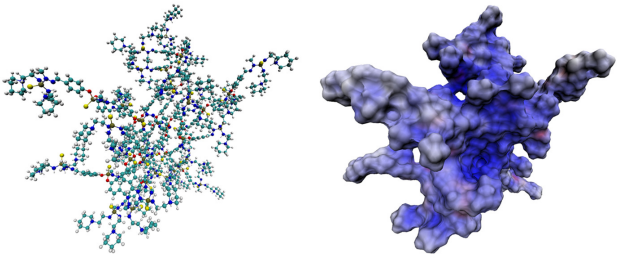

(c)

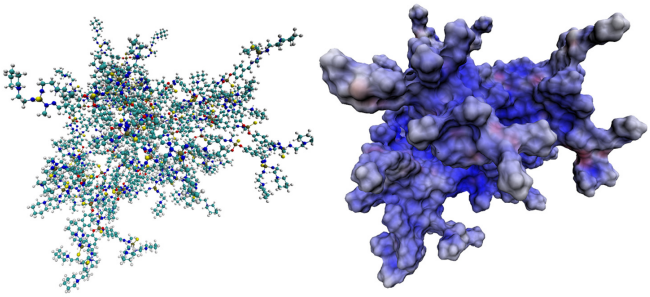

(d)

Figure 4.15: *Equilibrium configuration of mk*016 *dendrimers (left) and map of electrostatics interactions (right) founded using Adaptive Poisson-Boltzmann Solver (APBS) method: G1 (a); G2 (b); G3 (c); G4 (d).*

4.4 Discussion

In this work, the structural-physico-chemical profiles have been presented for 3 different functionalized dendrimers for gene therapy, which in this specific case could be applied in the treatment of lung inflammations.
Generally, in appropriate MD simulation, a suitable force field is important for the correct structural and dynamic predication and mechanism explanation. Here the chosen force field (GAFF) has been successfully applied for our dendrimers.
From the analysis it follows that the size, shape, effective charge and terminal characteristics of dendrimers, play significant role in their application as delivery vectors.
Primarily, the conformational stability analysis for all three dendrimers under investigation highlights different behaviours between the generations in terms of conformational arrangement and variation during the simulation time.
The related results show that the ability of dendrimers to change their structural conformation is strongly dependent on the generation, with a proportional relation.
From data it proves that all dendrimers structures undergo considerable structural changes in presence of solvent compared to vacuum, with a collapse that reduces its whole occupation area. The phenomenon is more pronounced in the case of higher generations (G3, G4). Thus, it leads to different binding characteristics between generations because of different structures obtained.
Furthermore, it has been demonstrated that with the growing of generation the structure of macromolecules changes; on one hand, the lower generations exhibit flexible conformations, on the other hand, G3 and mostly G4 show more rigid and compact conformations. In higher generation dendrimers the numerous branching terminal units create a kind of cover around internal ones, keeping inside the hydrophobic parts of dendrimer. DM dendrimers are the ones who exhibit the higher hydrophilic component (with higher percentage of SASA values reported).
Correctly, the analysis of Radial Distribution Function of Cl ions around charged amines of dendrimers terminal groups highlights the capacity to attract negative ions (Cl) present in the solvent, as a function of dendrimer generation and therefore dendrimer size. Indeed, the number of ions considerably grows with generation and high ones exhibit low surface and very high energy. From data results the presence of high peak for all generations in a specific distance from amines that correspond to the area of high atomic density and also low atomic mobility; it takes into accounts the interaction distance between two charged atoms and indicates that a large part of the Cl takes part in the interaction.
Moreover, from APBS analysis emerges that the existence of many charged terminals conducts G3-G4 dendrimers to be surrounded by a positive potential, which may allow the formation of multivalent interactions with nucleic acid; differently, lower generation dendrimers may neutralize the siRNA electrostatic surface in the binding

region. As a consequence, the binding with siRNA might show different features, comparing different generations and dendrimers.

4.5 Conclusion

Here we wanted to compare three different types of dendrimers (DP, DM and DG) in order to study their structural and electrostatic characteristics.
These MD simulations provide significant informations about the design of dendrimer size, shape, or surface properties for applications in nanomedicine, as in the treatment of lung inflammation with gene therapy.
The development of highly-efficient and low-toxicity macromolecules as good carriers will allow advances in understanding of interactions involved in the gene deliver process.

Chapter 5

Characterization Of Dendrimer-siRNA Complexes

This chapter presents a molecular modelling strategy to design optimized dendrimer-based carries for siRNA to be delivered by inhalation route in COPD treatment. In details, in silico simulations have been performed to evaluate the siRNA-dendrimer interaction. Classical MD has been employed to ensure an appropriate siRNA loading and delivery in presence of different dendrimers functionalized by pyrolidinium, piperazinium and morpholidinium surface groups.

5.1 Introduction

The design of efficient delivery technologies is an important key for a successfully medical treatment with silencing interference RNA (siRNA). The advantages of siRNA therapy for treatment of lung inflammation as COPD have been established. In addition, the use of nanoparticles as carriers in siRNA therapy, with a special focus on cationic polymers and dendrimers, has been proven in several research studies [20],[18],[22].
For example, the main characteristics of PAMAM and PEI dendrimers for efficient siRNA deliveries and potent gene silencing have been widely exposed in recent times [95], [83], [62], [81], [96]. In the last years several approaches have been promoted to achieve this goal.
Generally, dendrimer functionalization modifies the interaction properties in particular for what concern the ability of binding siRNA molecules. In details, mechanical properties of dendrimers, such as surface properties, in terms of charge distribution may affect the free energy of interaction which lately drives the siRNA delivery in loco.
A good delivery technology should guarantee the release from the endosomal pathway (endosomal escape). The negatively charged nucleic acids are generally not

able to spontaneously cross the likewise negatively charged cell membranes to reach the cytoplasm or cell nucleus on their own, however, may be ingested by the endo-/lysosomal pathway.
Recent studies have demonstrated that rigid polycationic dendrimers are able to reorganize their peripheral groups to generate a large number of contacts with the nucleic acid [80]. They found that flexible dendrimers, originally conceived to create multivalent interactions with nucleic acids, generate only few contacts, revealing the role of molecular flexibility in the binding phenomenon. The efficacy of PAMAM dendrimers and PEI polymers has been demonstrated to strongly depend on its structure, molecular mass and charge density; however, significant cytotoxicity strongly limits its application [83].
Therefore, the above mentioned siRNA-dendrimer based nanocarrier seems to be a promising strategy to increase siRNA concentrations in AMs, reducing dose and ensuring biocompatibility. However, in order to design an ad hoc dendrimer-based system suitable for inhalator purpose and able to guarantee a high TNF-alfa silencing, an accurate evaluation of the physicochemical and molecular properties of the different dendrimers in complex with the nucleic acid is necessary.
In this context molecular modelling helps to better understand mechanism of binding and delivery by a specific analysis with atomic resolution, it proves to be a powerful strategy in nanocarrier characterization of physical-chemical properties and mechanism of action. Evaluation of siRNA-dendrimer interaction at the atomistic level has been employed to ensure an appropriate loading and delivery of the therapeutic agent. At present three types of dendrimer, called $16/CEF/051$, $16/CEF/294$ and $mk016$, of three different generations have been investigated for gene delivery.
This work provides results that will be used for future design of selective nucleic acids carriers characterized by a good complexation stability and ability of the delivery system.

5.2 Materials and Methods

Molecular Dynamics simulations have been performed with the aim of evaluating the siRNA-Dendrimer interaction. In particular, three siRNA-dendrimer complexes have been developed in presence of different functionalization.
Whereas in the previous Chapter three types of dendrimer have been analysed in the unbound condition, here we intend to investigate the complexation with siRNA in order to evaluate how the macromolecules are capable of an internal reorganization due binding. Enhanced sampling techniques such as Umbrella Sampling can be applied to improve the sampling efficiency of classical MD, allowing the estimation of the siRNA-dendrimer adsorption free energy.

5.2.1 RNA Structure Model

Starting from the stoichiometry and the knowledge about the physical and chemical properties of related atoms and bonds a 3D model of siRNA has been developed. This specific siRNA sequence is composed by a sense strand:

$$5' - pGUCUCAGCCUCUUCUCAUUCCUGct - 3' \tag{5.1}$$

and by an antisense strand:

$$5' - AGCAGGAA\underline{U}G\underline{A}G\underline{A}A\underline{G}A\underline{G}G\underline{C}U\underline{G}A\underline{G}A\underline{C}A\underline{U} - 3' \tag{5.2}$$

where the lower case letters indicate *2'-deoxyribonucleotides*, underlined capital letters represent *2'-O-methylribonucleotides* and *p* is a phosphate residue. The model consists of 50 nucleotides and it has been selected as a siRNA model for the present work. The relative starting coordinates were built to be in the canonical B-form of the AMBER NAB tool and its structure is presented in figure below.

5.2.2 Building of siRNA-dendrimer Complex Mode

With the purpose of building a complex, together with the structure of nucleic acid, the models of three different polycationic dendrimers were built (Fig. 5.1, right). They consist of several repeating units and are differentiated by their terminal groups, as widely described in Chapter 3.
Here, for convenience, those dendrimers are labelled as follows:

1. dendrimer $16/CEF/051$, which is labelled **DP**, has *pyrolidinium* terminal group
2. dendrimer $16/CEF/294$, which is labelled **DM**, has *morpholinium* terminal group
3. dendrimer *mk*016, which is labelled **DG**, has *piperidinium* terminal group

Generation	G1	G2	G3
Repetitive Units	6	12	24

Overall, nine molecular systems have been prepared: for all dendrimers 3 generations have been considered, discriminated by the growing number of their repetitive units. Each one of them has been put in complex with siRNA; the complexes were created by placing dendrimers in close proximity of siRNA at 2 nm of distance (considering their Center of Mass as reference). The obtained systems were again solvated in a periodic box of $12 \times 12 \times 12$ nm with a solute containing TIP3P water molecules and the proper amount of Na+ and Cl- ions useful for system neutralization was added:

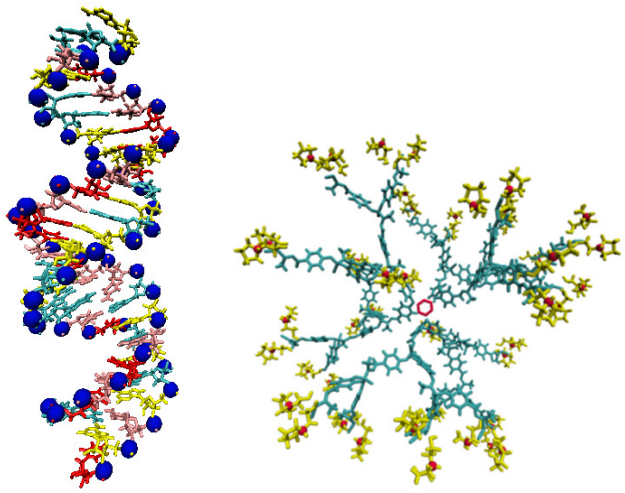

(a) (b)

Figure 5.1: *Molecular models representation of siRNA (a) and DP dendrimer (G3, b) used for simulations (images taken from VMD). To clarify siRNA uraciles are colored in red, guanines in cyan, cytosines in pink and adenine in yellow, while the phosphores are represented as blue balls. Within G3 dendrimer, the central residue (CORE) is colored in red, the repetitive (REP) branch units in cyan and the surface terminal groups are represented in yellow.*

it reproduces the 150 mM ionic concentration. An example of the model is shown in Fig. 5.2 and the main characteristics of the simulated systems are summarized in the Table 5.1.

5.2.3 Molecular Dynamics Simulations

Here molecular dynamics (MD) is used to investigate the local mechanism of binding between siRNA molecules and different cationic dendrimers, providing informations about the structural conformations and binding behavior [70], [97]. Thus, the molecular dynamics simulations take fully into account the siRNA flexibility together with the presence of explicit solvent and ions.
Before starting with the MD simulations, all the molecular systems were minimized and then equilibrated at 300 K by 200 ps molecular dynamics in the canonical NVT ensemble. This stage was followed by two steps of density equilibration run (each one of 200 ps) under NPT conditions with explicit solvent and pressure set to 1 bar to obtain a reliable equilibrated configuration. Finally, the production dynamic lasted for 50 ns has been performed under periodic boundary condition at 300 K and 1 atm using the Langevin thermostat, and 10 angstrom for the cutoff value. The neighbour list of 1.1 nm length was updated using the Verlet neighbour search algorithm every 50 time-steps.

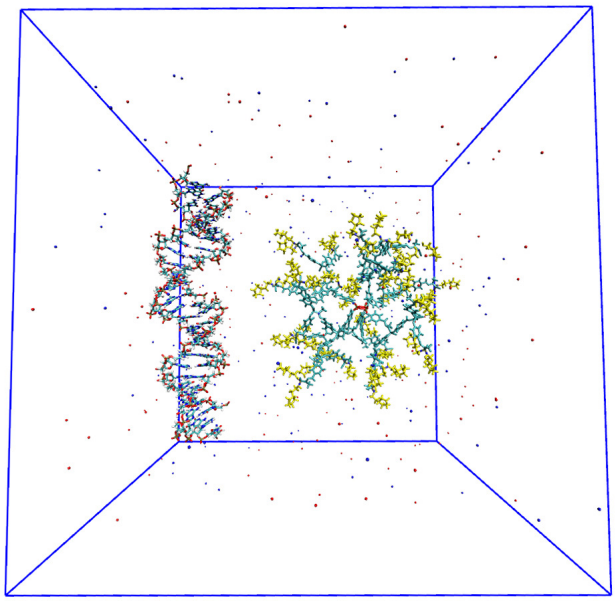

Figure 5.2: *Snapshot of siRNA and DP dendrimer (G3) models in a box of 12×12×12 nm for molecular dynamics simulations. Water molecules are omitted for clarity. Cl- and Na+ are colored in yellow and red respectively and represented as dots.*

Every complex system was simulated using Gromacs-5 [78], a molecular dynamics package designed for biomolecular systems exploited also for dendrimer systems in the previous Chapter. To treat long-range electrostatic effects, the particle mesh Ewald (PME) approach has been adopted [98] and the SHAKE algorithm was used to constrain all bonds involving hydrogen atoms [99].
For parametrization of dendrimeric structures, as explained in Chapter 3, the calculation method of *Antechamber* [100], module of AMBER 16, has been used: it assigns parameters and force field types that are consistent with the **General Amber Force Field** (GAFF) [101]. Consequentely, GAFF and TIP3P model [102] have been employed for dendrimers and water molecules, respectively. All the images derived from the MD simulations have been visualized by the VMD software [93].

5.2.4 Analysis

Since all dendrimer systems have been already evaluated previously (see Chapter 3), before studying complex systems, an accurate analysis on the siRNA has been performed. In details, the evaluation over time of principal system parameters, as Radius of Gyration (R_g) and Solvent-Accessible Surface Area (SASA) have been executed.
Then, after the siRNA-dendrimer complex development and the trajectories analysis, in order to identify the equilibrium states of every system, a conformational stability

System	Dendrimer charge	siRNA charge	Number of Na+ and Cl- atoms	Number of water molecules	Total number of atoms
siRNA-DP **G1**	+12	-50	222	85371	87592
siRNA-DP **G2**	+24	-50	284	109848	112647
siRNA-DP **G3**	+48	-50	338	124941	128826
siRNA-DM **G1**	+12	-50	222	85395	87628
siRNA-DM **G2**	+24	-50	284	109887	112710
siRNA-DM **G3**	+48	-50	338	124932	128865
siRNA-DG **G1**	+12	-50	222	85374	87631
siRNA-DG **G2**	+24	-50	284	109830	112701
siRNA-DG **G3**	+48	-50	338	124719	128748

Table 5.1: *Main features of the molecular systems simulated in this work.*

estimation has been done, in terms of time evolution of RMSD as good indicator of convergence of the structures.

Equilibrium Quantitative Analysis of siRNA-dendrimer Complex

With the purpose of studying the equilibrium conformations of all complex, cluster analysis was performed, following the same steps of the only dendrimer systems presented in the previous Chapter. In the average-linkage method, the cluster similarity is assessed by computing the mean distance between members of each cluster, where the distance between structures is given by the Root Mean Square Deviation (RMSD) of the atomic positions after optimal superposition. Each system snapshot was considered as part of a cluster when its distance to any element of the cluster was less than a critical threshold.
After obtaining the equilibrium configurations, a quantitative analysis of the systems in terms of Radius of Gyration (R_g), Solvent Accessible Surface Area (SASA), Buried Surface Area (BSA), Root Mean Square Fluctuation, Contact Probability and Radial Distribution Function has been performed. In details, with the aim of describing the conformational modifications of every dendrimer and siRNA upon binding, the values of the Radius of Gyration of the dendrimer within the complex (Rg_{den}), of the siRNA within the complex (Rg_{rna}), of the dendrimer terminal groups (Rg_{ter}) and of the whole complex ($Rg_{complex}$) have been calculated over the equilibrium simulation. R_g is not a true measurement of radius, but is defined as the root-mean-square distance between each atom and the center of mass of the structure considered; it gives important informations on the geometrical structure of the systems under investigation:

$$R_g^2 = \frac{1}{N}\sum_{k=1}^{N}(r_k - r_{mean})^2 \tag{5.3}$$

Another molecular issue, derived from the data collected for the analysis, is the so-called molecular Solvent-Accessible Surface Area (SASA), which describes the area over which contact between solute and solvent can occur. The estimation of accessible area calculation has been used to determine the Buried Surface Area (BSA). This measurement was calculated to evaluate the relevant contact area between siRNA and all dendrimer during the binding complex. Otherwise, concerning the study of siRNA interaction with polycation dendrimers and with the purpose of quantifying its flexibility, the root-mean-square fluctuation (RMSF) of siRNA sequence has been calculated and it is defined as:

$$RMSF = \frac{1}{N}\sum_{i}\sqrt{\frac{1}{T}\sum_{t=1}^{T}(r_i(t) - < r >_i)^2} \tag{5.4}$$

Moreover the Contact Probability between siRNA atoms and dendrimer ones has been computed in order to elucidate the effect of dendrimer conformational properties and its molecular geometry on the complex.
The contact probability for each siRNA base pair has been calculated using the following procedure [103]. Trajectory snapshots are extracted from 50 ns of each MD simulation, for each one the distance between a base pair in siRNA and all residues of the interfacing dendrimer is calculated. If at least one distance value among the residue-residue distances is under a chosen threshold (0.28 nm), the base is considered in contact with the interfacing dendrimer in that snapshot. The number of contact snapshots divided by the number of total snapshots taken out from the MD trajectories is the contact probability associated with the siRNA residue.
Furthermore, with the aim of exploring the effect of siRNA binding on the distribution of dendrimer atoms, several measurements of Radial Distribution Function (RDF) have been computed for all the systems of interest.
The Radial Distribution Function or pair correlation function $g_{AB}(r)$ between particles of type A and B is defined as:

$$g_{AB}(r) = \frac{< \rho_B(r) >}{< \rho_B >_{local}} = \frac{1}{< \rho_B >_{local}} \frac{1}{N_A} \sum_{i \in A}^{N_A} \sum_{j \in B}^{N_B} \frac{\delta(r_{ij} - r)}{4\pi r^2} \tag{5.5}$$

with $< \rho_B(r) >$ the particle density of type B at a distance r around particles A, and $< \rho_B >_{local}$ the particle density of type B averaged over all spheres around particles A with radius r_max, usually half of the box length.

Energetic Analysis

As made also for dendrimer systems (Chapter 3), the APBS package [94] was used to compute the electrostatic potentials, by applying the linearized Poisson-Boltzmann

equation using single Debye-Huckel sphere boundary condition on a 65×65×65 grid with a spacing of 1 angstrom centered at the COM of the molecular system.
The dielectric constants of the solute and the solvent were set to 4 and 80, respectively [104], [105]. In addition, the MM-PBSA Method has been used to calculate binding energies of siRNA-dendrimer complexes. Specifically, this method gives the different components of energy, in terms of MM (Molecular Mechanics), PB (Poisson-Boltzmann) and SA (Surface Area) energy values. Its goal consists of integrating high-throughput molecular dynamics (MD) simulations with binding energy calculations. The tool also allows to obtain the residue wise energetic contribution to total binding energy using energy decomposition scheme, which provides important informations about contributing residues to siRNA-dendrimer association. In particular, g_{mmpbsa} [106] is a tool that has been developed to enable the use of the MM-PBSA method in conjunction with the GROMACS package. In general terms, the binding free energy of a dendrimer with siRNA in solvent can be expressed as

$$\Delta G_{binding} = G_{complex} - (G_{dendrimer} + G_{siRNA}) \tag{5.6}$$

where, $G_{complex}$ is the total free energy of the siRNA-dendrimer complex and $G_{dendrimer}$ and G_{siRNA} are total free energies of the isolated macromolecule and nucleic acid in solvent, respectively. Furthermore, the free energy for each individual entity can be given by

$$G_x = < E_{MM} > -TS + < G_{solvation} > \tag{5.7}$$

where x is the dendrimer or siRNA or the complex. $< E_{MM} >$ is the average molecular mechanics potential energy in a vacuum. TS refers to the entropic contribution to the free energy in a vacuum where T and S denote the temperature and entropy, respectively. The last term $< G_{solvation} >$ is the free energy of solvation, which is the energy required to transfer a solute from vacuum into the solvent. The potential energy E_{MM} includes the energy of both bonded as well as nonbonded interactions, and it is calculated based on the molecular mechanics (MM) force-field parameters, as described in Chapter 2. In the MM-PBSA approach, it is calculated using an implicit solvent model. The solvation free energy is expressed as the following two terms

$$G_{solvation} = G_{polar} + G_{nonpolar} \tag{5.8}$$

where G_{polar} and $G_{nonpolar}$ are the electrostatic and nonelectrostatic contributions to the solvation free energy, respectively. The electrostatic term is estimated by solving the Poisson Boltzmann (PB) equation, which is a second order nonlinear elliptic partial differential equation, given by

$$\nabla[\epsilon(r)\nabla\varphi(r)] - \epsilon(r)\kappa(r)^2 sinh[\varphi(r)] + \frac{4\pi\rho(r)}{kT} = 0 \tag{5.9}$$

where $\phi(r)$ is electrostatic potential, $\epsilon(r)$ is the dielectric constant and $\rho(r)$ is the fixed charge density. κ^2 is related to the reciprocal of Debye length which is dependent on the ionic strength of the solution. Unfortunately, this method does not take into account the entropic term and therefore in principle is unable to give the absolute binding energy; the tool is useful for calculating relative binding energies, decomposing energy contributions on a per residue basis.

5.3 Results

5.3.1 Conformational Stability Analysis

SiRNA System Analysis

For a first check of the stability of siRNA structure, a conformational analysis was performed: here results for the time evolution of Solvent Accessible Surface Area and Radius of Gyration for 100 ns of MD simulation are reported (Fig. 5.3).
In particular, a stable value around 97 nm^2 of SASA is shown by simulation data, thus, concerning the trend of R_g over time, after a little reorganization there are not visible variations of the value that reaches almost to the beginning of the simulation 2.4 nm. The resulting data are synthesized in the Table 5.2, in which the hydrophobic and the hydrophilic components of the SASA are distinguished and for which the second is greater and predominant with a calculated value of $\sim$ 72.09 percentage of the total. From the measurements obtained of R_g and SASA over time it follows that siRNA system is stabilized and it can be used together with every dendrimer model already prepared in order to build the complex systems, which are the topic of interest in this thesis work.

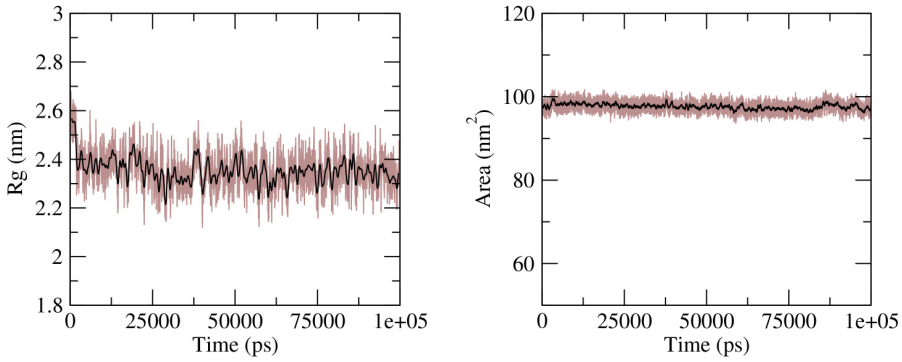

Figure 5.3: *Time evolution of Radius of Gyration (left) and Solvent Accessible Surface Area (right) for siRNA over 100 ns of MD simulation.*

Rg (nm)	Total SASA (nm^2)	Hydrophobic component (% of total)	Hydrophobic component (% of total)
2.40 ± 0.1	97.63 ± 1.07	27.91 ± 1.3	72.09 ± 1.4

Table 5.2: *Radius of Gyration (left) and Solvent Accessible Surface Area components (right) as a percentage of total (average value and standard deviation) for equilibrated siRNA.*

Complex System Analysis

Concerning with the complexation between siRNA and dendrimer, before conducting an equilibrium investigation some conformational stability analysis has been performed. Here is reported the time evolution of Root-Mean-Square Deviation (RMSD) in order to evaluate the system stability during MD simulation.
The relative plots are presented in Fig. 5.4 for whole complex, distinguishing dendrimer and siRNA RMSD. The RMSD data show that all the systems converge to the equilibrium with good stability. Moreover, the plots highlight for all considered components the parameter reach a plateau, showing a relative stable trend after $\sim$ 25 ns. It mainly happens for all siRNA-DG complex systems and siRNA-DP for G1 and G2, differently for siRNA-DM G2 and siRNA-DP G3 to whom the stability is reached only after $\sim$35 ns of simulation, before which occurs a reorganization of the whole structure.
These observations further confirm that complex systems such as presently studied need more time to reach equilibrium compared to a simple one, as dendrimer systems presented in the previous chapter that needed less stabilization time.
To evaluate the interaction area between siRNA and dendrimer along the simulation time, their relative Buried Surface Area (BSA) has been studied. The results for the three systems are plotted in Fig. 5.5, discriminating dendrimer generations.
From the pictures is evident that all the complexes were formed around 15 ns of simulation; in details,all siRNA-G1 dendrimer reach a stable complex configuration after just 5 ns.
Differently, the others (expecially DM-G3/G2 and DG-G3/G2) exhibit a longer feature with dendrimer and siRNA detached, until the time of binding after $\sim$ 15 ns of simulation or later.
All other dendrimers fit with siRNA structure in a binding configuration in a very short time, however the visible fluctuations in the graphs reflect the movement and the adaptation of the two structure (siRNA and dendrimer) before the formation of a stable complex.

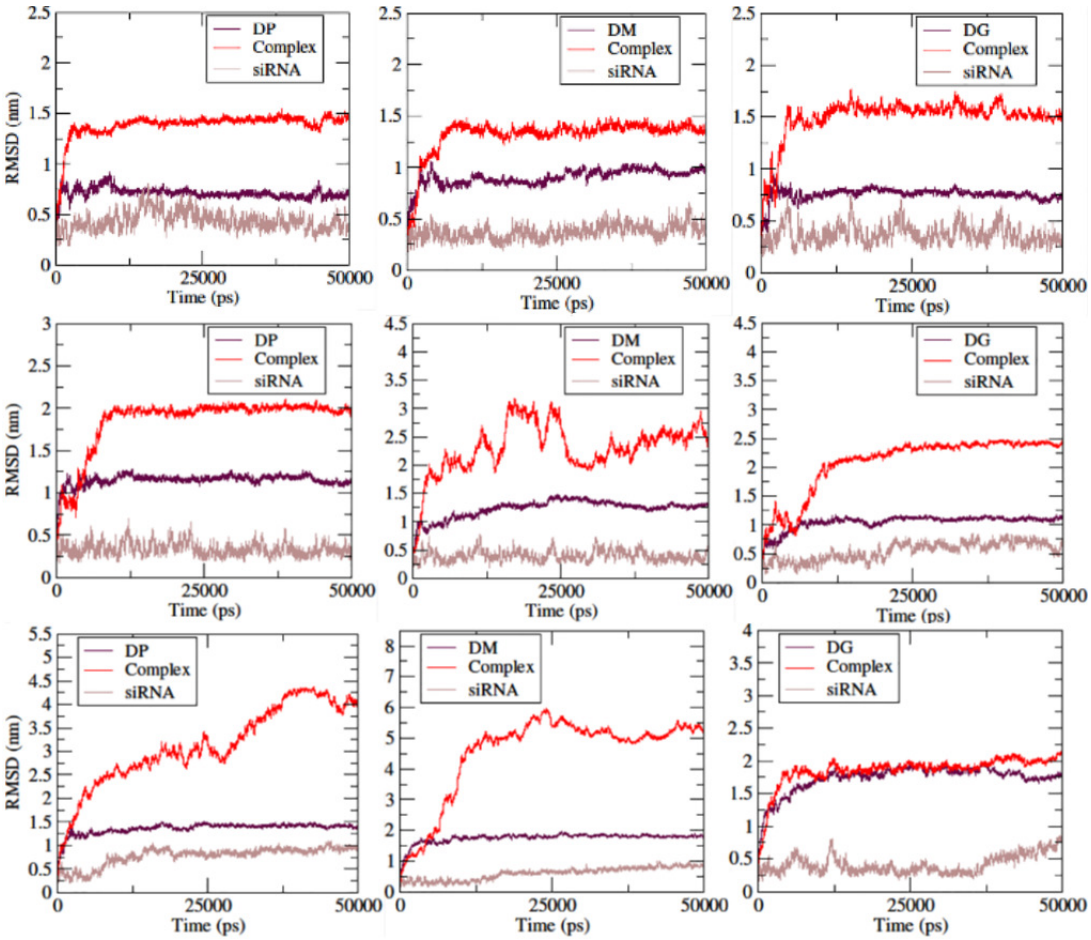

Figure 5.4: *Time evolution of total Root-Mean-Square Deviation (RMSD) distinguishing the whole complex, siRNA and dendrimer components, for all dendrimer generations: G1; G2; G3.*

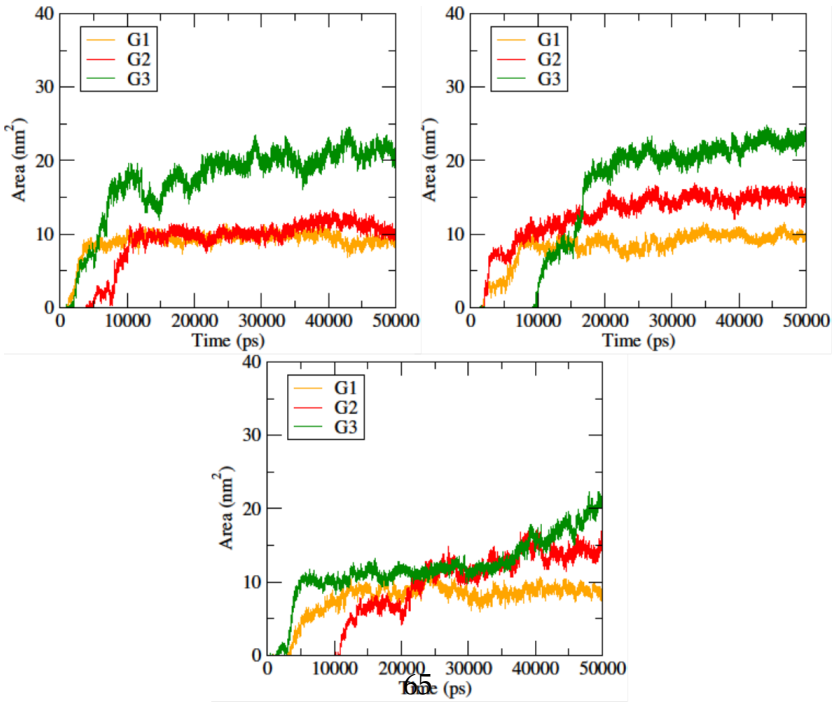

Figure 5.5: *Time evolution of Buried Surface between siRNA and three types of dendrimers: DP (a); DM (b); DG (c), distinguishing three generations.*

5.3.2 Equilibrium Quantitative Analysis of siRNA-dendrimer Complex

The Cluster Analysis has been used to find the best equilibrium configuration for the complexes.
As done previously for unbound dendrimers, for each molecular system the center of the most populated cluster has been considered as input for the equilibrium quantitative analysis and for electrostatic calculations of the siRNA-dendrimer complexes. It represents more than 80% of the MD trajectory; the resulting snapshots of the equilibrated siRNA-dendrimer complex configurations are reported in Fig. 5.6-5.8.

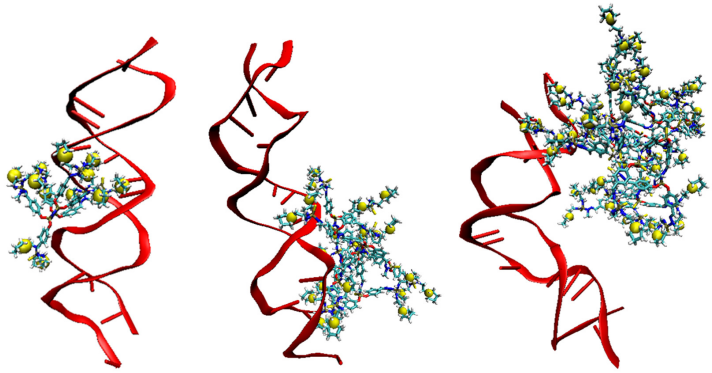

Figure 5.6: *Equilibrium configuration of the binding between siRNA (red) and DP dendrimer, distinguishing dendrimers generations: G1 (a); G2 (b); G3 (c). Ions of dendrimer terminal groups are highlighted in yellow.*

In detail, in the pictures nucleic acids are represented as red ribbons and surface amines that carry a one charge are represented as spheres coloured in yellow; the core of dendrimer is highlighted with the red color and for clarity water and ions are not shown. However, this specific representation of complex models helps to better understand the differences between the siRNA binding modalities of globular dendrimers (as generation 4) and flexible ones (lower generations). This behaviour together with the different electrostatic interactions inside the complex will be investigate using APBS method.
The snapshots related to all G3 dendrimers highlight a significant decrease of siRNA length during the MD simulation, caused by a winding around the dendrimer.
The reason here can be found in the presence of the terminal uracil in the nucleic acid strand, which add flexibility and with its proximity to dendrimer can wrap itself around it.

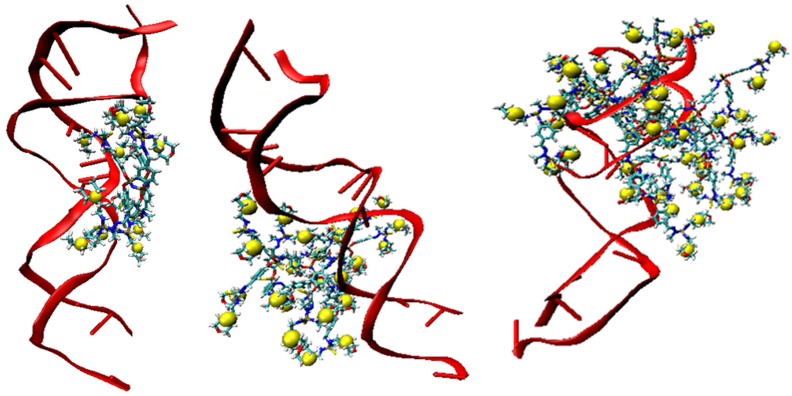

Figure 5.7: *Equilibrium configuration of the binding between siRNA (red) and DM dendrimer, distinguishing dendrimers generations: G1 (a); G2 (b); G3 (c). Ions of dendrimer terminal groups are highlighted in yellow.*

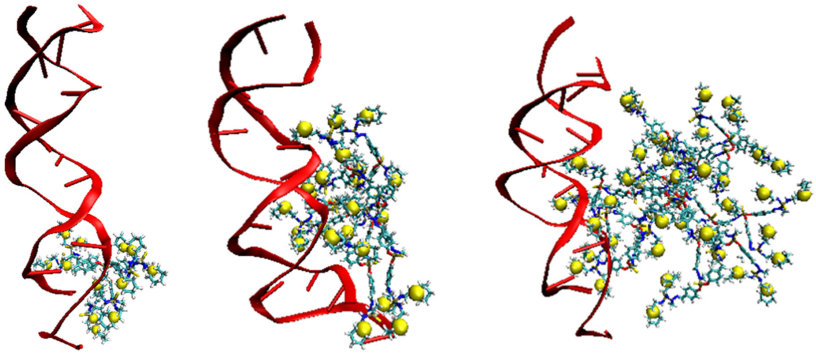

Figure 5.8: *Equilibrium configuration of the binding between siRNA (red) and DG dendrimer, distinguishing dendrimers generations: G1 (a); G2 (b); G3 (c). Ions of dendrimer terminal groups are highlighted in yellow.*

The results of quantitative analysis are here discussed in order to find remarkable characteristics of every siRNA-dendrimer system under investigation.
During the binding to an oppositely charged macromolecule, the bases of siRNA involve in the interaction undergo some alteration and become locally distorted to accommodate the dendrimer moieties.
This involves in a local stretching of the phosphate backbone that alters and reduces some degree of freedom at the binding zone[107].

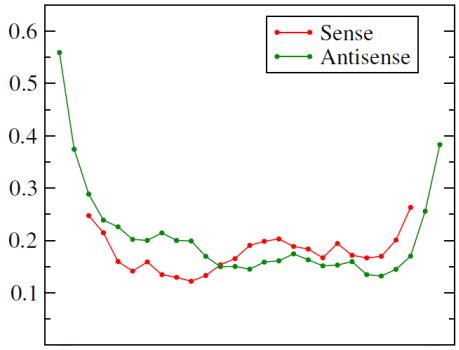

Figure 5.9: *Representation of RMS fluctuations of siRNA base pairs within the complex.*

RMS fluctuations of siRNA base pairs within the complex have been computed. The structural flexibility of border bases of siRNA during the binding process is confirmed by a significant raise in RMSF of border nucleotides of siRNA antisense strand (Adenine and Guanine, as shown in Fig. 5.9).
The value of RMSF increases over 0.6 nm and it is directly related to a higher solvent exposure after a partial siRNA opening.
The antisense strand is more exposed to dendrimer contact because of the presence of four unpaired nucleotides, which are located at the two extremes (Adenine-Guanine and Adenine-Uracil, respectively).
Moreover, in order to identify the nucleotides that are mainly responsible for siRNA-dendrimer interaction by contact probability plots, for each system MD trajectory at 300 K was analysed. The siRNA residues contact probability to dendrimer has been calculated, applying a distance cut-off of about 0.28 nm (roughly the diameter of a water molecule).
SiRNA bases mainly responsible for complex interaction have been identified by contact probability plots (Fig. 5.10-5.12).
As a result, analysing all systems specific residues most frequently involved in the binding. Considering DP dendrimers, particularly, uracil and cytosine are the mostly part of the contact area with over the 90% of siRNA contact probability, except for G2 which exhibit a value around 85%. Thus, comparing all different macromolecules, nucleotides are strongly involved in the interaction with DP dendrimers, as demonstrated by the high contact probability values.
Moreover, also in siRNA/DM-G2 and siRNA/DG-G3 interaction interface participate primarily cytosines and uracils of sense and antisense strands, with high contact probability around 90%.
Otherwise, lower contact probability values and lower number of nucleotides involving the interaction were detected in case of all siRNA-G1 dendrimers (and also G2), which have weaker electrostatic attraction caused by fewer positively charged amine groups available for the interaction.

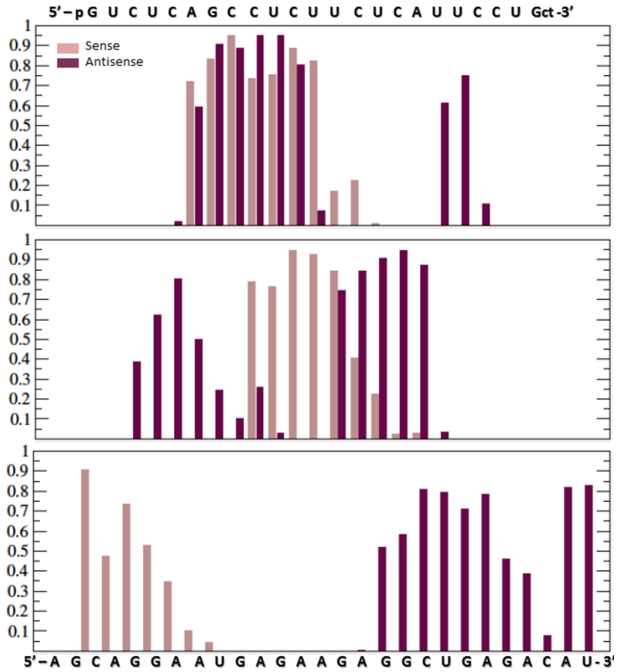

Figure 5.10: *Nucleotides that are mainly responsible for siRNA-dendrimer interaction have been identified by contact probability plots in case of DP, DM and DG generation one systems.*

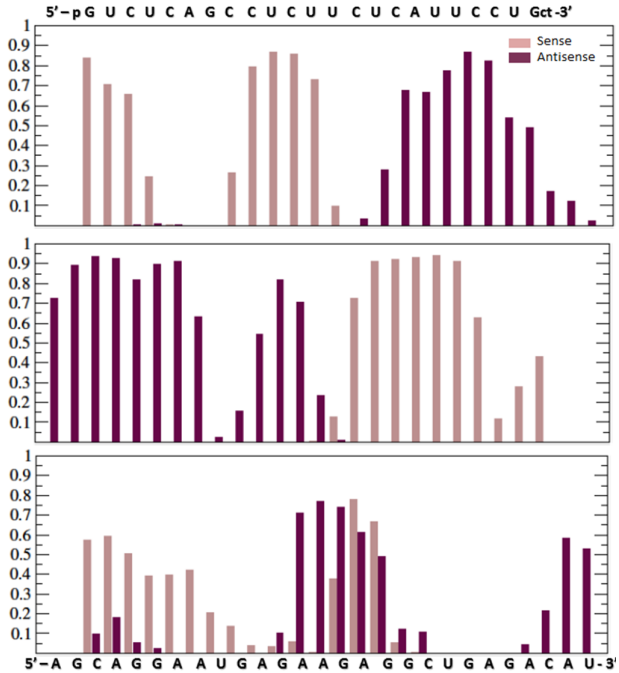

Figure 5.11: *Nucleotides that are mainly responsible for siRNA-dendrimer interaction have been identified by contact probability plots in case of DP, DM and DG generation two systems.*

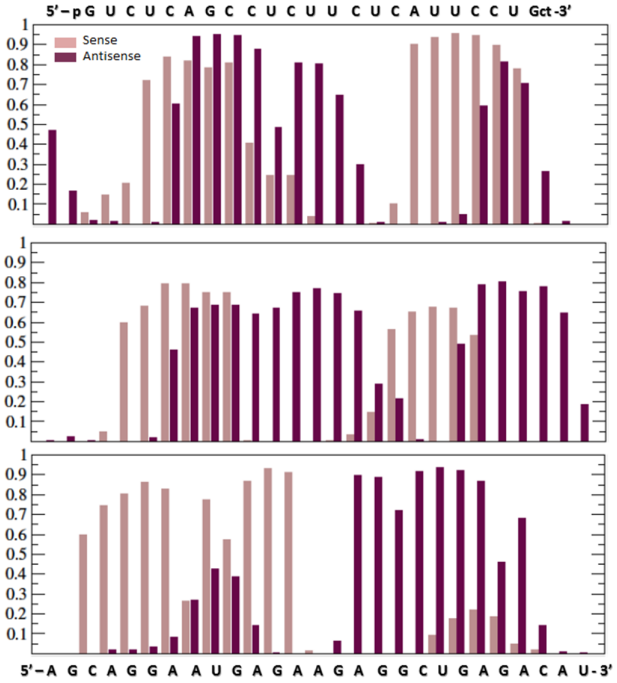

Figure 5.12: *Nucleotides that are mainly responsible for siRNA-dendrimer interaction have been identified by contact probability plots in case of DP, DM and DG generation three systems.*

Furthermore, we have analyzed the MD trajectories in order to characterize the conformational changes of dendrimers upon binding.
Considering the flexibility/rigidity ratio as one of the five critical parameters (size, shape, surface chemistry, flexibility/rigidity, and molecular geometry) [84], the value of the Radius of Gyration of the whole complex and those of the dendrimer and siRNA in binding condition has been evaluated for all equilibrated systems.
In fact, the level of reorganization in a specific structure is provided by these R_g values.
The averages of Radius of Gyration obtained from the analysis are summarized in Table 5.3 along with the relative standard deviations; we observe that with the increase of generation grows the value of R_g due to the greater amine density and branching units.
In the Fig. 5.13 are represented the average values and the error bars of R_g as function of dendrimer generation, comparing the case of siRNA and the three dendrimers within the complex.
Particularly, siRNA R_g presents no significant variations between dendrimers generations and the value remains around 2.25 nm; differently, with the increase of generation R_g of all three dendrimers grows from $sim1$ nm (for G1) to $\sim$ 2.35 nm (with a maximum value of 2.47 for DG dendrimer).

System	R_g(nm) **Complex**	R_g(nm) **siRNA**	R_g(nm) **Den**	R_g(nm) **Ter**
siRNA-16/CEF/051 **G1**	2.15 ± 0.04	2.12 ± 0.05	1.00 ± 0.12	1.20±0.03
siRNA-16/CEF/051 **G2**	2.32 ± 0.09	2.30 ± 0.05	1.40 ± 0.03	1.68±0.02
siRNA-16/CEF/051 **G3**	6.05 ± 0.21	2.24 ± 0.04	1.78 ± 0.05	2.09±0.03
siRNA-16/CEF/294 **G1**	2.27 ± 0.07	2.23 ± 0.04	1.02 ± 0.03	1.20±0.01
siRNA-16/CEF/294 **G2**	4.75 ± 0.26	2.28 ± 0.05	1.34 ± 0.03	1.58±0.02
siRNA-16/CEF/294 **G3**	7.48 ± 0.23	2.25 ± 0.05	1.80 ± 0.08	2.06±0.03
siRNA-mk016 **G1**	2.37 ± 0.06	2.31 ± 0.06	1.00 ± 0.03	1.15±0.02
siRNA-mk016 **G2**	2.13 ± 0.03	2.25 ± 0.04	1.42 ± 0.04	1.66±0.02
siRNA-mk016 **G3**	2.41 ± 0.05	2.24 ± 0.06	1.90 ± 0.03	2.23±0.02

Table 5.3: *Average value and standard deviation of Radius of Gyration (R_g) of the Complex, as composed by dendrimer and siRNA, of the single nucleic acid (siRNA), of the dendrimer for different generations.*

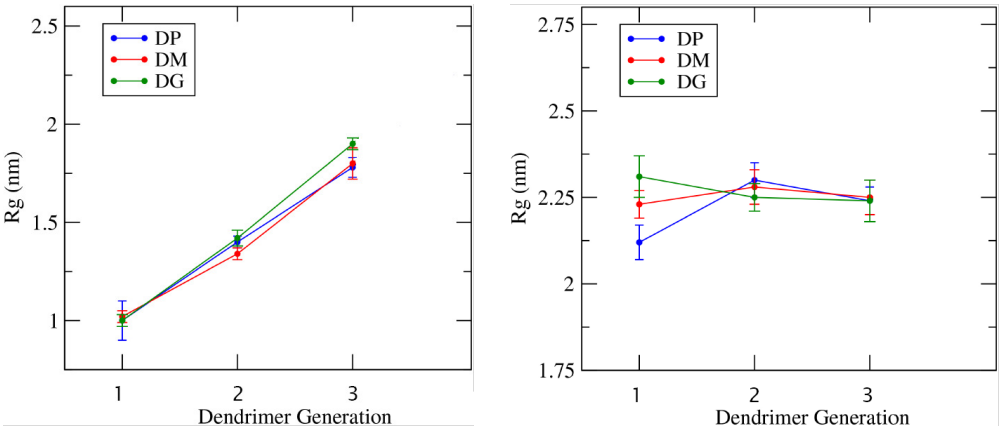

Figure 5.13: *Average value and error bar of R_g as a function of dendrimer generation. (a) Comparison of Rg of all dendrimers; (b) comparison of R_g value for siRNA in complex with dendrimers.*

In addition, all R_g of dendrimers are characterized by small fluctuations, which implies that they undergo very little deformation during the simulations. In the binding process the biggest part of the siRNA double helix still remains outside the dendrimer, and this reflects in the R_g of siRNA being larger than the dendrimer one. Moreover, the siRNA is a duplex, and the base pairing/stacking interactions between the opposite strands concur to confer an intrinsic rigidity to the overall structure, preventing a substantial wrapping of the nucleic acid around the dendrimer surface. The highest value of R_g is reached by the DM complex for which indeed is found a particular dovetail between siRNA and dendrimer (as seen in relative snapshot above).

Moreover, the different adaptability of smaller (G1) and biggest generations (G3) have an impact on the dendrimer-siRNA complexes, thus the second ones present charged amine terminal groups that electrostatically repulse to each other, contributing to form a broader structure, judging by the values of radius of gyration.
Another interesting consideration concerns the changes in conformation of dendrimers upon binding that can be assessed by comparing the R_g of the dendrimer and of cationic end groups, the higher values of this second ones reflects the orientation of external charged groups on the periphery toward the siRNA. The average value of total SASA for siRNA is 97.96 nm^2 with a hydrophobic percentage of 27.3 $\pm$ 1.3 and hydrophilic 72.7 $\pm$ 2.0 % of the total.
The values obtained for all dendrimers are not nearly different to the ones related to only dendrimers system and show a prevalence of hydrophobic component, with a percentage around 88 for DP and DG and around 82 for DM dendrimers. Below in Fig. 5.14 are reported the average values and relative error bars, comparing dendrimer and siRNA SASA components.

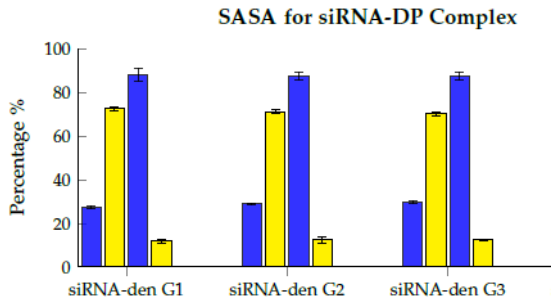

(a)

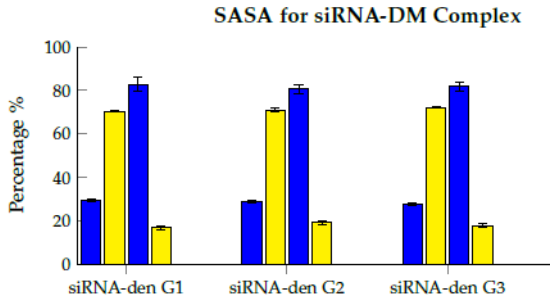

(b)

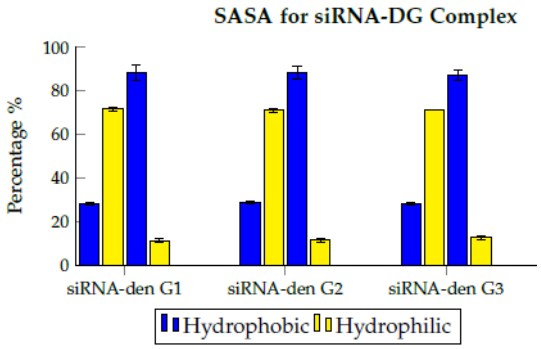

(c)

Figure 5.14: *Histograms of average values, comparing dendrimer and siRNA SASA components.*

The R_g considerations are also supported by the analysis of the solvent-accessible surface area SASA, for which histograms that distinguish hydrophobic and hydrophilic component for dendrimers and for siRNA have been reported within the complex. From results, it is highlighted the prevailing hydrophobic and the hydrophilic components of dendrimer and acid nucleic, respectively. In details, comparing the values with the ones founded in the previous chapter for unbounded dendrimers, there are no significant variations in the SASA of dendrimers in complex with siRNA. The highest percentage of hydrophilic component (around 18 % of total SASA) for the dendrimer remains evident in compared to others, due to atomic

constitution of morpholinium (terminal groups), with a maximum average value of 19.4 % for DM-G2 dendrimer.
Moreover, the RDF profiles calculated over equilibrium configurations suggest how the structures may behave in space over time.

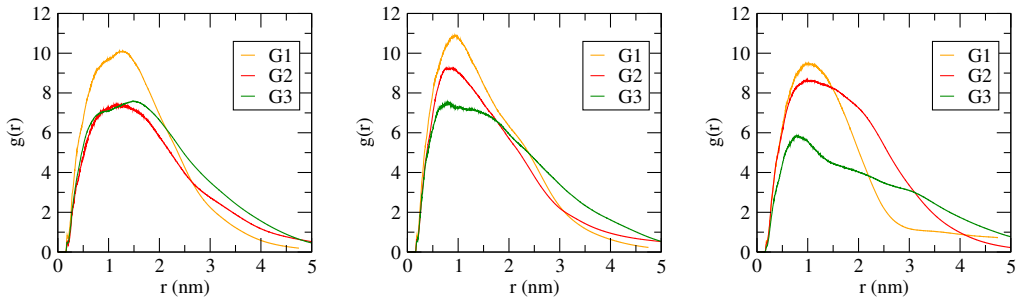

Figure 5.15: *Equilibrium Radial Distribution Function (RDF) of dendrimer in reference to siRNA for all generations of three dendrimers: DP (a); DM (b); DG (c).*

On one hand, in the RDF plots sharp peaks correspond to a large number of atoms confined both spatially and temporally, on the other hand large features correspond to less confined, rapidly reorganizing domains.
Concerning the RDF of whole dendrimer in reference to siRNA (Fig. 5.15), the radial distance over which density remains almost constant increases with increasing dendrimer generation. For high generation dendrimers (G3), there is a constant density zone from 1 to 3.5 nm of distance, signifying the compact nature of the higher generation dendrimer. This may be a consequence of the higher level of extended branches on the dendrimer as observed in the simulation snapshots of the dendrimers and it provides informations about the spatial arrangement of the terminal groups. Otherwise, for lower dendrimer generations a region of high density is visible near the phosphates of siRNA, since the branches are not spread out. In each case, the density shows a maximum and the overall density decays more gradually. The peak of the radial distribution function shifts with the increase in generation and the result is that the higher generation dendrimers are more rigid when compared to the lower generation dendrimer. This phenomenon is accentuated by the electrostatic repulsion between a higher number of terminal groups.
The non-uniformity in peak height in the RDF profile suggests a difference in the ability of the two regions to readily vibrate. The rigid core region is forbidden from free vibrations in comparison to the oscillations that occur at the terminal groups of the dendrimer. In general, each layer of surface groups added to the further generation tends to saturate the surface of the dendrimer, meaning the molecule is less able to orient its active groups toward the target to optimize the interactions and

the efficiency of the scaffold to use each surface group decreases, it results in a switch from flexible to rigid behaviour of dendrimers in the binding with siRNA.

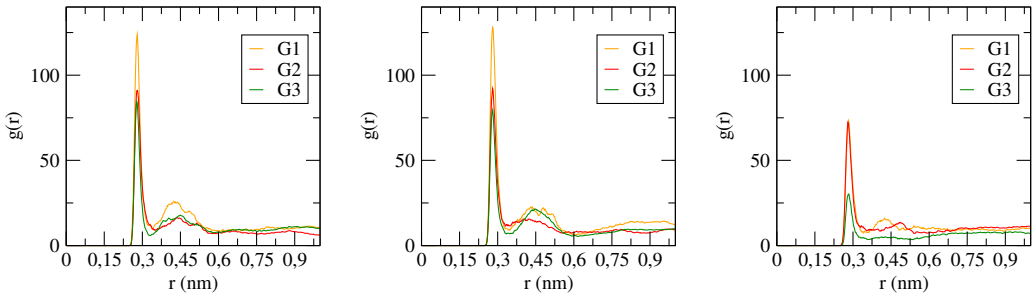

(a) (b) (c)

Figure 5.16: *Equilibrium Radial Distribution Function (RDF) of amine groups around O1P and O2P siRNA atoms for all generations of three dendrimers: DP (a); DM (b); DG (c). Only charged amine groups are considered for the calculation.*

In addition, the equilibrium RDF of amine groups around O1P and O2P siRNA atoms has been studied in order to investigate the nature of the interactions between protonated amine groups and siRNA phosphate group oxygen atoms, as done in previous works [108], and the results are shown in Fig. 5.16.
The pictures are characterized by two different peaks at 2.7 and 4.3 angstrom, in agreement with previous computational observations [109]. Importantly, the first peak assesses the primary interaction resulting from the hydrogen bond between the amine hydrogen atoms and the phosphate oxygen, while the second peak is related to the water-mediated hydrogen bonding. In the Table 5.4 the average number of amine groups of each dendrimer for different generations, interacting with siRNA O1P and O2P atoms averaged over the last 20 ns of each Molecular Dynamics trajectory at 300 K has been reported. It shows the percentage of amine groups that participate in the interaction with oxygen and phosphate atoms of siRNA. Furthermore, the principal differences observed in terms of peak heights have been calculated by the measurement of contacts between the amine nitrogen atoms involved in primary or secondary interactions with the phosphate oxygens over the last 20 ns of MD trajectory at 300 K.
For an integral analysis of interactions within the complex, the RDF of charged amine groups around electronegative atoms in siRNA grooves has been developed (Fig. 5.17).
In details, G1-dendrimers are able to interact with a high number of phosphate groups through their amine groups, following by G2 ones. It is due to the flexible nature of their structures and it's a crucial point because these dendrimers exhibit the alignment of their backbone with the siRNA phosphate groups in the major grooves. Otherwise, the flexibility loss moving to higher generations and it follow

System	Total amines groups	**Primary** %	**Secondary** %	% **Total Amines**
siRNA-16/CEF/051 **G1**	12	83	17	100
siRNA-16/CEF/051 **G2**	24	54	4	58
siRNA-16/CEF/051 **G3**	48	50	15	65
siRNA-16/CEF/294 **G1**	12	75	8	83
siRNA-16/CEF/294 **G2**	24	46	13	59
siRNA-16/CEF/294 **G3**	48	35	10	45
siRNA-mk016 **G1**	12	67	8	75
siRNA-mk016 **G2**	24	71	12	83
siRNA-mk016 **G3**	48	23	13	36

Table 5.4: *Average number of amine groups of each dendrimer for different generations, interacting with siRNA O1P and O2P atoms averaged over the last 20 ns of each Molecular Dynamics trajectory at 300 K.*

that dendrimers are not capable so well to align with the siRNA's phosphate groups. DP dendrimers show the best ability of aligning with siRNA backbone (except for DP-G2), with high values of amine groups interacting with siRNA (100 % of total for DP-G1).

Moreover, also amine groups of DP-G3 despite their stiffness, interact with the electronegative atoms in the siRNA backbone with average values of 65 and 38 % of total (Table 5.5). It is evident that the terminal groups of the first three generations of dendrimers present high spatially connected with the siRNA structure, for which the majority of distribution state at a distance lower than 2 nm; with the increase of generation the spatial density changes.

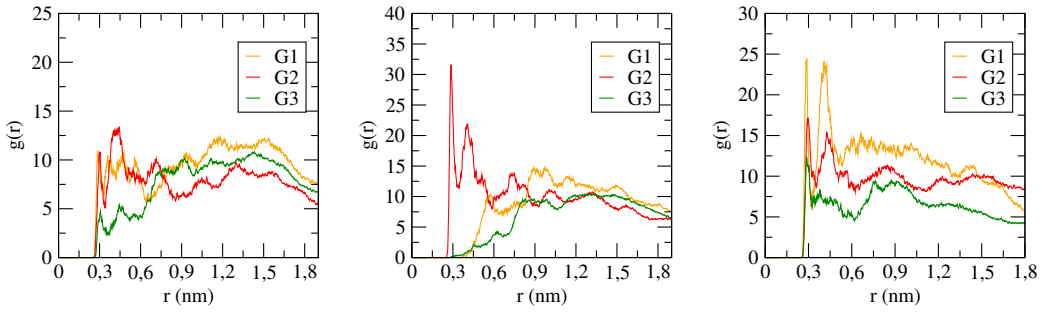

Figure 5.17: *Equilibrium Radial Distribution Function (RDF) of amine groups around electronegative atoms in siRNA grooves for three dendrimers for all generations of three dendrimers: DP (a); DM (b); DG (c). Only charged amine groups are considered for the calculation.*

System	Total amines groups	**Primary** %	**Secondary** %	% **Total Amines**
siRNA-16/CEF/051 **G1**	12	17	8	25
siRNA-16/CEF/051 **G2**	24	8	17	25
siRNA-16/CEF/051 **G3**	48	8	15	23
siRNA-16/CEF/294 **G1**	12	8	17	25
siRNA-16/CEF/294 **G2**	24	12	13	25
siRNA-16/CEF/294 **G3**	48	4	12	16
siRNA-mk016 **G1**	12	25	25	50
siRNA-mk016 **G2**	24	13	17	30
siRNA-mk016 **G3**	48	4	6	10

Table 5.5: *Average number of amine groups of each dendrimer for different generations, interacting with electronegative atoms in siRNA grooves averaged over the last 20 ns of each Molecular Dynamics trajectory at 300 K.*

Equilibrium Evaluation of Charges Effect

The equilibrium binding conformations were analysed to describe the electrostatic potential of the resulting complex. Particularly, the electrostatic potentials were computed using the APBS package, by applying the Poisson-Boltzmann equation. The resulting configurations are reported below. The siRNA structure together with the representation of charge distribution and the map of electrostatic interactions founded using Adaptive Poisson-Boltzmann Solver (APBS) method, showing prevalence of negative net charges on the surface of siRNA (Fig. 5.18).

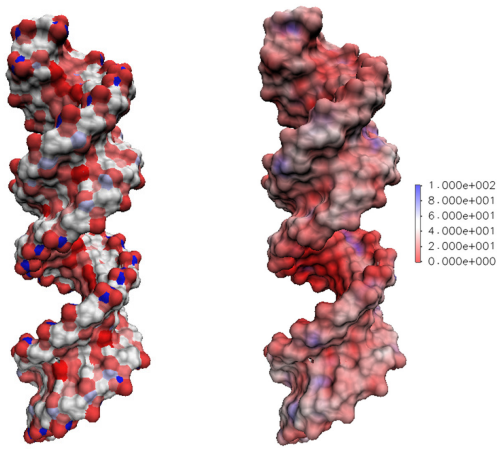

Figure 5.18: *SiRNA representations: the equilibrated structure (left). Map of electrostatics interactions founded using Adaptive Poisson-Boltzmann Solver (APBS) method for siRNA (right, snapshot of the simulation after cluster analysis).*

An accurate investigation of the electrostatic map leads to find different typologies

of binding regions (results are presented in Fig. 5.19-5.21).
Firstly, the negative electrostatic potential of the siRNA is visible in all the complexes. For dendrimers of high generation only a limited part of the charged surface groups interacts actively with siRNA while a larger part of charged amines is back folded. On the other hand, dendrimers of lower generations (flexible), appear to exert both electrostatic and hydrophobic interaction with the siRNA.
This phenomenon leads to formation of merged complexes that appear to be a single neutralized or barely charged entity; it is emphasized for dendrimers of G1 and G2 where the neutralization at the binding of siRNA and dendrimer is visible as a white color in the APBS map. Thus, all dendrimers of first and second generation are able to neutralize the siRNA.
Otherwise, all dendrimers of third generation behave as rigid systems in binding with siRNA leading to complexes of charged patches, as shown in figure where they exhibit a positive net charge and are surrounded by a positive potential, while a negative net charge extends on nucleic acid. This positive potential may allow the formation of multivalent interactions with other siRNA molecules.
Finally, dendrimers of third generation (and also DM-G2) show an intermediate binding behaviour with siRNA, because is both affected by hydrophobic and electrostatic forces which are distributed over a larger and more rigid molecule.

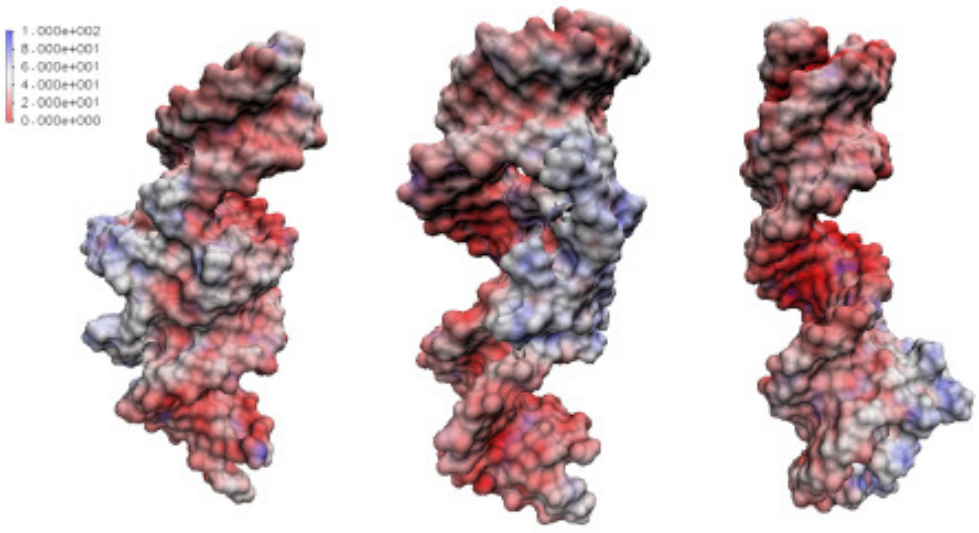

Figure 5.19: *Map of electrostatics interactions founded using Adaptive Poisson-Boltzmann Solver (APBS) method, for generation one of all dendrimers (snapshot of the simulation after cluster analysis): DP (a); DM (b); DG (c).*

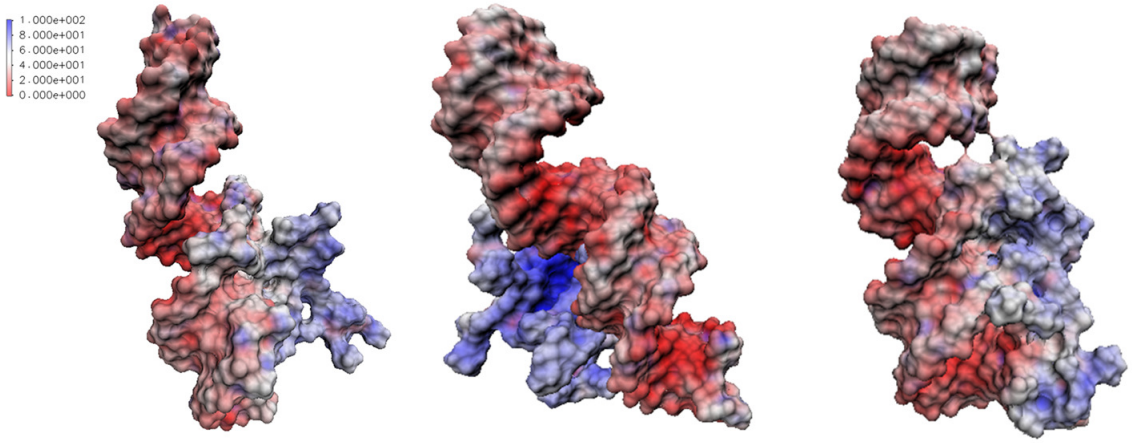

Figure 5.20: *Map of electrostatics interactions founded using Adaptive Poisson-Boltzmann Solver (APBS) method, for generation two of all dendrimers (snapshot of the simulation after cluster analysis): DP (a); DM (b); DG (c).*

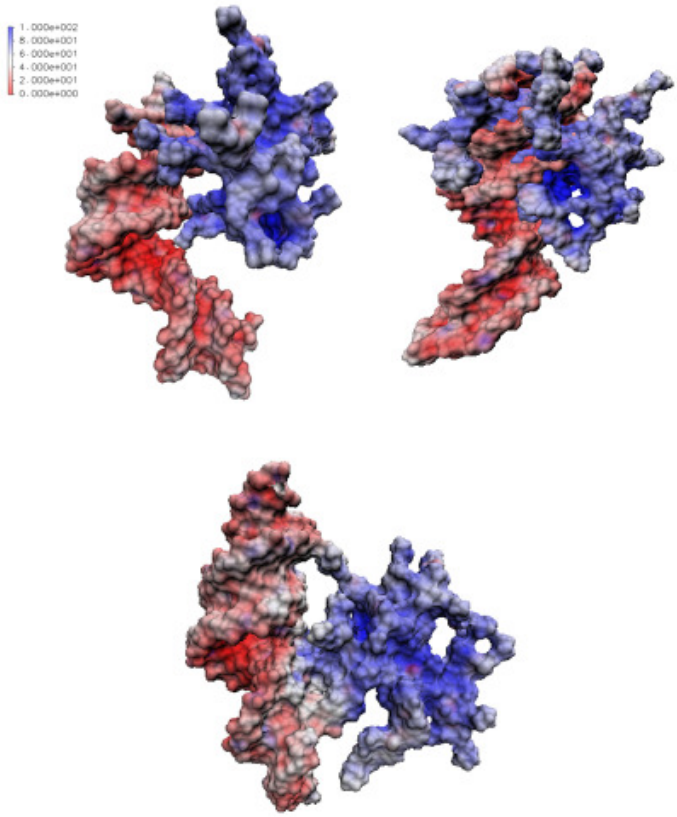

Figure 5.21: *Map of electrostatics interactions founded using Adaptive Poisson-Boltzmann Solver (APBS) method, for generation three of all dendrimers (snapshot of the simulation after cluster analysis): DP (a); DM (b); DG (c).*

Binding Energy Evaluation

To calculate the average binding energy and the associated confidence intervals, a bootstrap analysis was performed, using gg_mpbsa tool.
By decomposing the total dendrimer/nucleic acid interaction energy for each binding residue, we were able to point the attention on those residues that actively participate to the binding.
In order to obtain the average contribution of all residues (of dendrimer and siRNA) to the binding energy, it was used a python script.
Below are plotted the energetic contribution of single residues of the complex (Fig. 5.22-5.24).
All the plots reported the first 50 residues, as shown in the pictures, belonging to siRNA, thay are separated from the dendrimer residues by a red line. Clearly, with the increase of dendrimer generation grows also the number of residues.
From pictures is visible that the principal dendrimer energetic contribution comes from terminal groups of dendrimer, highlighted by a colored square, otherwise core and other internal branches do not make significant contribution.
For complex with dendrimers of first and second generation, the contribution is given primarily by all terminal groups of dendrimers, denoting their flexible behaviour and the high binding nature that their form with siRNA.
Differently, with the increase of generation (and also the number of peripheral units), not all terminal groups participate in binding and the energetic contribution of siRNA is almost of the same order then the dendrimer one.
As has already been observed by related snapshots, for DP-G3 dendrimer the contribution comes from a large number of terminal groups and evenly from all the siRNA strands, it reflects the different binding conformation which is formed for this complex.

In addition, to calculate average binding energy, a python script has been used and here are reported the resulting average and standard deviation values of all energetic components including the binding energy for all different dendrimers.
The Tables 5.6-5.8 below contain average values and standard deviations for all the systems (compared for different dendrimer generation).
The energetic contributions consider Van der Waals, Electrostatic, Polar Solvation, Sasa apolar component and binding energy.
Because of the limits of gg_mpbsa tool [106], this energy calculation does not take into account the entropy term, which is fundamental to a correct estimate of free energy.

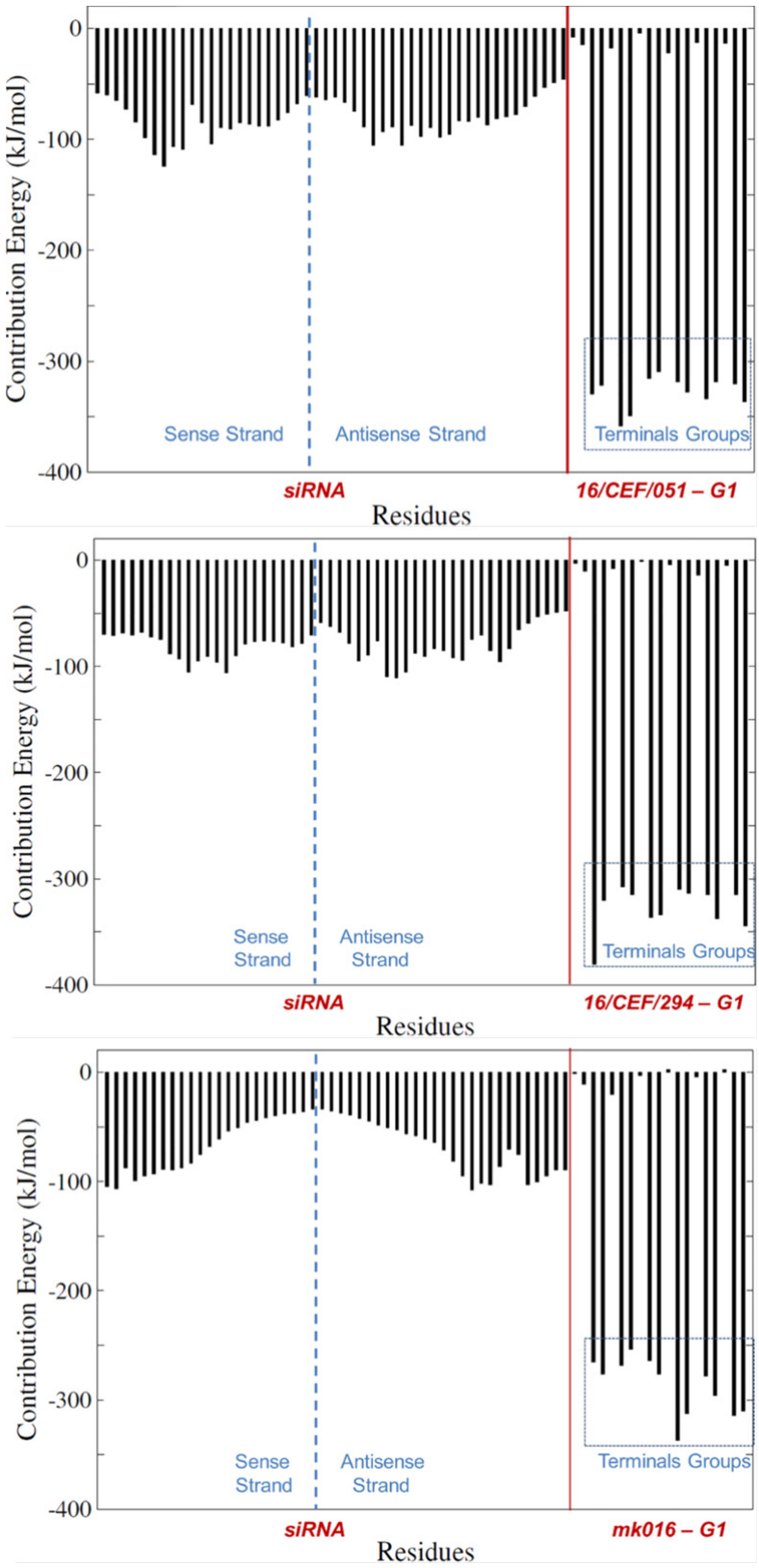

Figure 5.22: *Contribution of residues to the binding energy found with MM-PBSA method, for all dendrimer: G1.*

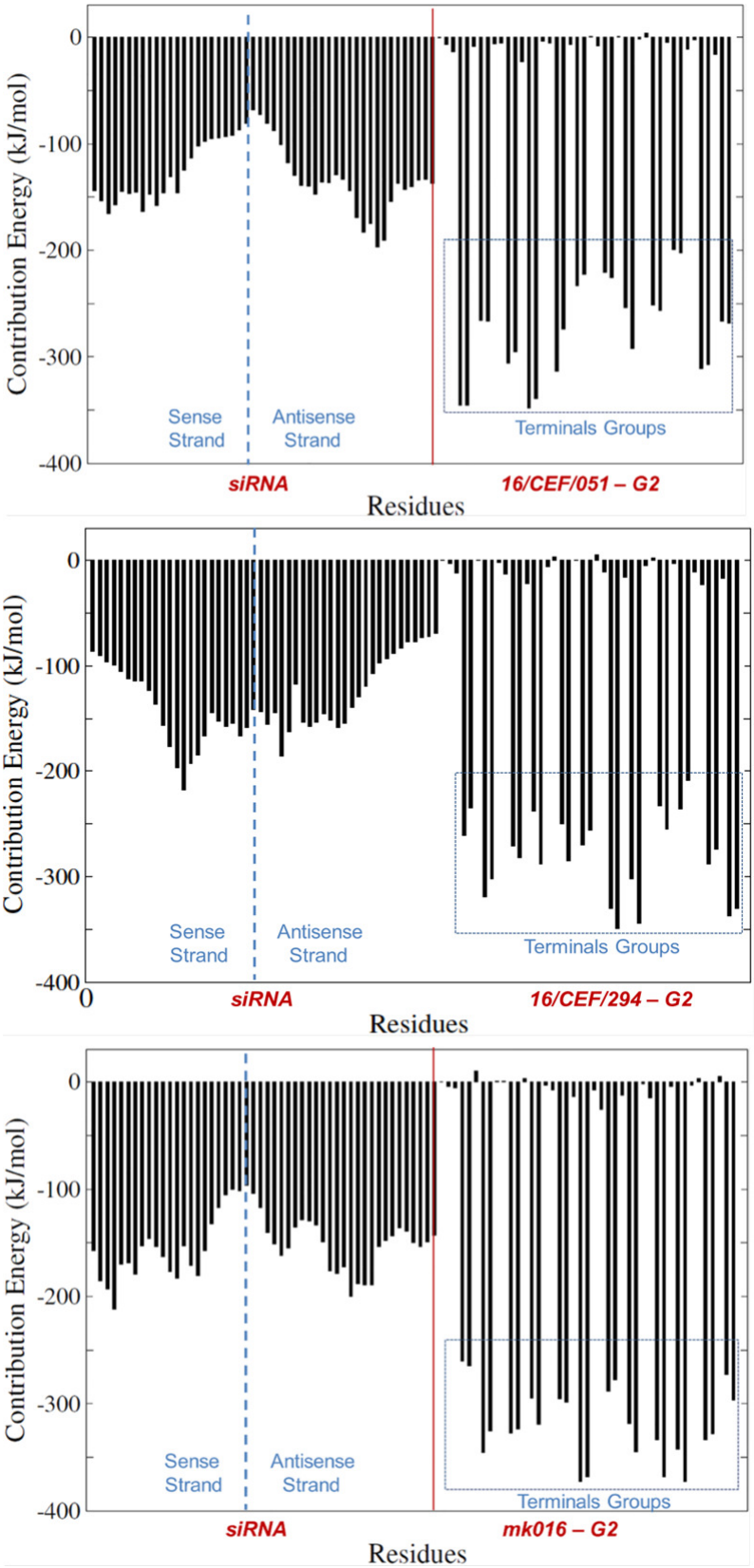

Figure 5.23: *Contribution of residues to the binding energy found with MM-PBSA method, for all dendrimer: G2.*

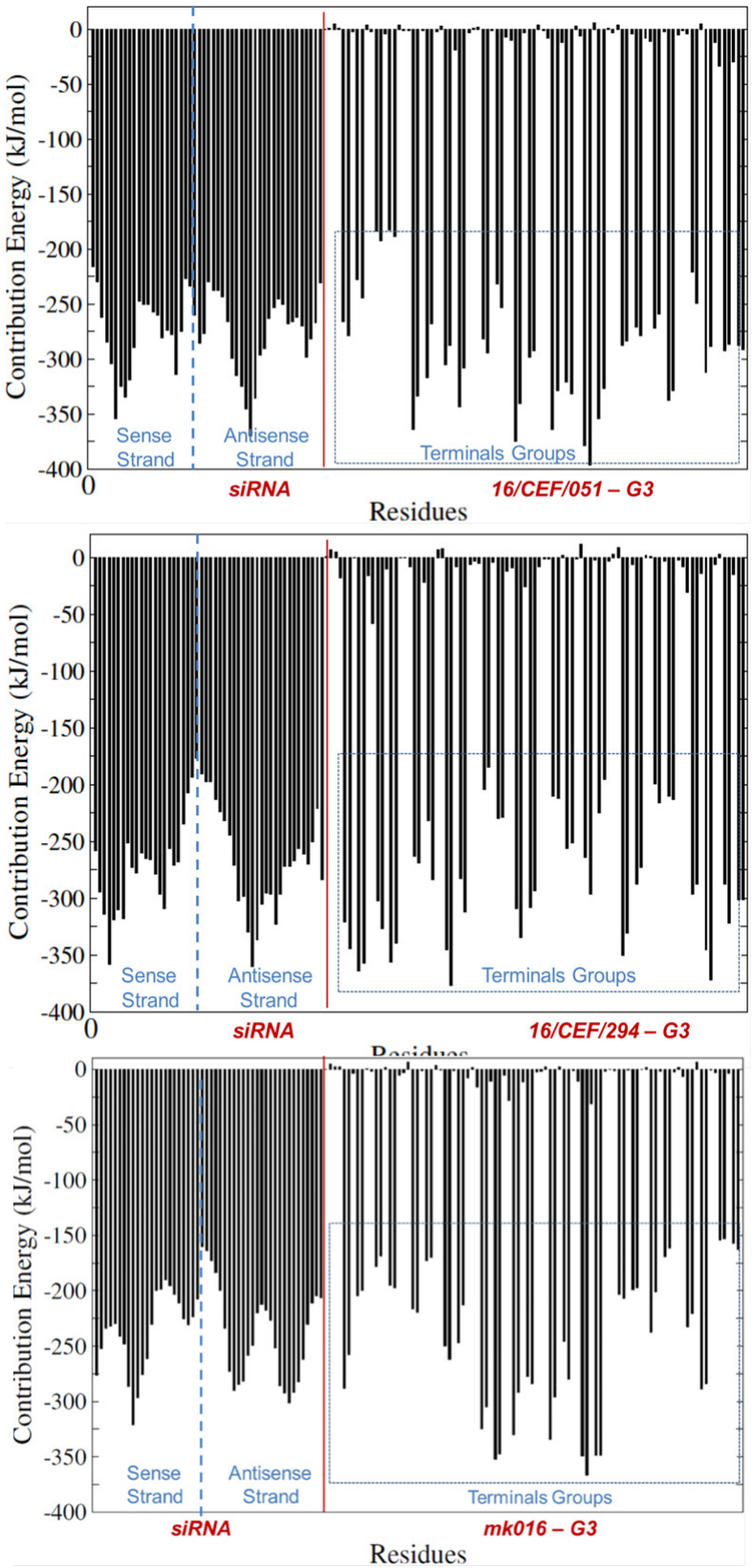

Figure 5.24: *Contribution of residues to the binding energy found with MM-PBSA method, for all dendrimer: G3.*

Energy Components (kJ/mol)	siRNA-DP G1	siRNA-DP G2	siRNA-DP G3
Van der Waals	-394.15±42.6	-428.73±51.6	-965.94±58.1
Electrostatic	-10218.96±207.3	-15602.62±440.6	-33122.32±118.9
Polar Solvation	2522.70±182.2	2755.50±302.4	6177.66±234.1
SASA	-41.69±3.4	-45.99±4.5	-92.90±2.9
Binding	-8132.11± 187.4	-13321.84±416.0	-28003.50±54.2

Table 5.6: *Average and standard deviation of all Energetic Components for siRNA − DP complex.*

Energy Components (kJ/mol)	siRNA-DM G1	siRNA-DM G2	siRNA-DM G3
Van der Waals	-385.90±47.3	-688.83±18.3	-1113.24±14.9
Electrostatic	-9895.50±213.2	-16807.93±136.6	-32292.32±82.4
Polar Solvation	2351.55±270.0	4040.18±61.0	6059.15±28.1
SASA	-41.61±3.9	-67.83±0.2	-98.66±2.5
Binding	-7971.46± 118.2	-13524.42±57.0	-27445.07±122.9

Table 5.7: *Average and standard deviation of all Energetic Components for siRNA − DM complex.*

Energy Components (kJ/mol)	siRNA-DG G1	siRNA-DG G2	siRNA-DG G3
Van der Waals	-357.22±45.0	-543.42±115.0	-648.55±132.1
Electrostatic	-8643.93±198.3	-17794.19±597.9	-25777.22±2133.1
Polar Solvation	2092.98±265.2	2970.64±494.9	2696.56±592.0
SASA	-39.49±3.8	-55.83±10.3	-62.10±10.2
Binding	-6947± 141.2	-15422.80±289.8	-23791.31±170.3

Table 5.8: *Average and standard deviation of all Energetic Components for siRNA − DG complex.*

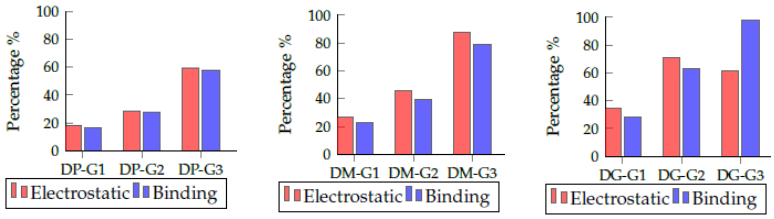

(a) (b) (c)

Figure 5.25: *Histograms of electrostatic contribution and binding energy of siRNA-dendrimers systems: DP (a); DM (b); DG (c).*

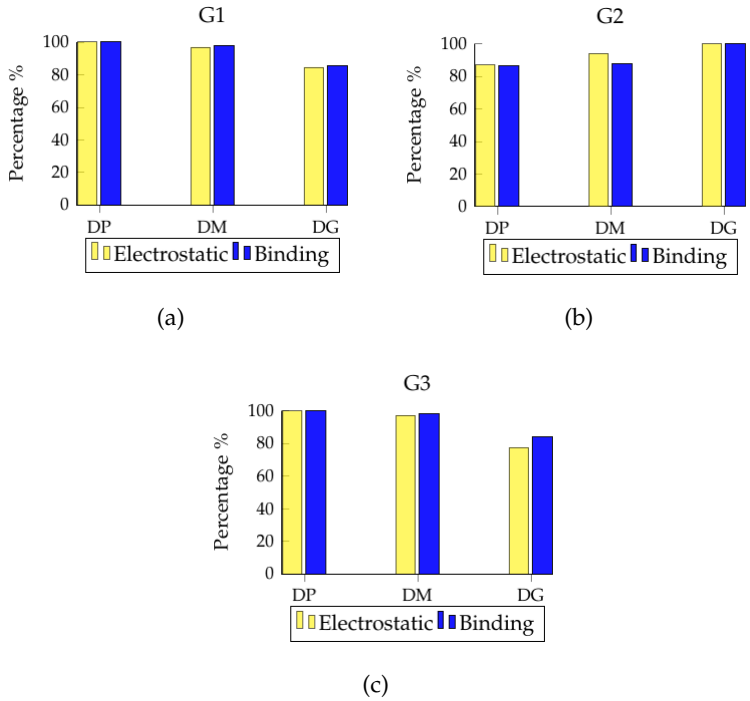

Figure 5.26: *Histograms of electrostatic contribution and binding energy of siRNA-dendrimers systems: G1 (a); G2 (b); G3 (c).*

In addition, the histograms in Fig. 5.25 report the percentage values of electrostatic average contribution and binding energy between different generations of the same dendrimer. It highlights that both the values grows with generation, thanks to the presence of a growing number of charges atoms interacting. Otherwise, the histograms in Fig. 5.25 report the percentage values of electrostatic average contribution and binding energy between same generations of different dendrimers. SiRNA-DP complexes exhibit higher values for G1 and G3, while for G2 siRNA-DG seems to be the complex with the maximum electrostatic and binding contributions.

5.4 Discussion

Owing to several possible applications in gene therapy, the development of molecular systems composed of nucleic acids and macromolecules catches attention in current scientific research. Moreover, the delivery of genetic materials into cells represents a great solution for therapeutic purposes. Among all possible molecule designs devoted to interact with nucleic acids, here the focus is put on the siRNA-dendrimer complex formation at atomistic level.
Molecular dynamics has been used to evaluate interactions between the nucleic acid and the macromolecules along the complex building. In details, 50 ns of MD simulations in the water environment have been carried out for nine siRNA-

dendrimer systems. Here most likely interacting sites were identified, thanks to the description of siRNA and dendrimer conformational changes due to the binding process. From the inspection of all systems emerge a significant information. It is the difference between terminal groups that leads to quantifiable variations in the energetic of binding as well as different conformational responses within the complexes [80]. From the analysis the siRNA-dendrimer complexation seems to be a multi-step process with an initial fast electrostatic binding, mainly driven by charged atoms, followed by slower structural global rearrangements. Our results suggest that DP dendrimers manifest highest binding efficacy.

Moreover, the equilibrium binding conformations have been further investigated to evaluate the electrostatic potential and the charge neutralization mechanisms of the siRNA-dendrimer complex. In particular, data highlight the predominant siRNA-dendrimer interaction between the electronegative phosphates present on siRNA backbone and charged amines of dendrimer terminal groups. In addition, the MD simulations also show siRNA groove binding of the dendrimers.

Furthermore, quantitative examination of the electrostatic contribution suggests interesting differences in the dendrimer binding regions. While G1 and G2 were able to neutralize the siRNA electrostatic potential in the binding region, all G3 were surrounded by a positive potential, which may allow the formation of multivalent interactions with other siRNA molecules. This phenomenon may become significant for larger generation dendrimers, which reveal more compact and rigid configurations. All G1 and G2 dendrimers exhibit the ability to use their surface residues more uniformly, avoiding preferential binding spots into the binding site. This leads to a uniform vibrational behaviour of N and P charged atoms of dendrimer and siRNA and thus in a stable binding for these complexes.

The analysis also show that cytosine and uracil of siRNA play a dominant role in the siRNA-dendrimer contact surface, especially in case of DP dendrimer, wherein nucleotides exhibit high values of contact probability. The results of siRNA-dendrimer contact probability have been compared to residues contribution on electrostatic potential for the equilibrium binding conformations, showing the dominant role of ions of dendrimer terminal groups in the binding process.

Moreover, for a complete analysis of interactions within the complex, the radial distribution function of charged amine groups around electronegative atoms in siRNA grooves has been developed. In details, all G1-dendrimers are able to interact with a high number of phosphate groups through their amine groups, also G2 ones show similar behaviour. It may be due to the flexible nature of their structures and it represents a crucial point because these dendrimers exhibit the alignment of their backbone with the siRNA phosphate groups in the major grooves. Differently, a loss of flexibility moving to higher generations has been reported and it follows that dendrimers are not capable so well to align with the siRNA's phosphate groups.

From results DP dendrimers show the best ability of aligning with siRNA backbone (except for DP-G2), with high values of amine groups interacting with siRNA (100 % of total for DP-G1). Also amine groups of DP-G3, despite their stiffness, interact with the electronegative atoms in the siRNA backbone.
Moreover, in order to identify the nucleotides that are mainly responsible for siRNA-dendrimer interaction, MD trajectory at 300 K was analysed for each system. The siRNA residues contact probability with dendrimer has been calculated, applying a distance cut-off of about 0.28 nm (roughly the diameter of a water molecule). SiRNA bases mainly responsible for complex interaction have been identified by contact probability plots. As a result, all systems have been analysed with the aim of locating specific residues that most frequently involve in the binding. Considering DP dendrimers, particularly, uracil and cytosine nucleotides cover the mostly part of the contact area with over the 90% of siRNA contact probability, whereas G2 exhibits a value around 85%. Thus, comparing all different macromolecules, nucleotides are strongly involved in the interaction with DP dendrimers, as demonstrated by the high contact probability values. Moreover, also in siRNA/DM-G2 and siRNA/DG-G3 interaction interface participate primarily cytosines and uracils of siRNA, with high contact probability around 90%. Otherwise, lower contact probability values and lower number of nucleotides involving the interaction were detected in case of all siRNA-G1 dendrimers, which have weaker electrostatic attraction caused by fewer positively charged amine groups available for the interaction.

5.5 Conclusion

We wanted to evaluate the characteristics of three different types of dendrimers (DP, DM and DG) in complex with a model of siRNA in order to study the structural and electrostatic behaviour in the binding condition. With the support of MD simulations we obtained several important informations about the peculiarity of the complexes, which show to be dependent on size, conformation, or surface properties of both dendrimer and nucleic acid. The analysis shows good binding configurations in case of complex between siRNA and DP dendrimers. The work presented here provides great insights into the complexation mechanism, elucidating how binding modes are influenced by the physico-chemical properties of different interacting dendrimers. Thus, these analysis could be useful for further investigations on interaction to assist the design/development of potent and selective RNA drug carrier systems and to achieve the best compromise between complexation stability and release ability. Furthermore, these results may advantage the evaluation of treatment of lung inflammation with gene therapy and other several applications in nanomedicine. In fact the development of highly-efficient macromolecules as good carriers will allow advances in understanding of interactions involved in the gene deliver process.

Chapter 6

Conclusions And Future Perspective

In summary, considering the safety issues and other drawbacks of viral approach, the nonviral vectors for siRNA delivery are increasingly concerned as the alternatives of viral ones. Among versatile non-viral vectors, dendrimers have been shown excellent characteristics as nanocarrier in gene therapy, therefore the small interfering RNA (siRNA) targeting tumor necrosis factor alpha (TNF-alfa) was used in complex with dendrimers for gene silencing in COPD treatment.
In the last years significant researches have been carried out to develop dendrimer-based nanomedicine for the delivery of drugs and nucleic acids. A detailed quantitative analysis of the physical interactions between dendrimers and bioactive agents or biomolecules is a crucial step in understanding the delivery mechanisms.
In this connection, computational molecular methods represent a powerful tool to provide quantitative and dynamic informations in order to determine ligands mechanism of action and differences in their therapeutic potential. This work presents a molecular dynamics method to study the complex of three types of functionalized dendrimers to siRNA at 150 mM salt concentration.
In this thesis the attention is focused on the investigation of different complexation between the funzionalized nanocarriers and siRNA on the atomic scale. With the purpose of investigating the effect of molecular geometry, dendrimer flexibility and charge density, three dendrimers configurations have been considered for the calculation: $16/CEF/051$, $16/CEF/294$ and $mk016$ with growing repeating units, corresponding to 3 different generations. We found that the positively charged surface of dendrimers induces not only increased cellular uptake through charge mediated interactions. Moreover, the data show a higher efficacy in term of siRNA-dendrimer binding for $16/CEF/051$ and $16/CEF/294$, which present pyrolidinium or piperazinium surface groups, respectively. Whereas morpholidinium terminals lead to a lower effect, especially in case dendrimers of generation 3.

Moreover, the influence of macromolecules architecture on the rigid and flexible behaviour in binding siRNA has been studied, recognizing the role of dendrimer generation on the complex composition.
The thesis does not pretend to be an exhaustive overview but elucidates main passages of the siRNA-dendrimer complexation at nanoscale level by MD simulations. It provides new contributions into the definition of flexibility properties and puts the attention on binding efficiency, suggesting new paradigms in the design of molecules devoted to interact with nucleic acids.
Further investigations are needed in order to better characterize the free energy landscape. In this regard, an interesting avenue for future computational studies could be the use of enhanced sampling computational methods, like umbrella sampling and metadynamics, which are very powerful tools able to elucidate the energetic reasons behind binding mechanisms.
These informations may be relevant to better understand ligand mechanism of action and peculiarities in their therapeutic potential and may open the prospective of dendrimer-base practical production for siRNA delivery in the future.

Ringraziamenti

Vorrei innanzitutto ringraziare il professor Gastone Castellani, per aver appoggiato la mia proposta di una tesi svolta presso l'Istituto Dalle Molle di studi sull'intelligenza artificiale di Lugano (CH).
Un ringraziamento speciale va al Prof. Andrea Danani, per avermi dato la possibilità di svolgere il mio lavoro presso il centro di ricerca, per avermi accolta con entusiasmo nel suo gruppo e per la disponibilità e la fiducia dimostratemi. Desidero inoltre ringraziare il Dott. Marco Agostino Deriu per avermi seguita con attenzione e costanza in questi mesi e avermi guidata nel mondo della dinamica molecolare. Grazie anche al resto del gruppo di ricerca per il prezioso aiuto fornitomi in questi mesi, a Martina e Stefano per il supporto e la simpatia.
Infine, un grande Grazie alla mia famiglia e alle persone a me vicine, per avermi sempre sostenuta e accompagnata in questo percorso con l'affetto di sempre.

Bibliography

[1] Mark D Eisner, Nicholas Anthonisen, David Coultas, Nino Kuenzli, Rogelio Perez-Padilla, Dirkje Postma, Isabelle Romieu, Edwin K Silverman, and John R Balmes. An official american thoracic society public policy statement: Novel risk factors and the global burden of chronic obstructive pulmonary disease. *American journal of respiratory and critical care medicine*, 182(5):693–718, 2010.

[2] Theo Vos, Abraham D Flaxman, Mohsen Naghavi, Rafael Lozano, Catherine Michaud, Majid Ezzati, Kenji Shibuya, Joshua A Salomon, Safa Abdalla, Victor Aboyans, et al. Years lived with disability (ylds) for 1160 sequelae of 289 diseases and injuries 1990–2010: a systematic analysis for the global burden of disease study 2010. *The Lancet*, 380(9859):2163–2196, 2013.

[3] Rafael Lozano, Mohsen Naghavi, Kyle Foreman, Stephen Lim, Kenji Shibuya, Victor Aboyans, Jerry Abraham, Timothy Adair, Rakesh Aggarwal, Stephanie Y Ahn, et al. Global and regional mortality from 235 causes of death for 20 age groups in 1990 and 2010: a systematic analysis for the global burden of disease study 2010. *The Lancet*, 380(9859):2095–2128, 2013.

[4] Gillina FG Bezemer, Seil Sagar, Jeroen Van Bergenhenegouwen, Niki A Georgiou, Johan Garssen, Aletta D Kraneveld, and Gert Folkerts. Dual role of toll-like receptors in asthma and chronic obstructive pulmonary disease. *Pharmacological reviews*, 64(2):337–358, 2012.

[5] R Rodriguez-Roisin. Copd exacerbations· 5: Management. *Thorax*, 61(6):535–544, 2006.

[6] S James, Christopher K Finch, and Nathan A Pinner. Corticosteroids in the treatment of acute exacerbations of chronic obstructive pulmonary disease. *International Journal of COPD*, 9:421–430, 2014.

[7] Ana L Kersul, Amanda Iglesias, Ángel Ríos, Aina Noguera, Aina Forteza, Enrique Serra, Alvar Agustí, and Borja G Cosío. Molecular mechanisms of inflammation during exacerbations of chronic obstructive pulmonary disease. *Archivos de Bronconeumología ((English Edition))*, 47(4):176–183, 2011.

[8] Peter J Barnes. Alveolar macrophages as orchestrators of copd. *COPD: Journal of Chronic Obstructive Pulmonary Disease*, 1(1):59–70, 2004.

[9] Seiichiro Sakao, Koichiro Tatsumi, Hidetoshi Igari, Yuji Shino, Hiroshi Shirasawa, and Takayuki Kuriyama. Association of tumor necrosis factor α gene promoter polymorphism with the presence of chronic obstructive pulmonary disease. *American journal of respiratory and critical care medicine*, 163(2):420–422, 2001.

[10] Mario Cazzola, Maria Gabriella Matera, Paola Rogliani, and Clive Page. Treating systemic effects of copd. *Trends in pharmacological sciences*, 28(10):544–550, 2007.

[11] Maria Gabriella Matera, Luigino Calzetta, and Mario Cazzola. Tnf-α inhibitors in asthma and copd: we must not throw the baby out with the bath water. *Pulmonary pharmacology & therapeutics*, 23(2):121–128, 2010.

[12] So Jin Lee, Aeju Lee, Seung Rim Hwang, Jong-Sung Park, Jiyeon Jang, Myung Sook Huh, Dong-Gyu Jo, Soo-Young Yoon, Youngro Byun, Sun Hwa Kim, et al. Tnf-α gene silencing using polymerized sirna/thiolated glycol chitosan nanoparticles for rheumatoid arthritis. *Molecular Therapy*, 22(2):397–408, 2014.

[13] I De Godoy, Michael Donahoe, William J Calhoun, Juliet Mancino, and Robert M Rogers. Elevated tnf-alpha production by peripheral blood monocytes of weight-losing copd patients. *American Journal of Respiratory and Critical Care Medicine*, 153(2):633–637, 1996.

[14] Sabina A Antoniu, Florin Mihaltan, and Ruxandra Ulmeanu. Anti-tnf-α therapies in chronic obstructive pulmonary diseases. *Expert opinion on investigational drugs*, 17(8):1203–1211, 2008.

[15] Francesco Menzella, Mirco Lusuardi, Carla Galeone, and Luigi Zucchi. Tailored therapy for severe asthma. *Multidisciplinary respiratory medicine*, 10(1):1, 2015.

[16] Rodrigo Athanazio. Airway disease: similarities and differences between asthma, copd and bronchiectasis. *Clinics*, 67(11):1335–1343, 2012.

[17] Giuseppe Murdaca, Francesca Spanò, Miriam Contatore, Andrea Guastalla, Ottavia Magnani, and Francesco Puppo. Pharmacogenetics of etanercept: role of tnf-α gene polymorphisms in improving its efficacy. *Expert opinion on drug metabolism & toxicology*, 10(12):1703–1710, 2014.

[18] Mengyao Zheng, Giovanni M Pavan, Manuel Neeb, Andreas K Schaper, Andrea Danani, Gerhard Klebe, Olivia M Merkel, and Thomas Kissel. Targeting

the blind spot of polycationic nanocarrier-based sirna delivery. *ACS nano*, 6(11):9447–9454, 2012.

[19] Gemma Navarro, Jiayi Pan, and Vladimir P Torchilin. Micelle-like nanoparticles as carriers for dna and sirna. *Molecular pharmaceutics*, 12(2):301–313, 2015.

[20] Christine Dufès, Ijeoma F Uchegbu, and Andreas G Schätzlein. Dendrimers in gene delivery. *Advanced drug delivery reviews*, 57(15):2177–2202, 2005.

[21] Clare E Thomas, Anja Ehrhardt, and Mark A Kay. Progress and problems with the use of viral vectors for gene therapy. *Nature Reviews Genetics*, 4(5):346–358, 2003.

[22] Swati Biswas and Vladimir P Torchilin. Dendrimers for sirna delivery. *Pharmaceuticals*, 6(2):161–183, 2013.

[23] Meredith A Mintzer and Eric E Simanek. Nonviral vectors for gene delivery. *Chemical reviews*, 109(2):259–302, 2008.

[24] Jiangyu Wu, Weizhe Huang, and Ziying He. Dendrimers as carriers for sirna delivery and gene silencing: a review. *The Scientific World Journal*, 2013, 2013.

[25] Michael Monaghan and Abhay Pandit. Rna interference therapy via functionalized scaffolds. *Advanced drug delivery reviews*, 63(4):197–208, 2011.

[26] Ahmet M Denli and Gregory J Hannon. Rnai: an ever-growing puzzle. *Trends in biochemical sciences*, 28(4):196–201, 2003.

[27] Ala Daka and Dan Peer. Rnai-based nanomedicines for targeted personalized therapy. *Advanced drug delivery reviews*, 64(13):1508–1521, 2012.

[28] Andrew Fire, SiQun Xu, Mary K Montgomery, Steven A Kostas, Samuel E Driver, and Craig C Mello. Potent and specific genetic interference by double-stranded rna in caenorhabditis elegans. *nature*, 391(6669):806–811, 1998.

[29] Sayda M Elbashir, Jens Harborth, Winfried Lendeckel, Abdullah Yalcin, Klaus Weber, and Thomas Tuschl. Duplexes of 21-nucleotide rnas mediate rna interference in cultured mammalian cells. *nature*, 411(6836):494–498, 2001.

[30] Antti Nykänen, Benjamin Haley, and Phillip D Zamore. Atp requirements and small interfering rna structure in the rna interference pathway. *Cell*, 107(3):309–321, 2001.

[31] Xiaoxuan Liu, Palma Rocchi, and Ling Peng. Dendrimers as non-viral vectors for sirna delivery. *New Journal of Chemistry*, 36(2):256–263, 2012.

[32] Lisha Zhang, FX Gu, JM Chan, AZ Wang, RS Langer, OC Farokhzad, et al. Nanoparticles in medicine: therapeutic applications and developments. *Clinical pharmacology and therapeutics*, 83(5):761–769, 2008.

[33] Yuriko Higuchi, Shigeru Kawakami, and Mitsuru Hashida. Strategies for in vivo delivery of sirnas. *BioDrugs*, 24(3):195–205, 2010.

[34] Lars Aagaard and John J Rossi. Rnai therapeutics: principles, prospects and challenges. *Advanced drug delivery reviews*, 59(2):75–86, 2007.

[35] Carol A Sledz and Bryan RG Williams. Rna interference in biology and disease. *Blood*, 106(3):787–794, 2005.

[36] Aimee L Jackson, Steven R Bartz, Janell Schelter, Sumire V Kobayashi, Julja Barchard, Mao Mao, Bin Li, Guy Cavet, and Peter S Linsley. Expression profiling reveals off-target gene regulation by rnai. *Nature biotechnology*, 21(6):635–637, 2003.

[37] MJ Hope, BASQF Mui, S Ansell, and QF Ahkong. Cationic lipids, phosphatidylethanolamine and the intracellular delivery of polymeric, nucleic acid-based drugs (review). *Molecular membrane biology*, 15(1):1–14, 1998.

[38] Elias Fattal and Amélie Bochot. State of the art and perspectives for the delivery of antisense oligonucleotides and sirna by polymeric nanocarriers. *International journal of pharmaceutics*, 364(2):237–248, 2008.

[39] Lin Zhu and Ram I Mahato. Lipid and polymeric carrier-mediated nucleic acid delivery. *Expert opinion on drug delivery*, 7(10):1209–1226, 2010.

[40] Hui Yi Xue, Pengbo Guo, Wu-Cheng Wen, and Ho Lun Wong. Lipid-based nanocarriers for rna delivery. *Current pharmaceutical design*, 21(22):3140–3147, 2015.

[41] CP Lollo, MG Banaszczyk, and HC Chiou. Obstacles and advances in non-viral gene delivery. *Current opinion in molecular therapeutics*, 2(2):136–142, 2000.

[42] Giovanni Maria Pavan, Paola Posocco, Aaron Tagliabue, Marek Maly, Anastasia Malek, Andrea Danani, Enzio Ragg, Carlo V Catapano, and Sabrina Pricl. Pamam dendrimers for sirna delivery: computational and experimental insights. *Chemistry-A European Journal*, 16(26):7781–7795, 2010.

[43] Jie Wang, Ze Lu, M Guillaume Wientjes, and Jessie L-S Au. Delivery of sirna therapeutics: barriers and carriers. *The AAPS journal*, 12(4):492–503, 2010.

[44] Jovica D Badjić, Alshakim Nelson, Stuart J Cantrill, W Bruce Turnbull, and J Fraser Stoddart. Multivalency and cooperativity in supramolecular chemistry. *Accounts of chemical research*, 38(9):723–732, 2005.

[45] Mauri A Kostiainen, David K Smith, and Olli Ikkala. Optically triggered release of dna from multivalent dendrons by degrading and charge-switching multivalency. *Angewandte Chemie International Edition*, 46(40):7600–7604, 2007.

[46] Mauri A Kostiainen, Géza R Szilvay, Julia Lehtinen, David K Smith, Markus B Linder, Arto Urtti, and Olli Ikkala. Precisely defined protein–polymer conjugates: construction of synthetic dna binding domains on proteins by using multivalent dendrons. *Acs Nano*, 1(2):103–113, 2007.

[47] Jason E Gestwicki, Christopher W Cairo, Laura E Strong, Karolyn A Oetjen, and Laura L Kiessling. Influencing receptor- ligand binding mechanisms with multivalent ligand architecture. *Journal of the American Chemical Society*, 124(50):14922–14933, 2002.

[48] Pavel I Kitov and David R Bundle. On the nature of the multivalency effect: a thermodynamic model. *Journal of the American Chemical Society*, 125(52):16271–16284, 2003.

[49] Donald A. Tomalia et al. *Dendrimers and other dendritic polymers*. Wiley, 2001.

[50] Donald A. Tomalia. Birth of a new macromolecular architecture: dendrimers as quantized building blocks for nanoscale synthetic polymer chemistry. *Progress in Polymer Science*, 30(3):294–324, 2005.

[51] Donald A Tomalia, Jørn B Christensen, and Ulrik Boas. *Dendrimers, dendrons, and dendritic polymers: discovery, applications, and the future*. Cambridge University Press, 2012.

[52] Jonathan D Eichman, Anna U Bielinska, Jolanta F Kukowska-Latallo, and James R Baker. The use of pamam dendrimers in the efficient transfer of genetic material into cells. *Pharmaceutical science & technology today*, 3(7):232–245, 2000.

[53] Anne-Marie Caminade, Séverine Fruchon, Cédric-Olivier Turrin, Mary Poupot, Armelle Ouali, Alexandrine Maraval, Matteo Garzoni, Marek Maly, Victor Furer, Valeri Kovalenko, et al. The key role of the scaffold on the efficiency of dendrimer nanodrugs. *Nature Communications*, 6, 2015.

[54] Sahil P Chaplot and Ilva D Rupenthal. Dendrimers for gene delivery–a potential approach for ocular therapy? *Journal of Pharmacy and Pharmacology*, 66(4):542–556, 2014.

[55] Yu Gao, Ge Gao, Yun He, Taole Liu, and Rong Qi. Recent advancs of dendrimers in delivery of genes and drugs. *Mini reviews in medical chemistry*, 8(9):889–900, 2008.

[56] Sönke Svenson and Donald A Tomalia. Dendrimers in biomedical applications—reflections on the field. *Advanced drug delivery reviews*, 64:102–115, 2012.

[57] Megan E Fox, Francis C Szoka, and Jean MJ Fréchet. Soluble polymer carriers for the treatment of cancer: the importance of molecular architecture. *Accounts of chemical research*, 42(8):1141–1151, 2009.

[58] Francesca Aulenta, Wayne Hayes, and Steven Rannard. Dendrimers: a new class of nanoscopic containers and delivery devices. *European Polymer Journal*, 39(9):1741–1771, 2003.

[59] Tamis Darbre and Jean-Louis Reymond. Peptide dendrimers as artificial enzymes, receptors, and drug-delivery agents. *Accounts of chemical research*, 39(12):925–934, 2006.

[60] Giovanni M Pavan. Modeling the interaction between dendrimers and nucleic acids: a molecular perspective through hierarchical scales. *ChemMedChem*, 9(12):2623–2631, 2014.

[61] Mauri A Kostiainen, John G Hardy, and David K Smith. High-affinity multivalent dna binding by using low-molecular-weight dendrons. *Angewandte Chemie*, 117(17):2612–2615, 2005.

[62] Jiehua Zhou, Jiangyu Wu, Nadia Hafdi, Jean-Paul Behr, Patrick Erbacher, and Ling Peng. Pamam dendrimers for efficient sirna delivery and potent gene silencing. *Chemical communications*, (22):2362–2364, 2006.

[63] Mahesh L Patil, Min Zhang, Seema Betigeri, Oleh Taratula, Huixin He, and Tamara Minko. Surface-modified and internally cationic polyamidoamine dendrimers for efficient sirna delivery. *Bioconjugate chemistry*, 19(7):1396–1403, 2008.

[64] Dan Luo and W Mark Saltzman. Synthetic dna delivery systems. *Nature biotechnology*, 18(1):33–37, 2000.

[65] Emilyne Blattes, Alain Vercellone, Hélène Eutamène, Cédric-Olivier Turrin, Vassilia Théodorou, Jean-Pierre Majoral, Anne-Marie Caminade, Jacques Prandi, Jérôme Nigou, and Germain Puzo. Mannodendrimers prevent acute lung inflammation by inhibiting neutrophil recruitment. *Proceedings of the National Academy of Sciences*, 110(22):8795–8800, 2013.

[66] D Shcharbin, V Dzmitruk, A Shakhbazau, N Goncharova, I Seviaryn, S Kosmacheva, M Potapnev, E Pedziwiatr-Werbicka, M Bryszewska, M Talabaev, et al. Fourth generation phosphorus-containing dendrimers: prospective drug and gene delivery carrier. *Pharmaceutics*, 3(3):458–473, 2011.

[67] Yajie Zhang, Yafeng Wang, Chi Zhang, Jin Wang, Dejing Pan, Jianghuai Liu, and Fude Feng. Targeted gene delivery to macrophages by biodegradable star-shaped polymers. *ACS applied materials & interfaces*, 8(6):3719–3724, 2015.

[68] Vladimir P Torchilin. Multifunctional nanocarriers. *Advanced drug delivery reviews*, 64:302–315, 2012.

[69] Marcio J Tiera, Francoise M Winnik, and Julio C Fernandes. Synthetic and natural polycations for gene therapy: state of the art and new perspectives. *Current gene therapy*, 6(1):59–71, 2006.

[70] Giovanni M Pavan, Mauri A Kostiainen, and Andrea Danani. Computational approach for understanding the interactions of uv-degradable dendrons with dna and sirna. *The Journal of Physical Chemistry B*, 114(17):5686–5693, 2010.

[71] Hans Martin Senn and Walter Thiel. Qm/mm methods for biomolecular systems. *Angewandte Chemie International Edition*, 48(7):1198–1229, 2009.

[72] Wilfred F van Gunsteren, Dirk Bakowies, Riccardo Baron, Indira Chandrasekhar, Markus Christen, Xavier Daura, Peter Gee, Daan P Geerke, Alice Glättli, Philippe H Hünenberger, et al. Biomolecular modeling: goals, problems, perspectives. *Angewandte Chemie International Edition*, 45(25):4064–4092, 2006.

[73] Michael Levitt. The birth of computational structural biology. *Nature Structural & Molecular Biology*, 8(5):392–393, 2001.

[74] Alessandro Barducci, Riccardo Chelli, Piero Procacci, Vincenzo Schettino, Francesco L Gervasio, and Michele Parrinello. Metadynamics simulation of prion protein: β-structure stability and the early stages of misfolding. *Journal of the American Chemical Society*, 128(8):2705–2710, 2006.

[75] Massimiliano Bonomi, Alessandro Barducci, and Michele Parrinello. Reconstructing the equilibrium boltzmann distribution from well-tempered metadynamics. *Journal of computational chemistry*, 30(11):1615–1621, 2009.

[76] Mark A Murcko. Computational methods to predict binding free energy in ligand-receptor complexes. *Journal of medicinal chemistry*, 38(26):4953–4967, 1995.

[77] Jochen S Hub, Bert L De Groot, and David Van Der Spoel. g_wham-a free weighted histogram analysis implementation including robust error and autocorrelation estimates. *Journal of Chemical Theory and Computation*, 6(12):3713–3720, 2010.

[78] Berk Hess, Carsten Kutzner, David Van Der Spoel, and Erik Lindahl. Gromacs 4: algorithms for highly efficient, load-balanced, and scalable molecular simulation. *Journal of chemical theory and computation*, 4(3):435–447, 2008.

[79] Mathai Mammen, Seok-Ki Choi, and George M Whitesides. Polyvalent interactions in biological systems: implications for design and use of multivalent ligands and inhibitors. *Angewandte Chemie International Edition*, 37(20):2754–2794, 1998.

[80] Giovanni M Pavan, Meredith A Mintzer, Eric E Simanek, Olivia M Merkel, Thomas Kissel, and Andrea Danani. Computational insights into the interactions between dna and sirna with "rigid" and "flexible" triazine dendrimers. *Biomacromolecules*, 11(3):721–730, 2010.

[81] Giovanni M Pavan, Lorenzo Albertazzi, and Andrea Danani. Ability to adapt: different generations of pamam dendrimers show different behaviors in binding sirna. *The Journal of Physical Chemistry B*, 114(8):2667–2675, 2010.

[82] Giovanni M Pavan and Andrea Danani. Supporting the design of efficient dendritic dna and sirna nano-carriers with molecular modeling. *Current drug discovery technologies*, 8(4):314–328, 2011.

[83] G M Pavan, S Monteagudo, J Guerra, B Carrion, V Ocana, J Rodriguez-Lopez, A Danani, F C Perez-Martinez, and V Cena. Role of generation, architecture, ph and ionic strength on successful sirna delivery and transfection by hybrid ppv-pamam dendrimers. *Current medicinal chemistry*, 19(29):4929–4941, 2012.

[84] Donald A Tomalia. Dendrons/dendrimers: quantized, nano-element like building blocks for soft-soft and soft-hard nano-compound synthesis. *Soft Matter*, 6(3):456–474, 2010.

[85] Oxana Klementieva, Nuria Benseny-Cases, Alejandro Gella, Dietmar Appelhans, Brigitte Voit, and Josep Cladera. Dense shell glycodendrimers as potential nontoxic anti-amyloidogenic agents in alzheimer's disease. amyloid–dendrimer aggregates morphology and cell toxicity. *Biomacromolecules*, 12(11):3903–3909, 2011.

[86] Peter MH Heegaard and Ulrik Boas. Dendrimer based anti-infective and anti-inflammatory drugs. *Recent patents on anti-infective drug discovery*, 1(3):333–351, 2006.

[87] Myriam Hayder, Séverine Fruchon, Jean-Jacques Fournié, Mary Poupot, and Rémy Poupot. Anti-inflammatory properties of dendrimers per se. *The Scientific World Journal*, 11:1367–1382, 2011.

[88] Jérémy Ledall, Séverine Fruchon, Matteo Garzoni, Giovanni M Pavan, Anne-Marie Caminade, Cédric-Olivier Turrin, Muriel Blanzat, and Rémy Poupot. Interaction studies reveal specific recognition of an anti-inflammatory polyphosphorhydrazone dendrimer by human monocytes. *Nanoscale*, 7(42):17672–17684, 2015.

[89] S Rosenfeldt, M Ballauff, P Lindner, and L Harnau. Structure and interaction of flexible dendrimers in concentrated solution. *The Journal of chemical physics*, 130(24), 2009.

[90] Enguerran Vanquelef, Sabrina Simon, Gaelle Marquant, Elodie Garcia, Geoffroy Klimerak, Jean Charles Delepine, Piotr Cieplak, and François-Yves Dupradeau. Red server: a web service for deriving resp and esp charges and building force field libraries for new molecules and molecular fragments. *Nucleic acids research*, 39(suppl 2):W511–W517, 2011.

[91] Alan W Sousa da Silva and Wim F Vranken. Acpype-antechamber python parser interface. *BMC research notes*, 5(1):367, 2012.

[92] Berk Hess, Henk Bekker, Herman JC Berendsen, Johannes GEM Fraaije, et al. Lincs: a linear constraint solver for molecular simulations. *Journal of computational chemistry*, 18(12):1463–1472, 1997.

[93] William Humphrey, Andrew Dalke, and Klaus Schulten. Vmd: visual molecular dynamics. *Journal of molecular graphics*, 14(1):33–38, 1996.

[94] Nathan A Baker. Poisson–boltzmann methods for biomolecular electrostatics. *Methods in enzymology*, 383:94–118, 2004.

[95] Meredith A Mintzer, Olivia M Merkel, Thomas Kissel, and Eric E Simanek. Polycationic triazine-based dendrimers: effect of peripheral groups on transfection efficiency. *New Journal of Chemistry*, 33(9):1918–1925, 2009.

[96] Linda B Jensen, Giovanni M Pavan, Marina R Kasimova, Sandra Rutherford, Andrea Danani, Hanne M Nielsen, and Camilla Foged. Elucidating the molecular mechanism of pamam–sirna dendriplex self-assembly: Effect of dendrimer charge density. *International journal of pharmaceutics*, 416(2):410–418, 2011.

[97] GM Pavan and A Danani. Dendrimers and dendrons for sirna binding: computational insights. *Journal of Drug Delivery Science and Technology*, 22(1):83–89, 2012.

[98] Tom Darden, Darrin York, and Lee Pedersen. Particle mesh ewald: An n log (n) method for ewald sums in large systems. *The Journal of chemical physics*, 98(12):10089–10092, 1993.

[99] Vincent Kräutler, Wilfred F Van Gunsteren, and Philippe H Hünenberger. A fast shake algorithm to solve distance constraint equations for small molecules in molecular dynamics simulations. *Journal of computational chemistry*, 22(5):501–508, 2001.

[100] Junmei Wang, Wei Wang, Peter A Kollman, and David A Case. Automatic atom type and bond type perception in molecular mechanical calculations. *Journal of molecular graphics and modelling*, 25(2):247–260, 2006.

[101] Junmei Wang, Romain M Wolf, James W Caldwell, Peter A Kollman, and David A Case. Development and testing of a general amber force field. *Journal of computational chemistry*, 25(9):1157–1174, 2004.

[102] William L Jorgensen, Jayaraman Chandrasekhar, Jeffry D Madura, Roger W Impey, and Michael L Klein. Comparison of simple potential functions for simulating liquid water. *The Journal of chemical physics*, 79(2):926–935, 1983.

[103] Marco A Deriu, Gianvito Grasso, Ginevra Licandro, Andrea Danani, Diego Gallo, Jack A Tuszynski, and Umberto Morbiducci. Investigation of the josephin domain protein-protein interaction by molecular dynamics. *PloS one*, 9(9):e108677, 2014.

[104] Nathan A Baker, David Sept, Simpson Joseph, Michael J Holst, and J Andrew McCammon. Electrostatics of nanosystems: application to microtubules and the ribosome. *Proceedings of the National Academy of Sciences*, 98(18):10037–10041, 2001.

[105] Chuanying Chen and B Montgomery Pettitt. The binding process of a nonspecific enzyme with dna. *Biophysical journal*, 101(5):1139–1147, 2011.

[106] Rashmi Kumari, Rajendra Kumar, and Andrew Lynn. g_mmpbsa - a gromacs tool for high-throughput mm-pbsa calculations. *Journal of chemical information and modeling*, 54(7):1951–1962, 2014.

[107] Jonathan B Chaires. Energetics of drug–dna interactions. *Biopolymers*, 44(3):201–215, 1997.

[108] Diana A Kondinskaia, Andrei Yu Kostritskii, Alexey M Nesterenko, Alexandra Yu Antipina, and Andrey A Gurtovenko. Atomic-scale molecular dynamics simulations of dna–polycation complexes: Two distinct binding patterns. *The Journal of Physical Chemistry B*, 120(27):6546–6554, 2016.

[109] Jesse Ziebarth and Yongmei Wang. Molecular dynamics simulations of dna-polycation complex formation. *Biophysical journal*, 97(7):1971–1983, 2009.